Final Report

CRACKING PERFORMANCE EVALUATION OF ASPHALT BINDERS AT INTERMEDIATE TEMPERATURES

Contract No.: BDV31-977-83
Secondary No.: 00095360

Submitted to:

Florida Department of Transportation
605 Suwannee Street
Tallahassee, FL, 32399

Dr. Reynaldo Roque, P.E.
Dr. Yu Yan, P.E.
George Lopp

Department of Civil and Coastal Engineering
College of Engineering
365 Weil Hall, P.O. Box 116580
Gainesville, FL, 32611-6580
Tel: (352) 392-9537 extension 1458
Fax: (352) 392-3394

June 2020

DISCLAIMER

The opinions, findings, and conclusions expressed in this publication belong to the authors, and not necessarily the Florida Department of Transportation.

Prepared in cooperation with the Florida Department of Transportation.

SI (MODERN METRIC) CONVERSION FACTORS

SI* (MODERN METRIC) CONVERSION FACTORS

APPROXIMATE CONVERSIONS TO SI UNITS

Symbol	When You Know	Multiply By	To Find	Symbol
	LENGTH			
in	inches	25.4	millimeters	mm
ft	feet	0.305	meters	m
yd	yards	0.914	meters	m
mi	miles	1.61	kilometers	km
	AREA			
in²	square inches	645.2	square millimeters	mm²
ft²	square feet	0.093	square meters	m²
yd²	square yards	0.836	square meters	m²
ac	acres	0.405	hectares	ha
mi²	square miles	2.59	square kilometers	km²
	VOLUME			
fl oz	fluid ounces	29.57	milliliters	ml
gal	gallons	3.785	liters	l
ft³	cubic feet	0.028	cubic meters	m³
yd³	cubic yards	0.765	cubic meters	m³

NOTE: Volumes greater than 1000 l shall be shown in m³.

Symbol	When You Know	Multiply By	To Find	Symbol
	MASS			
oz	ounces	28.35	grams	g
lb	pounds	0.454	kilograms	kg
T	short tons (2000 lb)	0.907	megagrams	Mg
	TEMPERATURE (exact)			
°F	Fahrenheit temperature	$5(F-32)/9$ or $(F-32)/1.8$	Celcius temperature	°C
	ILLUMINATION			
fc	foot-candles	10.76	lux	lx
fl	foot-Lamberts	3.426	candela/m²	cd/m²
	FORCE and PRESSURE or STRESS			
lbf	poundforce	4.45	newtons	N
psi	poundforce per square inch	6.89	kilopascals	kPa

APPROXIMATE CONVERSIONS FROM SI UNITS

Symbol	When You Know	Multiply By	To Find	Symbol
	LENGTH			
mm	millimeters	0.039	inches	in
m	meters	3.28	feet	ft
m	meters	1.09	yards	yd
km	kilometers	0.621	miles	mi
	AREA			
mm²	square millimeters	0.0016	square inches	in²
m²	square meters	10.764	square feet	ft²
m²	square meters	1.195	square yards	yd²
ha	hectares	2.47	acres	ac
km²	square kilometers	0.386	square miles	mi²
	VOLUME			
ml	milliliters	0.034	fluid ounces	fl oz
l	liters	0.264	gallons	gal
m³	cubic meters	35.71	cubic feet	ft³
m³	cubic meters	1.307	cubic yards	yd³
	MASS			
g	grams	0.035	ounces	oz
kg	kilograms	2.202	pounds	lb
Mg	megagrams	1.103	short tons (2000 lb)	T
	TEMPERATURE (exact)			
°C	Celcius temperature	$1.8C + 32$	Fahrenheit temperature	°F
	ILLUMINATION			
lx	lux	0.0929	foot-candles	fc
cd/m²	candela/m²	0.2919	foot-Lamberts	fl
	FORCE and PRESSURE or STRESS			
N	newtons	0.225	poundforce	lbf
kPa	kilopascals	0.145	poundforce per square inch	psi

(Revised August 1992)

* SI is the symbol for the International System of Units. Appropriate rounding should be made to comply with Section 4 of ASTM E380.

1. Report No.	2. Government Accession No.	3. Recipient's Catalog No.

4. Title and Subtitle	5. Report Date
Evaluation of the Cracking Performance of Asphalt Binders at Intermediate Temperatures	June 2020
	6. Performing Organization Code 0054539

7. Author(s)	8. Performing Organization Report No.
Reynaldo Roque, Yu Yan, and George Lopp	

9. Performing Organization Name and Address	10. Work Unit No. (TRAIS)
University of Florida Department of Civil and Coastal Engineering 365 Weil Hall P.O. Box 116580 Gainesville, FL 32611-6580	
	11. Contract or Grant No. BDV31-977-83

12. Sponsoring Agency Name and Address	13. Type of Report and Period Covered
Florida Department of Transportation Research Management Center 605 Suwannee Street, MS 30 Tallahassee, FL 32399	Final 10/01/2017-06/01/2020
	14. Sponsoring Agency Code

15. Supplementary Notes

16. Abstract

The major objective of this research was to identify a binder parameter to effectively characterize binder cracking performance at intermediate temperatures. A laboratory experimental plan was developed that included six asphalt binders and twelve mixtures of two aggregate types. The linear amplitude sweep (LAS) test and the binder fracture energy (BFE) test were identified as candidate binder tests. Superpave IDT tests were performed to obtain mixture failure limit and damage rate, which were combined to evaluate mixture cracking performance.

Two versions of the LAS with three different failure definitions were employed to characterize the binder resistance to fatigue damage: the TP 101-14 and the G^R approach resulted in similar binder ranking. Moreover, the BFE test in its existing form was performed to determine the binder failure limit, i.e., fracture energy density (FED). Additionally, an alternative interpretation of the true stress-true strain curve was proposed and employed to obtain the binder damage rate. Results showed that binder FED and damage rate appeared to be inversely related: a binder with higher FED also had lower damage rate. The BFE binder N_f parameter that integrates binder FED and damage rate was used to evaluate the relative cracking performance of asphalt binders.

There is a fairly good correlation between LAS N_f parameter and mixture N_f parameter, except for the softest unmodified binder and the hybrid binder containing rubber. Correlations between binder and mixture results in terms of fracture properties and relative cracking performance were also examined: the binder FED parameter, which was inversely related to the binder damage rate parameter, was found to more suitably characterize the cracking performance of asphalt binders than the BFE binder N_f parameter. The BFE test following the TP 127 was recommended to evaluate binder cracking performance at intermediate temperatures.

17. Key Word	18. Distribution Statement
Asphalt binder, Asphalt mixture, Fracture energy density, Damage rate, Cracking performance, SBS polymer modification	No restrictions. This document is available to the public through the National Technical Information Service, Springfield, VA.22161

19. Security Classif. (of this report)	20. Security Classif. (of this page)	21. No. of Pages	22. Price
Unclassified	Unclassified	128	

Form DOT F 1700.7 (8-72)   Reproduction of completed page authorized

ACKNOWLEDGEMENTS

EXECUTIVE SUMMARY

Load-induced fatigue cracking (bottom-up and top-down) is one of the primary distress modes in asphalt pavements at intermediate temperatures. Asphalt binder, as the binding agent, plays a critical role in cracking resistance of asphalt mixtures. Accurate characterization and proper selection of fatigue-resistant asphalt binders could prolong the fatigue life of asphalt pavement. Currently, there is a lack of information about the role of asphalt binder and how damage progresses. Also, a fundamental approach is needed to effectively characterize asphalt binder and accurately determine its contribution to mixture cracking performance at intermediate temperature.

The main objective of this research was to identify a binder parameter to effectively characterize binder relative cracking performance at intermediate temperatures. According to the hot-mix asphalt-fracture mechanics model that has been shown to correlate well with field observations in Florida, it is important to consider both failure limit (e.g., fracture energy density), and damage rate as an entire system to predict mixture cracking performance. Thus, it seems logical that a binder parameter that is governed by the binder fracture energy density (FED) and damage rate is necessary to effectively characterize binder cracking performance.

To achieve the objective, a laboratory experimental plan was developed that included six asphalt binders, and twelve mixtures of two aggregate types. These binders which have been commonly used in Florida, were: three unmodified binders, one polymer-modified binder, one hybrid binder, and one high polymer-modified (HP) binder. Aggregates used throughout this research were Georgia granite and Florida limestone. Mixture design parameters for each aggregate type were held constant, so the only variable was binder type. This helped to isolate the effect of binder type and minimize the effect of mixture that may confound the effect of binder alone.

Two advanced binder tests, the linear amplitude sweep (LAS) test and the binder fracture energy (BFE) test, were identified as the candidate binder tests. More specifically, two versions of the LAS with three different failure definitions were employed to characterize the relationship of binder resistance to fatigue damage. Moreover, the BFE test in its existing form was performed to determine the binder failure limit (FED) and additionally, an alternative interpretation of the true stress-true strain curve was proposed and performed in this study to obtain the binder damage rate. The BFE binder N_f parameter that integrates binder FED and damage rate was used to evaluate the relative cracking performance of asphalt binders.

In terms of the LAS test, both AASHTO TP 101-12 and -14 resulted in questionable relative rankings of the six binders, i.e., soft virgin binder had fatigue life comparable to that of PG 76-22 PMA. This observation indicates that the failure definitions adopted by the two provisional standards may not be appropriate. The G^R approach yielded reasonable fatigue life (N_f) values of the six binders: HP exhibited superior performance, followed by PG 76-22 ARB and PG 76-22 PMA, and lastly, the three unmodified binders.

The BFE test provided consistent determination of the FED of the same six asphalt binders previously tested with the LAS test. As expected, FED results differentiated between unmodified, polymer-modified, hybrid, and heavily polymer-modified binders. Moreover, an

alternative interpretation of the BFE true stress-true strain curve was conducted to derive a parameter named creep strain rate per unit stress (CSR/S) to characterize binder damage rate. Complex shear modulus was used to determine binder elastic energy, which later was found to have no impact on the relative ranking of the six binders in terms of CSR/S. Stiffer binders had lower CSR/S values, indicating lower rates of damage accumulation. Also, the styrene-butadiene-styrene polymer binders exhibited notably lower CSR/S values than unmodified binders. Both observations agree with previous knowledge of mixture damage rate.

The Superpave IDT test was conducted to obtain mixture fracture properties. All mixtures were subjected to one condition protocol: short-term oven aging plus long-term oven aging. The relative cracking performance of asphalt mixtures was evaluated by using the mixture N_f parameter, which combined the mixture FED and damage rate. Florida limestone mixtures were found to have both lower failure limit and damage rate than Georgia granite mixtures, resulting in better relative cracking performance as indicated by the mixture N_f parameter. Relatively little difference was observed in FED between mixtures with unmodified and modified binders. However, significant reduction in mixture damage rate was achieved by the modified binders, especially the HP binder. Consequently, mixtures with modified binders had greater N_f values than mixtures with unmodified binders, regardless of the aggregate types.

Overall, there was a good correlation between LAS binder N_f parameter obtained from the LAS test-G^R approach and mixture N_f parameter determined based on Superpave IDT tests, except for PG 76-22 ARB. This discrepancy may be associated with the inadequacy of parallel plate binder tests (e.g., the LAS test) in characterizing asphalt binders containing rubber particles. Moreover, correlations between BFE and Superpave IDT test results in terms of fracture properties and relative cracking performance were also examined. SBS polymer modification appeared to increase binder FED but had negligible influence on mixture FED. However, SBS polymer reduced the damage rate of both asphalt binder and mixture. As a result, the difference in cracking performance of unmodified and modified binders depicted by the BFE binder N_f parameter was not proportionally reflected on the corresponding mixture N_f results. The binder FED, which was found to be inversely related to binder damage rate, more accurately captured the effect of binder type on mixture cracking performance. Therefore, the BFE test following the AASHTO TP 127 was recommended to evaluate binder cracking performance at intermediate temperatures.

TABLE OF CONTENTS

LIST OF FIGURES

LIST OF TABLES

CHAPTER 1 INTRODUCTION

1.1 Background

Load-induced fatigue cracking (bottom-up and top-down) is one of the primary distress modes in asphalt pavements at intermediate temperatures. Asphalt binder, as the binding agent, plays a critical role in cracking resistance of asphalt mixtures. Accurate characterization and proper selection of fatigue-resistant asphalt binders could prolong the service life of asphalt pavement. In the current PG specification, the fatigue performance of an asphalt binder is evaluated by the parameter G*sinδ, which is an indicator of total dissipated energy during cyclic loading. However, this parameter is measured within the linear viscoelastic range assuming energy estimated in this range is a good indicator of binder resistance to fatigue. Since the late 1990s, there has been increased focus on challenging this assumption, particularly for polymer-modified asphalts that have better fatigue resistance and show a nonlinear response to loading. Thus, there is a lack of information about the role of asphalt binder in damage progress. Also, a fundamental approach is needed to effectively characterize asphalt binder and accurately determine its contribution to mixture cracking performance at intermediate temperature.

In recent years, there have been significant efforts to accurately measure and characterize binder fatigue properties by means of damage characterization. The time sweep (TS) test proposed by Bahia et al. (2001) is a conventional fatigue test, which consists of applying repeated cyclic loading at a fixed load amplitude to a binder specimen by using the dynamic shear rheometer (DSR). However, the TS test is not a practical method for specification of asphalt binder fatigue resistance because of the uncertainty in testing time and poor testing repeatability (Hintz et al., 2011). Johnson and Bahia developed an accelerated asphalt binder fatigue test, called the linear amplitude sweep (LAS) test as a surrogate for the TS test. The LAS test consists a series of cyclic loads at systematically linearly increasing strain amplitudes to accelerate the rate of damage accumulation. The LAS test results can be analyzed using viscoelastic continuum damage (VECD), following Schapery's theory of work potential to model damage growth. The LAS test is based on the definition of fatigue damage, which is the degradation of material integrity under repeated loading. Johnson and Bahia proposed to use $|G^*| \cdot \sin\delta$ as the material integrity parameter and they used a power law function to model $|G^*| \cdot \sin\delta$ versus damage, from which the number of cycles that produce a given damage intensity can be determined. While the LAS test is promising, there are important concerns about its testing and analysis protocols. The level of damage accumulation to be used in the advanced fatigue life prediction model (VECD) is arbitrarily defined as a 35% reduction in undamaged $|G^*| \cdot \sin\delta$, which is similar to the controversial definition of fatigue failure in asphalt mixture (e.g., 50% reduction in initial stiffness).

Binder fracture energy density (FED), which is the energy a binder can tolerate before fracture, is an important property related to binder fatigue resistance. However, measurement of binder FED at intermediate temperature was not available until the development of a binder fracture energy (BFE) test by Roque et al. (2014). Binder FED

was found to be a fundamental material property independent of testing temperature (0–25°C) and loading rate, as opposed to other binder properties such as stiffness, failure stress, and failure strain. Additionally, previous work by Yan et al. (2017) showed failure limit parameter (i.e., FED) translated well from binder to mixture such that binders with higher FED resulted in higher mixture FED values. With a provisional AASHTO standard available, the BFE test now can be used to provide valuable information in terms of binder failure limit. However, this test in its current form is not suitable for determination of damage rate, which is another important property that potentially dominates binder cracking performance.

1.2 Objectives

The primary objective of this research was to identify a parameter that integrates binder failure limit and damage rate to effectively characterize binder cracking performance at intermediate temperatures. Detailed objectives of this project were:

- Identify an approach to determine a suitable rate of damage parameter for asphalt binders.
- Propose a parameter that integrates binder FED and damage rate.
- Evaluate the proposed binder parameter with mixture fracture properties and performance.

1.3 Scope

Six binders were employed, including three unmodified binders (PG 52-28, PG 58-22, and PG 67-22), one hybrid binder (PG 76-22 ARB), one polymer-modified binder (PG 76-22 PMA) and one heavily polymer-modified (HP) binder. Superpave PG binder tests were performed to evaluate specification compliance. Moreover, two versions of the LAS test were employed to characterize binder resistance to fatigue damage. Furthermore, the BFE tests including both the existing and the newly proposed approach were performed to evaluate the relative cracking performance of asphalt binders.

Twelve dense-grade Superpave mixtures were evaluated, corresponding to two aggregate types and six asphalt binders. The Superpave IDT test was conducted to obtain mixture fracture properties at 10°C. All mixtures were subjected to one condition level: short-term oven aging (STOA) plus long-term oven aging (LTOA). Mixture fracture properties and performance were compared with respect to the binder types. Additionally, correlations were examined between asphalt binder and mixtures in terms of fracture properties and performance.

1.4 Research Approach

To meet the objectives of the project, the research was categorized into tasks, summarized below:

- Task I — Literature Review: a literature review was conducted to gather and examine available information regarding the most recent and well-reported testing

methodologies to evaluate the cracking performance of asphalt binders at intermediate temperature, emphasizing the characteristics of binder damage growth. In addition, analytical approaches that model the fatigue behaviors of asphalt binders were also included in the literature review. Additionally, mixture fatigue models such as viscoelastic continuum damage (VECD) mechanics, dissipated energy ratio approach, UF HMA-FM model, dissipated pseudostrain energy, etc., were of great interest since binder fatigue research has in many ways traced the developments in mixture fatigue research.

- Task II — Identification of Candidate Test and Approach: this task identified candidate tests to determine a rate of damage parameter (e.g., energy dissipated per cycle) for asphalt binder. One promising test was LAS test, which uses cyclic loading with systematically increasing load amplitudes to accelerate damage and obtain sufficient damage accumulation. Another candidate test that can be used to characterize binder damage growth was the BFE test, with either an alternate interpretation of the true stress-true strain curve characteristics or a further developed version. Preliminary tests were conducted on the LAS and BFE tests following the AASHTO provisional standards.

- Task III — Experimental Design: findings from Tasks 1 and 2 were used to finalize a full testing plan and materials that were included in this study. All material selection was conducted in consultation with FDOT research panel. Anticipated factors that involved in the testing plan are shown in Figure 1-1.

Asphalt binder | PG 52-28 | PG 58-22 | PG 67-22 | PG 76-22 ARB | PG 76-22 PMA | High polymer

Asphalt mixture | Georgia granite | FL limestone | SP 12.5 Fine

Testing | Binder tests | BFE test | LAS test | Mixture tests | Superpave IDT @10°C
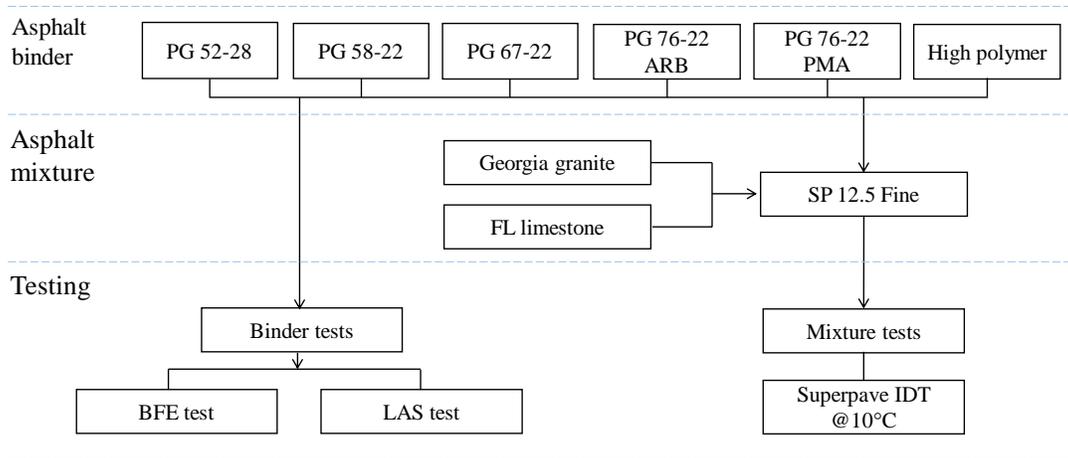
Figure 1-1. Flowchart for the experimental testing plan

- Task IV — Binder Evaluation: Superpave PG binder tests were conducted to evaluate specification compliance of selected binders. Two versions of the LAS tests with three different failure definitions were conducted to characterize binder resistance to fatigue damage. A binder rate of damage parameter was determined from the alternate interpretation of true stress-true strain curve from the BFE test. The relative cracking performance of selected binders was determined by using

the binder N_f parameter, which combined binder FED and damage rate (i.e., DCSE/cycle).

- Task V — Evaluation with Mixture Performance: mixture fracture properties were determined by performing the Superpave IDT tests and the relative mixture cracking performance was evaluated by using the mixture N_f parameter that combined mixture FED and damage rate. Mixture fracture properties and performance were compared with respect to the binder types. Moreover, correlations were examined between asphalt binder and mixtures in terms of fracture properties and cracking performance. Results of comparison and correlation provided insight on the relative effect of binder failure limit and damage rate on the cracking performance of asphalt binders.

CHAPTER 2 LITERATURE REVIEW

2.1 Introduction

Load-induced fatigue cracking is one of the primary distress modes in asphalt pavements at intermediate temperatures. In general, there are two mechanisms of fatigue cracking in asphalt pavements: bottom-up and top-down. Bottom-up cracks initiate at the bottom of the hot-mix asphalt (HMA) layer, where repeated applications of load cycles create high tensile strain, and damage progress up to the pavement surface. Conversely, top-down cracks initiate at the pavement surface and propagates downward through the HMA layer. Regardless of the mechanism, cracks typically initiate and propagate through the binder or the interface between binder and aggregate, as opposed to fracture through the aggregate. Thus, asphalt binder plays a critical role in cracking resistance of asphalt mixtures. Accurate characterization and proper selection of fatigue-resistant asphalt binders can prolong the fatigue life of asphalt pavements.

In Superpave performance grade (PG) specification, the fatigue performance of an asphalt binder is evaluated by the parameter $G^*\sin(\delta)$, which is an indicator of total dissipated energy during cyclic loading. However, the effectiveness of this parameter has been questioned by many researchers for several reasons, including 1) this parameter is measured at a small strain level (i.e., 1% constant strain) which may not introduce damage into the binder specimen; 2) not all the total dissipated energy is associated with damage; in fact a large portion can be delayed elastic energy; 3) this parameter assumes linear viscoelasticity whereas the behavior of polymer-modified binders can be highly nonlinear; 4) the meaning and appropriateness of linking cracking performance with intermediate temperatures are debatable. Overall, there is a lack of information about the role of asphalt binder in the damage progress.

In recent years, there has been a significant amount of research effort placed on the development of binder tests and associated data analysis procedures to accurately measure and characterize binder fatigue properties. This report organized the most recent and well-reported binder testing methodologies into two main categories: those using dynamic shear rheometer (DSR) to obtain rheological properties to determine binder fatigue life and those employing fracture mechanics and fracture properties as potentially better indicators of binder relative cracking performance. Mixture cracking models were also examined since binder fatigue research has in many ways followed the developments in mixture fatigue research.

2.2 Rheological Properties-Related Binder Tests

2.2.1 Time sweep test

The time sweep (TS) test proposed by Bahia et al. (2001) evaluates the fatigue damage by means of the degradation of material integrity under repeated loading. The TS procedure consists of applying repeated cyclic loading at a fixed loading frequency and amplitude to a binder specimen in either controlled-stress or controlled-displacement mode using the DSR. The TS test employs the 8-mm diameter parallel plates with a fixed

gap of 2 mm. Changes in complex shear modulus (G*) and phase angle (δ) with number of loading cycles are recorded for determination of binder fatigue life (Figure 2-1). The TS test allows for the binder to go beyond linear viscoelastic behavior and into the damage accumulation range. However, a unified means to clearly define fatigue failure, which is crucial to fatigue performance evaluation and prediction, is still missing in the TS test. Moreover, this test was determined not to be a practical method for specification of asphalt binder fatigue resistance because of the uncertainty in testing time (can be several hours) and poor testing repeatability (Hintz et al. 2011).
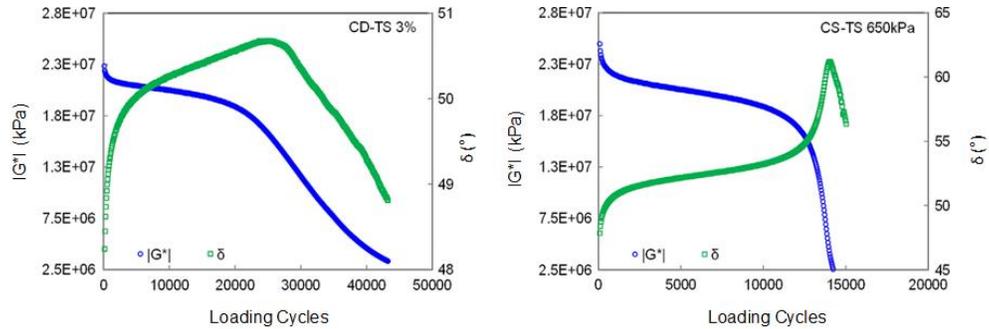
Figure 2-1. Binder responses during the TS tests: (a) controlled displacement loading mode; (b) controlled stress loading mode (Wang et al., 2016)

2.2.2 Binder yield energy test

Bahia and his co-workers made further attempts to introduce surrogate tests to estimate binder fatigue resistance in a relatively short period of time. This includes the binder yield energy (BYE) test and the linear amplitude sweep (LAS) test. The BYE test is a monotonic constant shear strain rate test that employs the DSR and measures the energy to "yielding" of binders (Johnson et al. 2009). Yield energy can be determined by integrating the area under the stress-strain curve to the maximum stress value (Figure 2-2). BYE tests were performed on several binders from an FHWA ALF project and the yield energy results of these binders were found to correlate well with the pavement cracking performance (i.e., the crack length at 100,000 passes) (Figure 2-3).
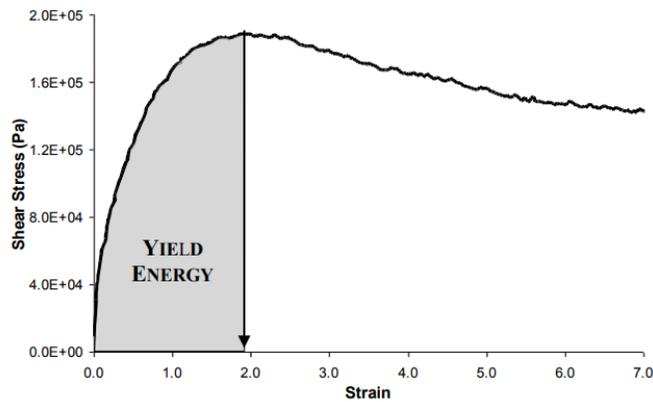
Figure 2-2. Determination of yield energy from the BYE test (Johnson et al. 2009)
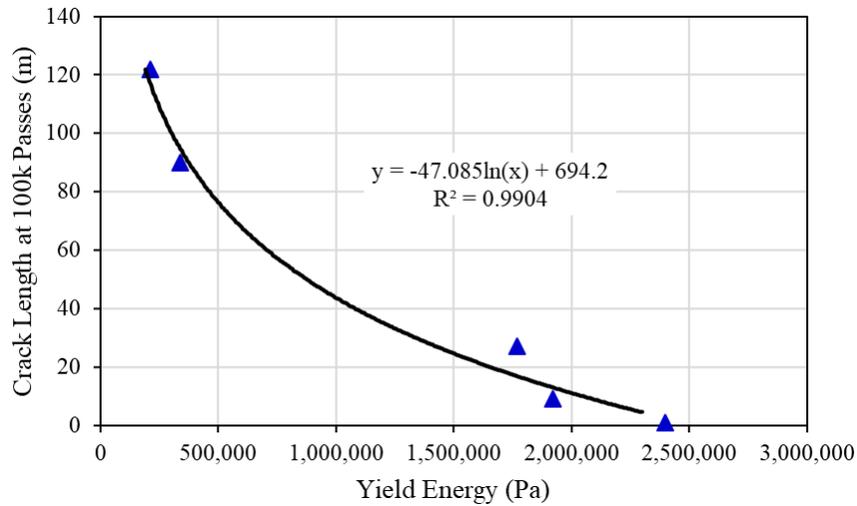
Figure 2-3. Correlation between binder yield energy and ALF pavement cracking performance (Johnson et al. 2009)

One method of quantifying damage is to relate the undamaged material properties to damaged material properties from destructive (damage-inducing) tests (Figure 2-4a). The undamaged properties are typically estimated from tests employing small loads, under the assumption that no damage is introduced. However, response of polymer-modified asphalt (PMA) binders from the BYE test, during which damage is assumed to have occurred, was found to be above the undamaged response of the same binder (Figure 2-4b). In other words, the increased shear strain did not reduce the material integrity or introduce damage. One potential reason for this observation was that undamaged responses determined from tests at small strain levels (less than 1%) may be inaccurate because polymer component has a more pronounced contribution to the properties at high strain (greater than 300%). It appears that the effect of polymer modification prevents the combined use of the BYE test and the viscoelastic constitutive model to accurately determine the characteristics of damage growth, which are essential for predicting the binder failure.
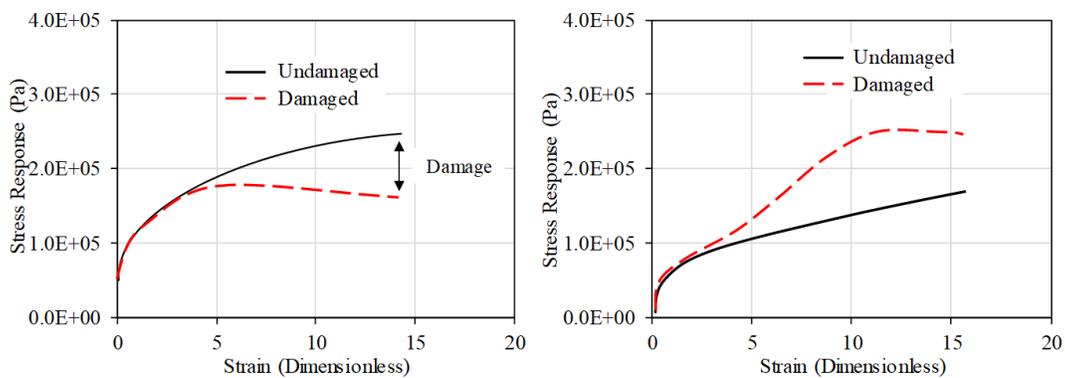
Figure 2-4. Damaged and undamaged responses: (a) ideal comparison; (b) comparison using BYE testing results of a PMA binder

2.2.3 Linear amplitude sweep test

The linear amplitude sweep (LAS) test was found to be more successful in measuring fatigue resistance of asphalt binders (Hintz et al., 2011). This test evaluates the ability of an asphalt binder to resist damage by employing cyclic loading at increasing amplitudes to accelerate damage. LAS tests are conducted in the DSR on rolling thin film oven (RTFO) plus pressure aging vessel (PAV)-aged binder specimens using the standard 8-mm parallel plate geometry with a 2-mm gap setting. The testing procedure includes 1) a frequency sweep, i.e., 100 cycles of sinusoidal loading at 0.1%, to obtain undamaged material properties and 2) an amplitude sweep, consisting of a total of 3,100 cycles of loads at systematically linearly increasing strain amplitudes from 0 to 30%, to accelerate the rate of damage accumulation. Note that the initial strain range in the LAS procedure was from 0 to 20%, which later was modified by Hintz et al. (2011) because significant material degradation of certain binders, e.g., PMA binders, is only achieved for strain levels above 20%. During the test, peak shear strain and peak shear stress are recorded every 10 load cycles, along with phase angle (δ, degrees) and dynamic shear modulus ($|G^*|$, Pa).

LAS testing results can be analyzed by using viscoelastic continuum damage (VECD) theory, which has been used extensively to model the complex fatigue behavior of asphalt mixtures. Application of VECD follows Schapery's theory of work potential to model damage growth (Equation 1).

$$\frac{dD}{dt} = \left(\frac{\partial W}{\partial D}\right)^{\alpha} \qquad (1)$$

where, t is time, W is work performed, D is damage intensity, and α is material constant related to rate at which damage progresses.

Quantification of work performed using dissipated energy follows work by Kim et al. (2006) (Equation 2). Equation 2 can then be substituted in Equation 1 and numerically integrated to determine damage intensity (D) (Equation 3).

$$W = \pi \cdot \gamma_0^2 \cdot |G^*| \sin\delta \qquad (2)$$

where, W is dissipated energy, γ_0 is shear strain, G^* is complex modulus and δ is phase angle.

$$D(t) = \sum_{i=1}^{N} [\pi \cdot I_D \cdot (|G^*|\sin\delta_{i-1} - |G^*|\sin\delta_i)]^{\frac{\alpha}{1+\alpha}} (t_i - t_{i-1})^{\frac{1}{1+\alpha}} \qquad (3)$$

where, I_D is the initial undamaged value of $|G^*|$.

As shown in Figure 2-5, Johnson and Bahia proposed using $|G^*|\cdot\sin\delta$ as the material integrity parameter and a power law to model $|G^*|\cdot\sin\delta$ versus damage (Equation 4). Equation 1 can be integrated to obtain a closed-form relation between number of

cycles to failure (N_f) and strain amplitude for a defined failure criterion (Equation 5 and Equation 6 which is a simplified version for Equation 5).
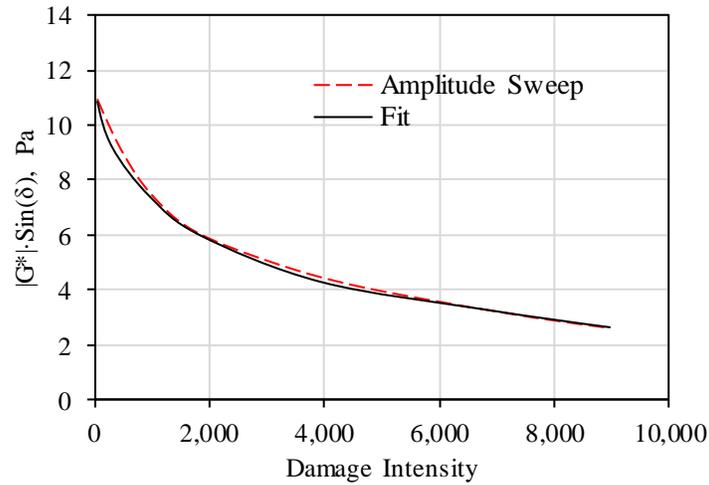
Figure 2-5. Binder $|G^*|\cdot\sin(\delta)$ versus damage plot with fitted curve (AASHTO TP 101-14)

$$|G^*|\sin\delta = C_0 - C_1(D)^{C_1} \tag{4}$$

where, C_0, C_1, and C_2 are model coefficients.

$$N_f = \frac{f(D_f)^k}{k(\pi\frac{I_D}{|G^*|}C_1C_2)^\alpha}|G^*|^{-\alpha}(\gamma_{max})^{-2\alpha} \tag{5}$$

where, k equals to $1+(1-C_2)\cdot\alpha$, f is loading frequency (Hz), $|G^*|$ is undamaged complex shear modulus, and D_f is damage accumulation at failure.

The advantage of using VECD is that results from a single test performed at a specific set of conditions can be used to predict the behavior of that material under any variety of alternative conditions (Figure 2-6).

$$N_f = A(\gamma_{max})^B \tag{6}$$

where, A equals to $\frac{f(D_f)^k}{k(\pi\frac{I_D}{|G^*|}C_1C_2)^\alpha}|G^*|^{-\alpha}$, and B equals to -2α.

While the LAS test is promising, the fatigue failure of asphalt binder where no catastrophic failure or fracture can be observed, is still not well-defined. In the work by Johnson (2010), the damage accumulation at failure (i.e., D_f in Equation 5) to be used in the VECD model is linked to a 35% reduction in undamaged $|G^*|\cdot\sin(\delta)$. This follows the traditional definition of fatigue failure in asphalt mixture (i.e., 50% reduction in initial stiffness/pseudo-stiffness), which is an arbitrarily selected criterion without theoretical or

phenomenological justification. In AASHTO TP 101-R16, damage accumulation at failure (D_f) is defined as the level of damage calculated by using $|G^*| \cdot \sin(\delta)$ value that corresponds to the peak shear stress on a shear stress versus shear strain curve (Figure 2-7). As damage accumulates, the materials no longer require a higher shear stress to maintain or increase the shear strain, indicating that a significant change in the material integrity occurs and the sample reaches fatigue failure. Wang et al. (2015) pointed out that peak stress should be regarded as the yield threshold of the material under increasing loading and the peak in phase angle, which normally occurs in the tests after the material yielded, should be used to define the ultimate failure or damage tolerance. However, the phase angle is not included in the VECD model framework and thus, the phase angle-based failure definition can only be used for determining the failure cycle from experimental data but not for further predictions.
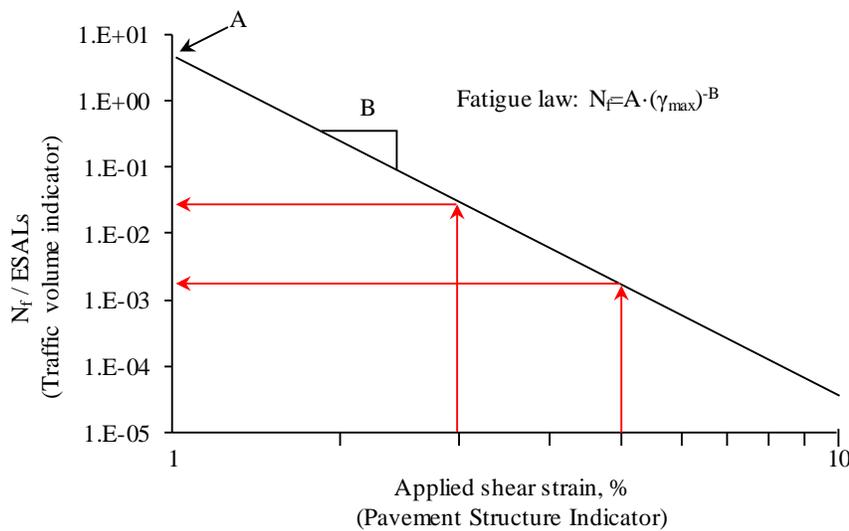
Figure 2-6. Traffic volume indicator (N_f) versus applied binder shear strain on a log-log scale (AASHTO TP 101-14)
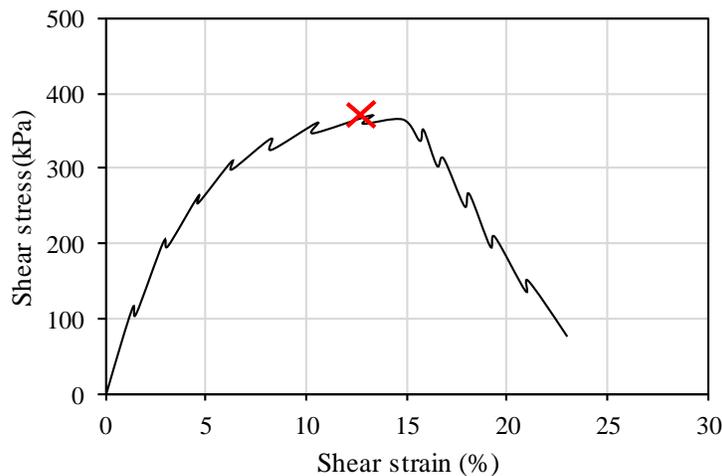
Figure 2-7. Illustration of stress-strain curve from the LAS amplitude sweep test

10

Wang et al. (2015) analyzed the LAS testing results in the pseudo-strain domain and eliminated the time-dependent effect of viscoelasticity (i.e., delayed elastic energy) from damage-associated energy by replacing physical strain with equivalent pseudo-strain. Moreover, the phase angle was excluded from the analysis. This simplifies the elliptical hysteresis loop in the stress-pseudo-strain space to a straight line, which represents the pseudo stiffness. Figure 2-8 shows the simplified pseudo-hysteresis loops representing the damage evolution in LAS tests. The undamaged line serves as a reference indicating the response of undamaged binder sample. As loading progresses, damage occurs in the specimen, resulting in the damaged line with reduced stiffness.

The area under the undamaged line represents the total pseudo-strain energy (PSE). For a given loading cycle, the total PSE can be separated into two parts: the released PSE (i.e., area with red lines) of the specimen due to damage and the stored PSE (i.e., area with black lines). When plotting the calculated stored PSE and released PSE for the entire LAS testing, there appears to be a maximum stored PSE, as shown in Figure 2-9. A peak in stored PSE indicates that failure has occurred because the material has lost its ability to store more PSE with increased input strain. Thus, the maximum stored PSE is selected as an energy-based failure criterion, and the corresponding number of cycles to failure (N_f) is reported as the indicator of the binder fatigue life. Wang et al. (2015) reported that the binder N_f, as determined by using the maximum stored PSE criterion with the LAS tests and by using the phase angle drop criterion with the TS tests, was comparable (Figure 2-10). They concluded that the maximum stored PSE is a reliable measure for defining binder fatigue life.
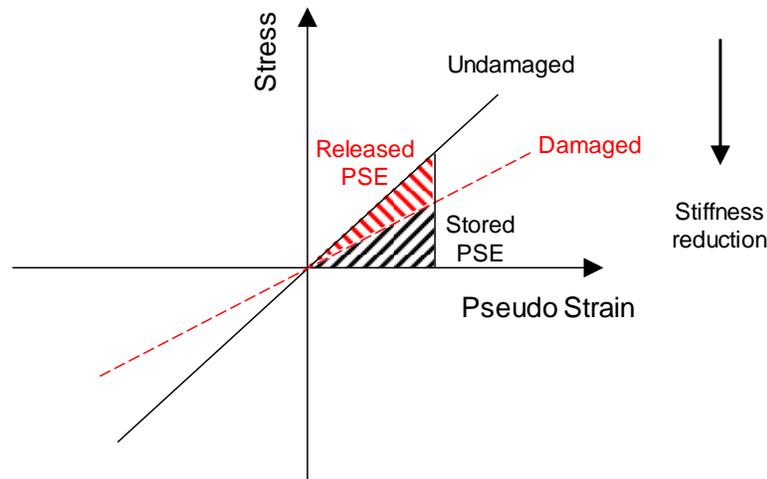
Figure 2-8. Schematic representation of undamaged and damaged lines (Wang et al. 2015)
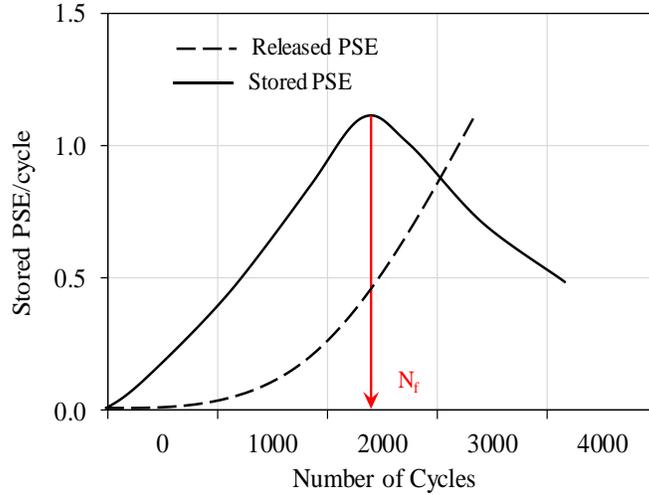
Figure 2-9. Illustration of the stored PSE failure definition for LAS testing results (Wang et al. 2015)
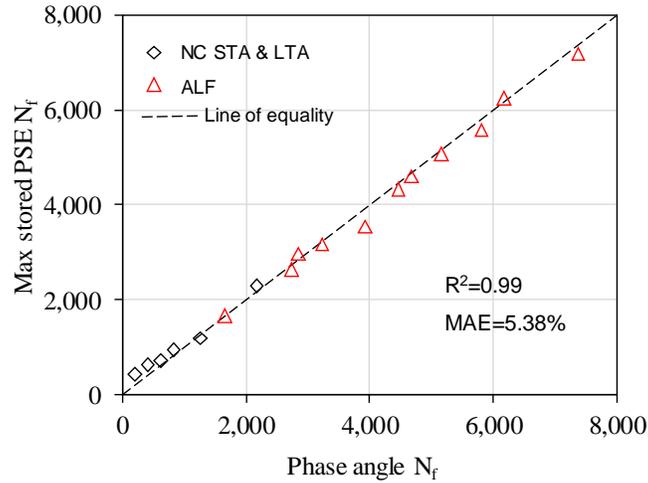
Figure 2-10. Fatigue life based on phase angle drop and maximum stored PSE criterion (Wang et al. 2015)

Zhang et al. (2013) evaluated the evolution of total released PSE of asphalt mixtures and identified a significant stable region where the rate of total released PSE, i.e., the slope of the total release PSE versus load cycles curve, is almost constant. Based on this observation, they proposed that the stable rate of total released PSE, entitled G^R, can be used to characterize the overall rate of energy loss during the fatigue test. Given that the total released PSE is calculated based on stiffness reduction, which is related to damage, the G^R parameter can also be used as the steady rate of damage accumulation. Sabouri and Kim (2014) modified the definition of G^R from "stable rate" to "average rate" and showed that there is a unique relationship between the average G^R and N_f that is independent of temperature and loading history for a given mixture tested under cyclic

uniaxial tension. The average G^R can be determined by using the averaged total released PSE divided by the number of cycles until failure (Equation 7).

$$G^R = \frac{\overline{W_r^R}}{N_f} = \frac{A/N_f}{N_f} = \frac{A}{(N_f)^2} \qquad (7)$$

where, G^R is average rate of total released PSE; $\overline{W_r^R}$ is average total released PSE; A is the area under the released PSE curve (Figure 2-9); and N_f is the fatigue life.

Wang et al. (2015) evaluated the feasibility of applying the G^R approach to analyze the TS and LAS binder testing results. They reported that the relationship between the average G^R and fatigue life (N_f) of a given binder is also independent of loading history, indicating that this relationship is fundamental. Figure 2-11 illustrates the relationship between G^R and N_f as determined based on binder testing results from different loading conditions, i.e., TS tests at different loading levels and LAS tests at different constant strain-amplitude rates. Moreover, they recommended that the relationship between G^R and N_f can be obtained by performing the LAS tests on the same binder sample at different constant strain-amplitude rates. Finally, this characteristic relationship can be incorporated into the S-VECD model by fitting a power law model between G^R and N_f, which allows for prediction of N_f at any strain amplitude.
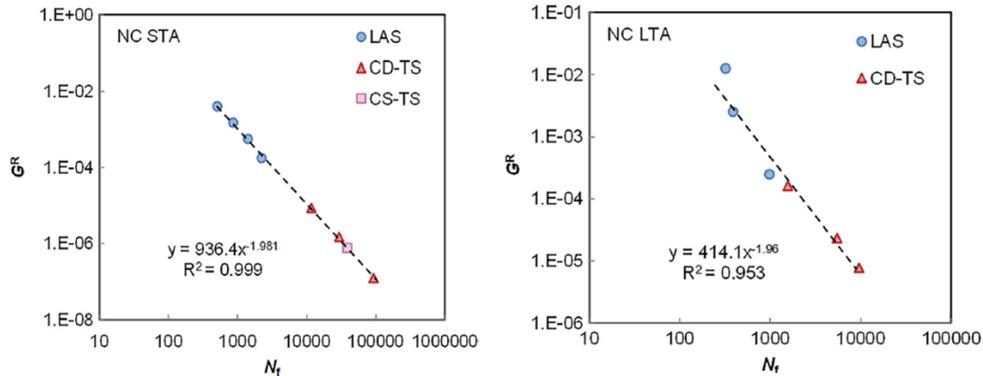
Figure 2-11. Correlation between G^R and N_f: (a) short-term aged; (b) long-term aged binders

2.3 Fracture Properties-Related Binder Tests

2.3.1 Edge fracture under torsion

Edge fracture refers to a circumferential crack forming at the periphery of a sample and propagating inward as loading is applied, effectively reducing the sample size (Aboutorabi, Ebbot and Gent., 1998). Figure 2-12 conceptually shows the edge fracture of a damaged DSR sample, where r_i is the initial sample radius, a is the crack length, and r is the radius of the intact portion of the sample. Anderson et al. (2001) attributed edge fracture in DSR testing of asphalt binders to "edge flow" caused by normal stresses.

However, Hintz et al. (2011) demonstrated that normal stresses were negligible compared with the torsional stresses, which rules out the flow instability as a cause of damage. Hintz and Bahia (2013a) compared the fracture morphology and trends in crack growth of the DSR binder samples with other materials (i.e., steel, rubber, and elastomers) under similar loading conditions (i.e., torsional fatigue loading). They concluded that edge crack, rather than changes in viscoelastic properties, results in changes in the load-carrying capacity during fatigue testing of asphalt binders in the DSR.
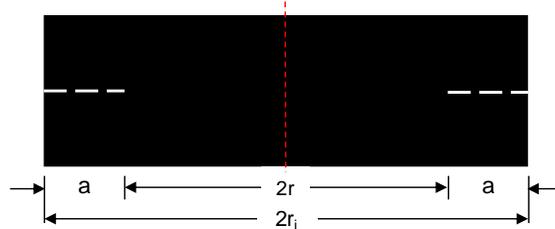
Figure 2-12. Schematic illustration of edge fracture in a DSR sample (Hintz and Bahia., 2013a)

Based on torsion prediction of crack length of DSR specimen, Hintz and Bahia (2013a) correlated the crack growth rate (da/dN) and the energy release rate (G_f) with crack length of binder samples. As shown in Figure 2-13, there appears to be two distinct stages of crack propagation: an increase in crack growth rate with crack length (i.e., shallow crack growth) followed by a decrease in crack growth rate (i.e., deep crack growth). Two explanations were provided regarding why crack growth rate decreases with increased crack length, including 1) energy for crack growth is derived from interior of the specimen, whose size keeps decreasing with increased crack length and 2) interaction between fractured surfaces increase as the crack becomes deep. Hintz and Bahia (2013a) proposed a fracture mechanics-based analysis framework for binder fatigue characterization and linked fatigue failure to the peak in energy release rate (G_f) and crack growth rate (da/dN), both of which occur at the same crack length corresponding to the transition from shallow to deep crack growth (Figure 2-14).
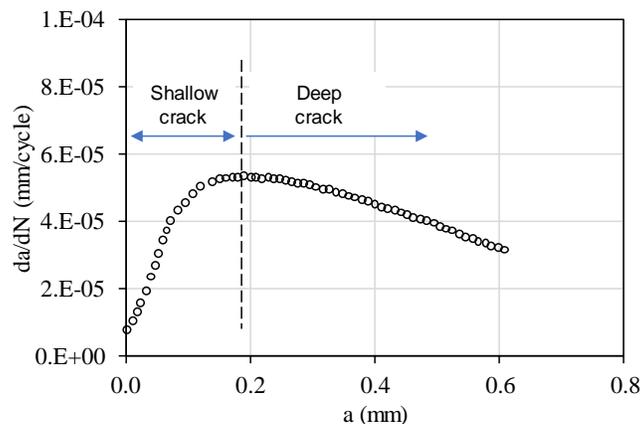
Figure 2-13. Crack growth rate versus crack length for a typical TS test (Hintz and Bahia., 2013a)
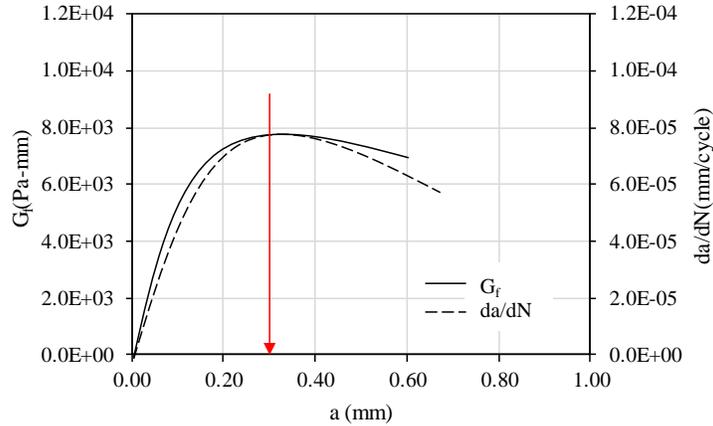
Figure 2-14. Failure definition based on energy release rate (G_f) and crack growth rate (da/dN) (Hintz and Bahia., 2013a)

Hintz and Bahia (2013b) further analyzed the binder crack growth rate as a function of crack length using LAS testing results. The crack growth rate was found to decrease within each strain step and jump abruptly between consecutive strain level (Figure 2-15). This observation was attributed to the loading method of the LAS amplitude sweep procedure, i.e., a linearly increased strain rate ranging from 0 to 30% at an interval of 1% and 100 cycles at each strain level. Since the LAS test does not allow for the determination of stable crack growth, the researchers recommended this test be used as a damage tolerance test rather than a fatigue test.
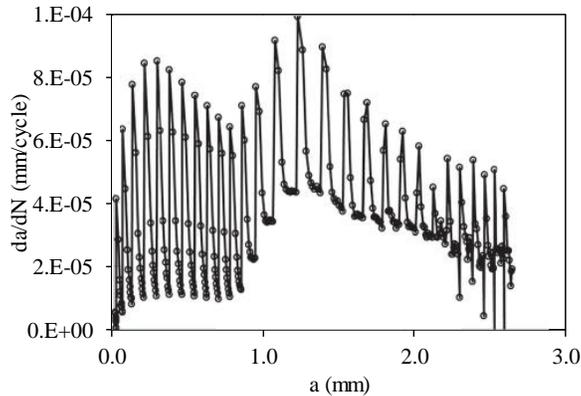
Figure 2-15. Crack growth rate versus crack length for a typical LAS test (Hintz and Bahia., 2013b)

In addition, Hintz and Bahia (2013b) modified the LAS amplitude sweep from a stepwise amplitude sweep to a continuously increased loading function, i.e., an increase of 0.1% strain every second for a total of 300 seconds. This change resulted in a smooth curve of crack growth rate versus crack length (Figure 2-16). The researchers proposed the crack length at failure (a_f), which corresponds to the crack length at the local minimum in crack growth rate, as a parameter to rank materials' relative damage tolerance. Effectiveness of the modified LAS failure criterion was validated by a good

correlation between the a_f results with the N_f results obtained from the TS tests (Figure 2-17). Of note, the TS test used the transition point from shallow to deep crack to define fatigue failure.
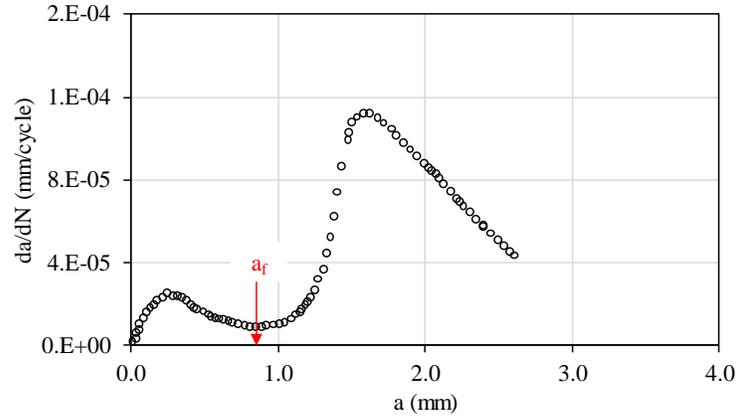
Figure 2-16. Crack growth rate versus crack length for modified LAS test (Hintz and Bahia., 2013b)
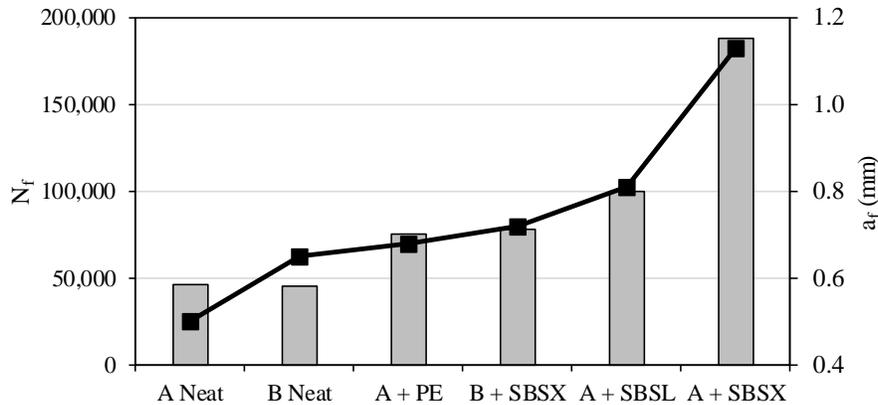
Figure 2-17. Correlation between a_f from modified LAS tests and N_f from TS tests (Hintz and Bahia., 2013b)

2.3.2 Double edge notched tension test

Andriescu et al. (2004) developed a double-edge notched tension (DENT) test to fracture ductile binders at intermediate temperatures (Figure 2-18). Data analysis of the DENT test followed the essential work of fracture method to separate the total energy into essential work (i.e., the work necessary for progression of fracture) and plastic work (i.e., the work necessary for plastic deformation before fracture). The essential work divided by the tensile yield stress gives an approximate critical crack tip opening displacement (CTOD), which is specified as a measure of binder strain tolerance in the ductile state (AASHTO T113-2015). Gibson et al. (2012) found that the CTOD parameter correlated well with FHWA-ALF mixture fatigue test results. However, they also pointed

out that the required number of replications and the scatter in the analysis as major drawbacks of the DENT tests.

Figure 2-18. DENT samples placed on loading pins (AASHTO TP113-2015)

Zhou et al. (2013) evaluated five different binder parameters/tests, including the G*sinδ, DENT test, the multiple stress creep recovery (MSCR) test, the elastic recovery (ER) test, and the LAS test, for characterizing fatigue performance of asphalt binders. They compared the results of binder tests with mixture push-pull tests and reported that 1) none of the G*sinδ, MSCR or LAS results showed a good correlation with mixture results and 2) the DENT and ER tests provided the same binder ranking, which is also in agreement with the one based on mixture results. In the end, they recommended the use of DENT test for purpose of binder fatigue specification, because DENT test is more fundamental whereas the ER test is purely empirical. However, the authors of this report want to point out that the MSCR and ER tests are not even intended for use as a tool for evaluation of binder fatigue cracking performance, although ER interestingly resulted in the same ranking as the DENT test in Zhou et al. (2013) work. Of note, the ongoing NCHRP 9-59 project is researching the potential application of DENT test for binder fatigue specification.

2.3.3 Binder fracture energy test

Binder fracture energy density (FED), which is the energy density a binder can tolerate before fracture, is an important property related to binder fatigue resistance. However, measurement of binder FED at intermediate temperature was not available until the development of a binder fracture energy (BFE) test by Niu et al. (2014). The BFE specimen geometry was designed to introduce a sufficient stress concentration at the middle section of a specimen where fracture is expected (Figure 2-19). The BFE tests were performed at a constant displacement rate of 500 mm/min, during which, time, force, and displacement data are recorded. The measured force and displacement are then transformed to true stress and true strain in the central cross-sectional area of the specimen, where fracture occurs by accounting for the change in cross-sectional area during testing. The binder FED is calculated as the area under the true-stress and true-strain curve until the stress peak (Figure 2-20).
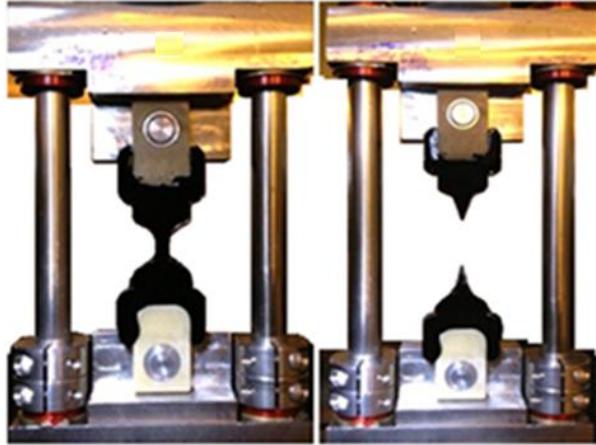
Figure 2-19. BFE specimen: (a) before fracture; (b) after fracture
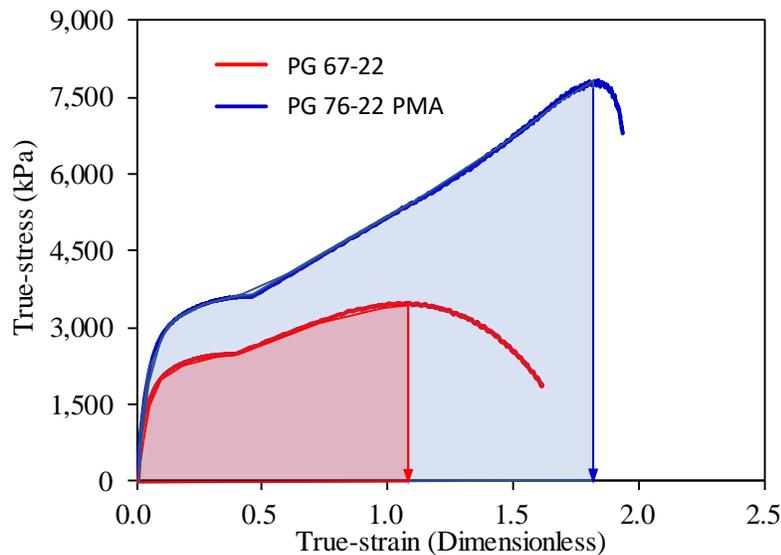
Figure 2-20. True stress-true strain curves for PG 67-22 and PG 76-22 PMA binders

Binder FED was found to be a fundamental material property, independent of testing temperature and loading rate (Figure 2-21), as opposed to other binder properties such as stiffness, failure stress, and failure strain. Moreover, the BFE test successfully differentiated elastomeric polymer-modified binders (i.e., SBS plus polypropylene composite and SBS plus oxidized polyethylene wax) from non-elastomeric polymer-modified binders (i.e., polyphosphoric acid) (Yan et al. 2015, 2016). Recent work by Yan et al. (2017) showed FED translated well from binder to mixture such that binders with higher FED resulted in higher mixture FED values. With a provisional AASHTO standard (i.e., TP 127-17) available, the BFE test can now be used to provide valuable information in terms of binder failure limit. However, this test in its current form is not suitable for determination of damage rate, which is another important property that potentially dominates binder cracking performance. Details regarding the importance of considering both failure limit and damage rate are provided in section 2.4.3.

18
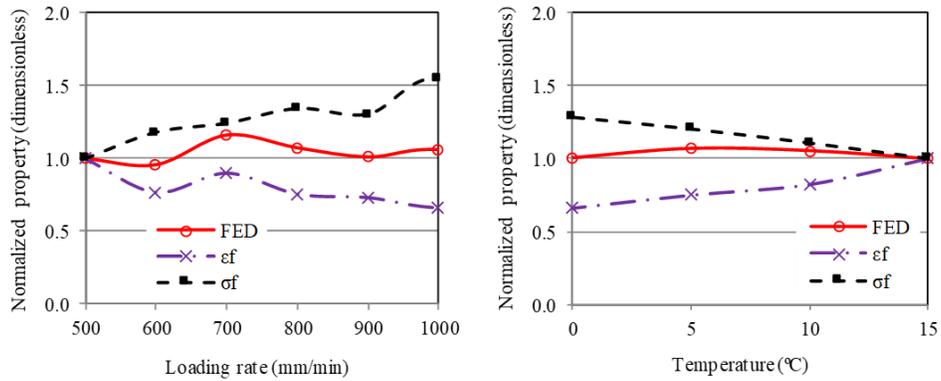
Figure 2-21. FED independence of (a) loading rate; (b) temperature (Yan et al., 2017)

2.4 Mixture Cracking Models

This section emphasizes mixture fatigue models since binder fatigue research has in many ways followed the developments in mixture fatigue research. The most common definition of fatigue failure that has been used in mixture fatigue model is a 50% reduction in initial modulus and the corresponding number of cycles to failure is denoted as N_{f50}. As previously mentioned, this definition of fatigue failure is an arbitrary assumption and does not accurately describe the damage capacity of asphalt mixtures.

The dissipated energy approach has shown great potential of providing a better definition of fatigue failure and giving a direct indication of damage accumulation or remaining life in asphalt mixtures. Asphalt binder is a viscoelastic material and it dissipates energy under mechanical work. When a load is initially applied to a mixture sample and then removed from it, the resulting stress and strain curves form a loop, called a hysteresis loop, and the area of the loop represents the dissipated energy in the load cycle (Figure 2-22). The following sections describe some of the models relevant to the dissipated energy concept, including dissipated energy ratio (DER), ratio of dissipated energy change (RDEC) and hot mix asphalt-fracture mechanics (HMA-FM) model. Of note, the VECD/S-VECD model and its applications were discussed in previous sections and were therefore, not included in this section.
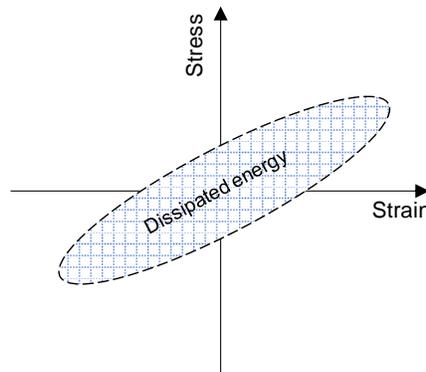
Figure 2-22. Illustration of stress-strain hysteresis loop of viscoelastic material

19

2.4.1 Dissipated energy ratio

In a mixture fatigue test, the stiffness decreases once the fatigue process starts and microcracks are induced in the material. Thus, the dissipated energy per loading cycle changes and usually increases for controlled stress tests and decreases for controlled strain tests. In general, there are two distinct stages in the mixture fatigue process: crack initiation and crack propagation. When fatigue damage goes from crack initiation to crack propagation, there is a significant change in the dissipated energy per loading cycle, which is independent of the mode of loading. Pronk (1995,1997) applied the rate-of-change in dissipated energy concept to define failure in mixture fatigue testing and proposed a parameter named dissipated energy ratio (DER) (Equation 8).

$$DER = \frac{\sum_{i=1}^{n} W_i}{W_n}$$

(8)

where, W_i is the dissipated energy at cycle i, and W_n is the dissipated energy at cycle n.

Bahia et al. (2001) applied the DER approach to characterize binder fatigue damage in a stress-controlled loading mode. As shown in Figure 2-23, the binder DER versus number of cycles curve can be divided into three stages: 1) the energy per cycle is dissipated in viscoelastic damping with negligible damage; 2) crack initiation starts and consumes an additional amount of energy beyond the viscoelastic damping; and 3) crack propagation begins with a noticeable increase in dissipated energy per cycle. Stage 3 is assumed to be the most critical one during which the healing and recovery is minimal due to the high rate of damage per cycle. A binder fatigue parameter, N_p, was proposed which refers to the number of loading cycles necessary for the binder to reach irrecoverable fatigue damage (stage 3). Bahia et al. (2001) pointed out that the DER approach is not useful for the controlled strain loading mode because it is almost impossible to clearly identify the inflection point corresponding to the transition point from stage 2 to stage 3.
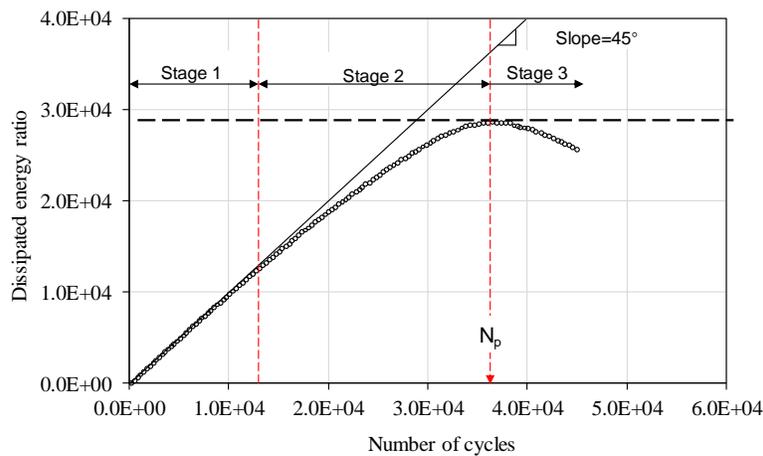
Figure 2-23. DER results of a stress-controlled TS test (Bahia et al. 2001)

2.4.2 Ratio of dissipated energy change

The definition of fatigue failure in the DER approach is based on total energy dissipated by the material during the fatigue test. However, the total dissipated energy can consist of energy dissipated in the form of mechanical work and heat generation, in addition to damage alone. Ghuzlan and Carpenter (2000) proposed a mixture fatigue parameter named ratio of dissipated energy change (RDEC). The RDEC parameter is determined based on a change in dissipated energy between load cycles (Equation 9), thus eliminating the energy dissipated due to mechanical work or heat generation and providing a truer indication of the damage being done to the mixture from one cycle to another.

$$\text{RDEC} = \frac{(DE_{n+1} - DE_n)}{DE_n} \qquad (9)$$

where RDEC is the ratio of dissipated energy change, DE_n is the dissipated energy produced in load cycle n, and DE_{n+1} is the dissipated energy produced in load cycle n+1.

During a mixture fatigue test, the damage curve represented by RDEC versus load cycles can be divided into three stages, as shown in Figure 2-24. Stage 1 starts with a high initial RDEC value, which then significantly decreases after a few load cycles. It can be hypothesized that a large portion of dissipated energy is being converted to damage as the mixture reorients itself to the repeated load applications. Stage 2, the plateau stage, tends to be lower and flatter, indicating that the mixture has developed a stable structure with relatively unchanged fatigue damage resistance. Stage 3 exhibits a rapidly increasing RDEC indicating more and more damage is occurring in the mixture. Failure is defined as the number of loading cycles (N_f) at which the change in the RDEC begins to increase dramatically. Moreover, the correlation between plateau value (PV) and the corresponding N_f appears to be independent of loading mode, indicating the PV is a more fundamental energy parameter to represent HMA fatigue behavior.
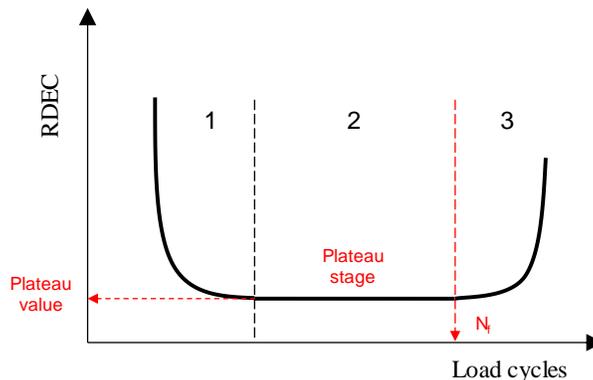
Figure 2-24. Illustration of RDEC versus load cycles curve with three distinctive stages under controlled stress loading mode (Carpenter et al. 2003)

Shen et al. (2006) employed the standard four-point bending beam test and evaluated the effectiveness of the RDEC parameter in assessing mixture fatigue behavior. They also reported that the RDEC parameter is applicable to asphalt binders and binder-filler mastics in terms of the fatigue characteristics. The relationship between PV and fatigue life (N_f) was found to be unique for asphalt mastic and asphalt mixtures. Most importantly, the PV and N_f curves of asphalt mastic and asphalt mixtures appear to be parallel with a shift between them, indicating the mixture fatigue behavior is strongly related to binder fatigue behavior (Figure 2-25). Shen et al. (2006) followed the traditional definition of fatigue failure (i.e., 50% reduction in initial stiffness) to determine fatigue life (N_f). This definition is debatable and has been challenged by Carpenter et al. (2003) as well as other researchers (Bahia et al., 2001; Wen and Bahia, 2009).
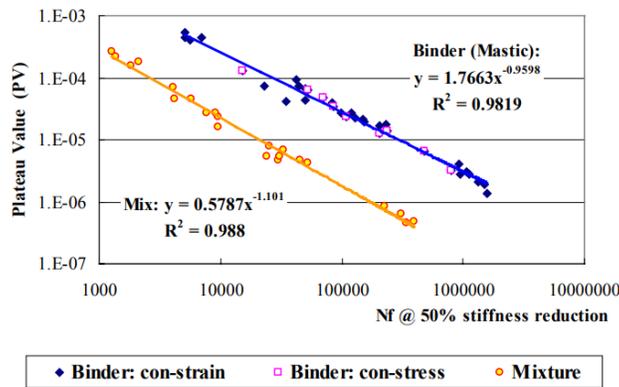
Figure 2-25. Plateau value versus load cycles to failure curves for asphalt binders, mastics, and mixtures (Shen et al., 2006)

2.4.3 Hot mix asphalt-fracture mechanics model

Roque and his co-workers (Zhang et al., 2001a, b; Roque et al., 2002) developed the HMA-FM model, which not only considers the failure limit of an asphalt mixture but also its rate of damage accumulation, to evaluate mixture cracking performance at intermediate temperatures. There are two types of mixture failure limit: dissipated creep strain energy limit ($DCSE_f$) or fracture energy density limit (FED_f), both of which have been identified as fundamental mixture properties, independent of mode of loading, rate of loading and specimen geometry (Birgisson et al., 2007). Failure limits can be determined from the stress-strain response of an asphalt mixture under the Superpave IDT fracture test: the FED_f is determined as the area under the stress-strain curve, while the $DCSE_f$ is the FED_f minus the elastic energy (EE) (Figure 2-26). The HMA-FM model assumes that damage can be quantified in terms of the viscous response (creep) of an asphalt mixture and therefore, the rate of damage accumulation, i.e., DCSE/cycle, is defined as the integral of the stress multiplied by the creep strain rate. For a repeated half-sine load consisting of a 0.1-s loading period followed by a 0.9-s rest period, the DCSE/cycle can be determined by using Equation 10.

$$DCSE/cycle = \frac{1}{20} \cdot \sigma \cdot CCR \qquad (\,10\,)$$

where, σ is the average stress and CCR is the viscous creep compliance rate, equals to the instantaneous slope of the compliance curve at 1,000 seconds obtained from the Superpave IDT creep compliance test.
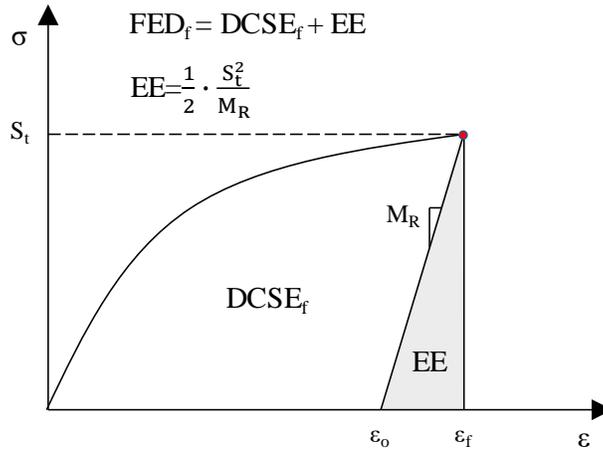
Figure 2-26. Determination of FED_f and $DCSE_f$ from a stress-strain diagram

Unlike traditional fatigue which assumes damage accumulates in a continuous manner, the HMA-FM model hypothesizes the distresses accumulate in a stepwise discontinuous way at an accelerated rate (Figure 2-27). A parameter named energy ratio, which was derived from the HMA-FM model, was determined to accurately distinguish between pavements that exhibited cracking and those did not, except for mixtures with excessively low or unusually high $DCSE_f$ (Roque et al., 2004). As part of NCHRP 01-42A, Roque et al. (2010) enhanced the HMA-FM model by including two submodels that account for aging and healing, both are known to have strong effects on mixture cracking performance. One output of the HMA-FM-E model is the crack initiation time, which has been shown to correlate well with field observations in Florida.
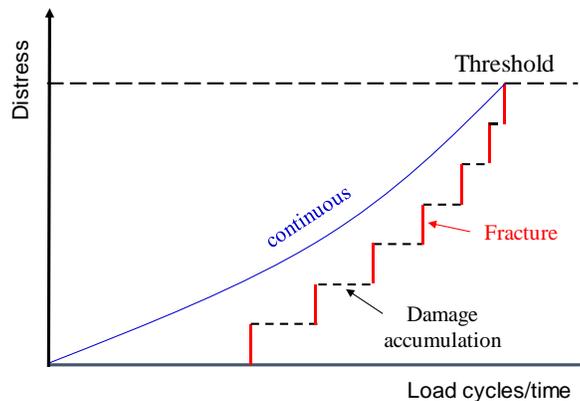
Figure 2-27. Stepwise discontinuous crack growth law used in the HMA-FM model

The HMA-FM model reveals the importance of considering both failure limit and damage rate as an entire system to predict cracking performance of asphalt mixtures. Thus, it seems logical that a binder parameter that is governed by the binder failure limit and damage rate is necessary to effectively characterize binder cracking performance. Whereas existing binder fatigue tests do not have a convincing definition of fatigue failure, the binder FED obtained from the BFE tests has been determined to be a fundamental failure limit of asphalt binder. Therefore, following the concepts presented in the HMA-FM model, it is anticipated that an energy-based binder cracking parameter can be identified by integrating binder FED value with binder damage rate whose determination was one objective of the current study.

2.5 Summary

Asphalt binder fatigue resistance plays a critical role in determining the fatigue life of asphalt pavements. However, the Superpave PG fatigue parameter (i.e., $G^*\sin\delta$) does not adequately characterize the binder fatigue resistance, especially for polymer-modified binders that have been widely used to enhance pavement performance. This report documented the most recent and well-documented binder testing methods as well as mixture models that have been or potentially can be used to more reliably evaluate binder cracking performance.

There is still a lack of accurate definition of fatigue failure in binder tests with DSR equipment, i.e., the TS and LAS tests. The conventional definition of fatigue failure, e.g., 50% reduction in initial modulus, has been challenged for a long time and studies have shown that binders with less than 50% residual modulus may have not reached their maximum damage capacity. Several alternative definitions have been proposed and according to these definitions, fatigue failure of asphalt binders is triggered by a dramatic change in binder response to load. This change has been referred to at the point where phase angle drops on a phase angle versus number of cycles curve, where stress peaks on a stress-strain curve, and where stored PSE peaks on a stored PSE versus number of cycles curve.

This chapter covered one application of fracture mechanics concepts and two binder fracture tests. The crack length at failure (a_f) parameter, which can be obtained from the edge crack growth rate versus crack length curve, correlates well with the TS N_f results. The DENT test applies the essential work of fracture method to separate essential and plastic work of fracture from the total work of fracture. The CTOD parameter, which is an indicator of binder strain tolerance at ductile state, also yield promising results in ranking binder fatigue performance. Because of its well-designed specimen geometry and data analysis procedure, the BFE test can be used to determine the binder FED, which is a measure of binder failure limit/fracture tolerance at intermediate temperatures.

Finally, three mixture parameters/models that involve dissipated energy were presented. The DER parameter describes the change in total dissipated energy between

loading cycles. The DER versus load cycle curve of binder exhibits an inflection point where microcracks are assumed to form into macrocracks. The RDEC parameter isolates the damage associated dissipated energy from the total dissipated energy and this parameter supposedly better captures the damage process than the DER parameter. The RDEC versus load cycle curves of binder results exhibit a relatively long stable stage yielding a parameter named plateau value (PV), which is recommended as an indicator of binder fatigue performance. The HMA-FM model emphasizes the importance of considering both failure limit and damage rate when evaluating mixture cracking performance. The HMA-FM model has successfully predicted field pavement performance. Since the mixture cracking performance is strongly affected by the asphalt binder, it seems logical to apply the concept of HMA-FM model to more accurately evaluate the binder cracking performance.

CHAPTER 3 IDENTIFICATION OF CANDIDATE TEST AND APPROACH

3.1 Introduction

The LAS test and the BFE test were selected as candidate tests: the former can introduce sufficient damage in binder specimens, whereas the latter accurately determines the binder failure limit at intermediate temperatures. Preliminary studies were performed to evaluate the LAS test and the BFE test following their AASHTO provisional standards. Based on these results, three approaches were presented and two were proposed for further development in this study: a recently revised LAS test with an energy-based definition of binder fatigue failure; and an alternative interpretation of the true stress-true strain curve of the BFE test. Note that binder damage rate obtained from the BFE test would be combined with the binder FED in a way that is analogous to the HMA-FM model. The derived binder parameter would be used to provide a complete assessment of binder relative cracking performance at intermediate temperatures.

3.2 Linear Amplitude Sweep Test

The LAS test uses cyclic loading with systematically increasing load amplitudes to accelerate the introduction of damage in binder specimens. The standardized LAS test has two main steps: 1) a frequency sweep is conducted as a fingerprint test to determine the undamaged material response of a binder sample and 2) a linearly oscillatory strain sweep is performed to measure the resistance of asphalt binder to fatigue damage. The testing temperature is the intermediate pavement temperature determined from the performance grade of the asphalt binder. Rolling thin film oven (RTFO) and pressure aging vessel (PAV) tests are conducted on virgin asphalt binders to simulate aging in production and during in-service life of asphalt mixtures, respectively. The LAS test now has an AASHTO provisional standard (TP 101), entitled *Estimating Fatigue Resistance of Asphalt Binders Using the Linear Amplitude Sweep*.

3.2.1 Frequency sweep test

Figure 3-1 shows the software setting of the standard rheometers available at State Materials Office (SMO) for the frequency sweep test. This test employs a constant strain of 0.1 percent (block 1) over a range of frequencies from 0.1 Hz to 30 Hz (block 2). The duration setting (block 3) recommended by the Modified Asphalt Research Center (MARC) resulted in invalid output data at frequencies lower than approximately 4.5 Hz (Table 3-1). After consulting a product specialist from the rheometer manufacturer, the duration setting was changed from "fixed meas. pt. duration" to "no time setting". This change allowed sufficient time for the rheometer to collect data. Table 3-2 presents the output data of the frequency test after changing the duration setting. Rheological properties, including complex modulus, phase angle and storage modulus, were successfully collected over the full range of frequency sweep.
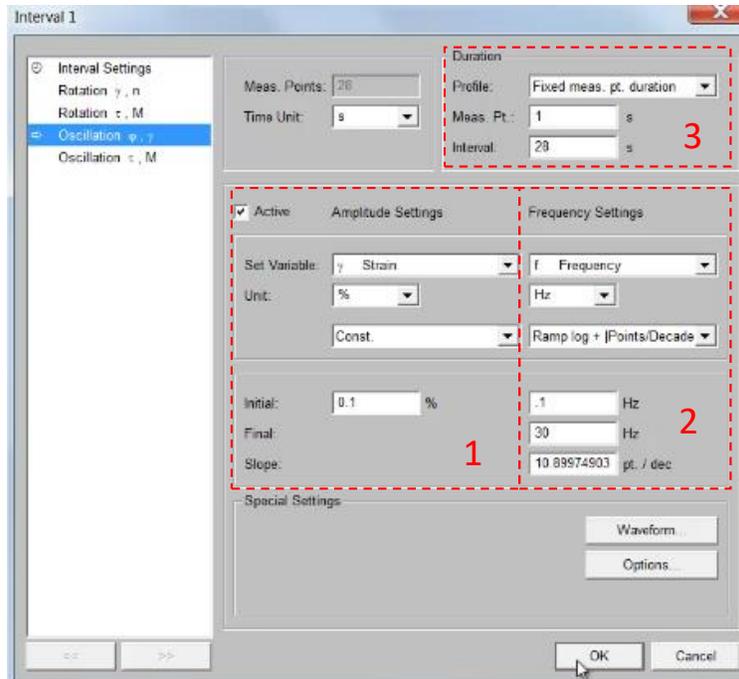
Figure 3-1. Software setting of the frequency sweep test

Table 3-1. Frequency sweep test output using the MARC duration setting

Meas. Pts.	Time	Frequency	Phase Angle	Complex Modulus	Storage Modulus
	[s]	[Hz]	[°]	[Pa]	[Pa]
1	invalid	—	—	—	—
Hidden content					
18	invalid	—	—	—	—
19	19	4.5	62.1	3.3E+06	1.6E+06
Hidden content					
28	28	30	50.3	1.5E+07	9.6E+06

Table 3-2. Frequency sweep test output using the modified duration setting

Meas. Pts.	Time	Frequency	Phase Angle	Complex Modulus	Storage Modulus
	[s]	[Hz]	[°]	[Pa]	[Pa]
1	1	0.1	50.2	2.8E+06	1.8E+06
Hidden content					
18	215	3.6	40.1	1.7E+07	1.3E+07
19	221	4.5	39.6	1.8E+07	1.4E+07
Hidden content					
28	283	30	35.5	3.7E+07	3.0E+07

3.2.2 Amplitude sweep test

Loading of the amplitude sweep test starts at a shear strain of 0.1% and proceeds in 1% strain increment until 30% strain is reached. This is achieved by setting 31 individual loading intervals of constant strain (e.g., 0.1%, 1%, 2% and so on). Figure 3-2 shows the software setting for the first interval, which applies a constant strain of 0.1% (block 1) at a constant frequency of 10 Hz (block 2). Each interval takes 10s and employs 100 load cycles. Peak shear strain and peak shear stress along with phase angle and dynamic shear modulus are recorded every 10 load cycles (1 s). Thus, the duration was set up to "fixed measuring point duration", which yields 1 measurement per second for a duration of 10s (block 3).
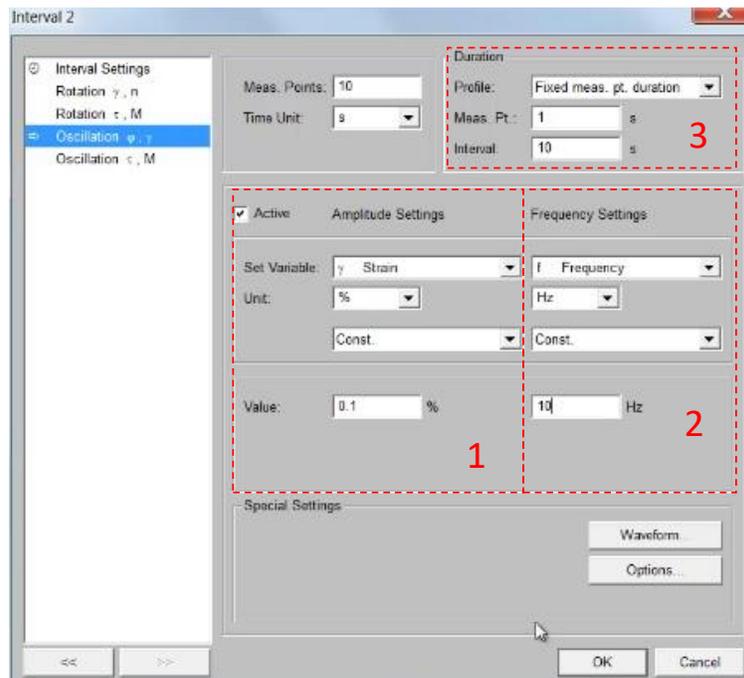
Figure 3-2. Software setting of the amplitude sweep test

The loading scheme of the amplitude sweep test in the AASHTO TP 101 has been changed. Figure 3-3 shows the loading scheme adopted in the original and the most recent versions of TP 101 published in 2012 and 2016. Hintz and Bahia (2013b) found that standard rheometers, as opposed to research rheometers, are incapable of instantaneously making abrupt adjustments (i.e., 1% strain increase between two intervals) in loading amplitude as is required in the LAS procedure. Therefore, the loading scheme of a linear ramp increasing at 0.1% per second to a maximum of 30% strain was employed in the TP 101(2014), as shown in Figure 3-4.
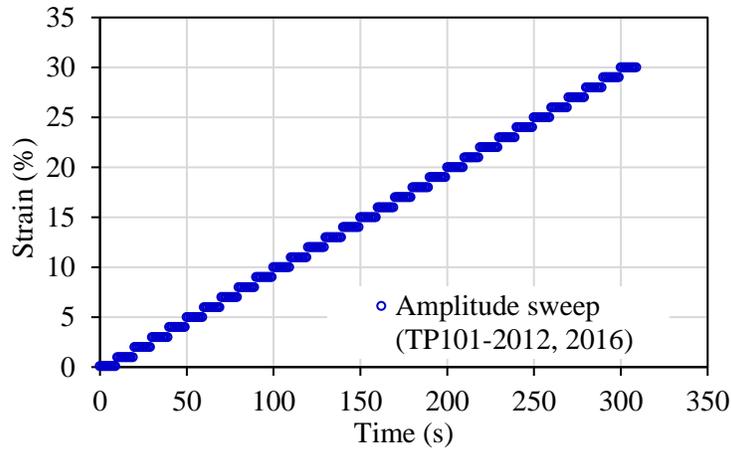
Figure 3-3. Stepped loading scheme for amplitude sweep test in TP 101-2012, 2016
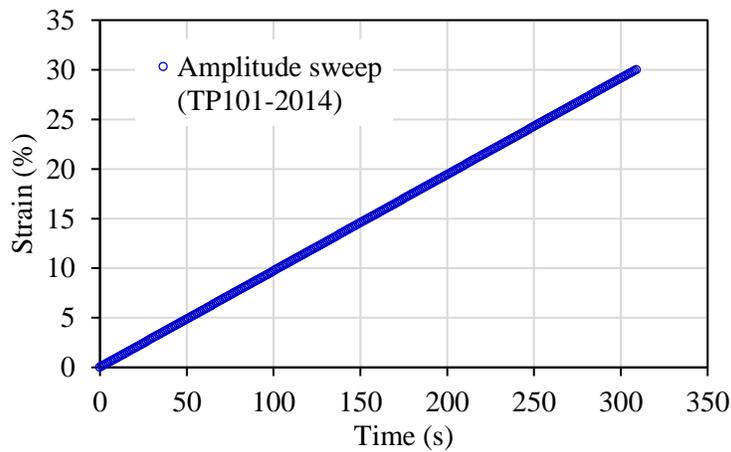
Figure 3-4. Continuous loading scheme for amplitude sweep test in TP 101-2014

3.2.3 Preliminary LAS testing results

The LAS tests were conducted on six different asphalt binders following the AASHTO TP 101(2016). Six binders commonly used in Florida were tested: PG 52-28, PG 58-28, PG 67-22, PG 76-22 Asphalt Rubber Binder (ARB), PG 76-22 Polymer-modified Asphalt (PMA) and heavily polymer-modified (HP) binder. The PG 76-22 ARB is a hybrid binder modified with a minimum of 7% rubber and an optional amount of SBS polymer. The HP binder contains approximately 7% SBS polymer.

Figure 3-5 shows the strain output of the amplitude sweep test performed on unmodified binders. The standard rheometer failed to provide precise control of strain during the amplitude sweep: a significant amount of strain values became erroneous at strain levels ranging from approximately 10% to 20%. The same observation was mentioned in a presentation by MARC who indicates this erratic trend can be eliminated by installing a software feature named direct strain oscillation (DSO) module (Hintz et al. 2011). Erroneous data output could also be associated with the fact that the assumption of

a constant geometry of DSR specimens becomes invalid once a crack is present (Hintz and Bahia, 2013b).
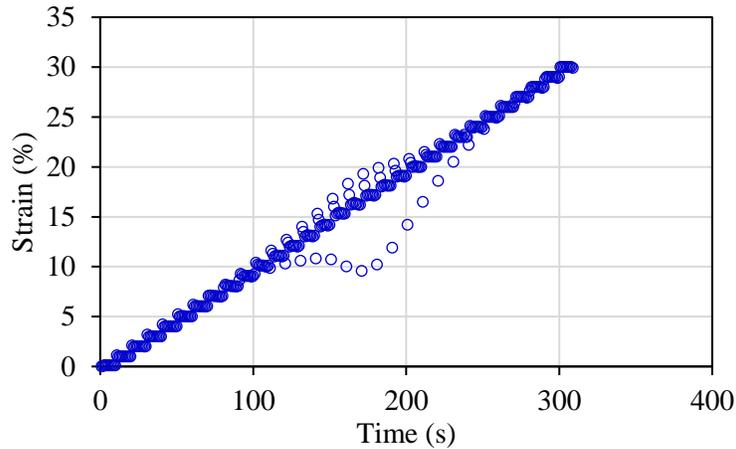
Figure 3-5. Strain output of amplitude sweep test conducted on unmodified binders

The PG 58-28 was used as an example of unmodified binders, and Figure 3-6 plotted the stress-strain curve. As expected, a significant amount of data points, which exhibits strain magnitudes that were unrealistically lower or higher than those within the same interval, was observed in the strain range of 10 to 20%. Consequently, the peak stress, which is the indicator of binder fatigue failure, could be mistakenly identified due to the presence of these outliers. Hintz et al. (2011) reported that a difference of about 8.5% in predicted binder fatigue parameter "A", which is an experimentally determined coefficient that is positively related to the predicted binder fatigue life, between rheometers with and without the DSO feature.
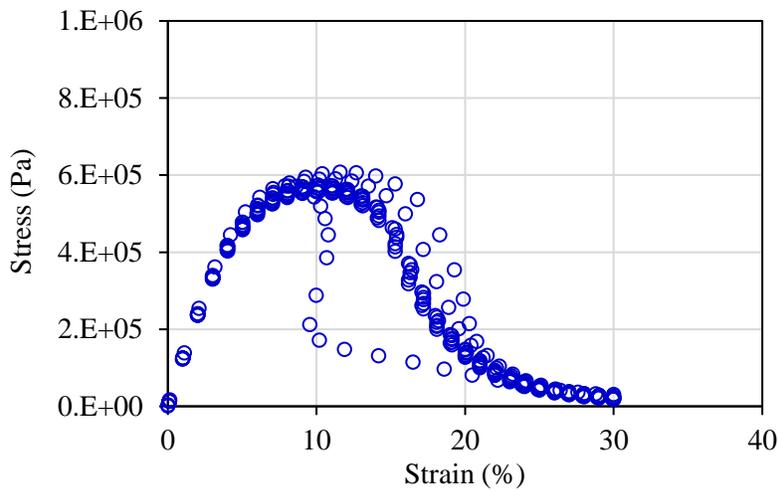
Figure 3-6. Stress versus strain curve of an unmodified binder: PG 58-28 binder

Figure 3-7 illustrates an example of strain output of the amplitude sweep test performed on modified binders. Errors were found to start at approximately 10% strain,

30

which is the same for unmodified binders, except that it continued until the end of loading. It appears that the presence of additives (e.g., polymer) made it more difficult for the standard DSRs to make quick and precise adjustments in the loading amplitude.
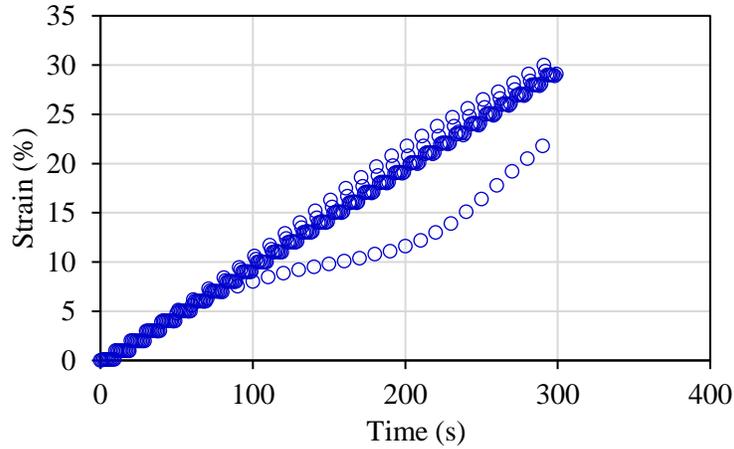
Figure 3-7. Strain output of amplitude sweep test conducted on modified binders

Figure 3-8 and Figure 3-9 show the stress-strain curves of the PG 76-22 PMA and HP binders, respectively. There appears to be a stress plateau where the relative change in stress is small and gradual as the strain increases, particularly for the HP binder. In this case, the standard rheometers (i.e., those without the DSO or a similar feature of accurate strain control) can easily result in greater than 8% error in fatigue life prediction of modified binders because the peak stress is used as the indicator of fatigue failure in the provisional standard. Regardless of these erroneous strain data points, the observation that modified binders exhibited a stress plateau instead of a clear stress peak raises a concern on the accuracy of the current binder failure definition.
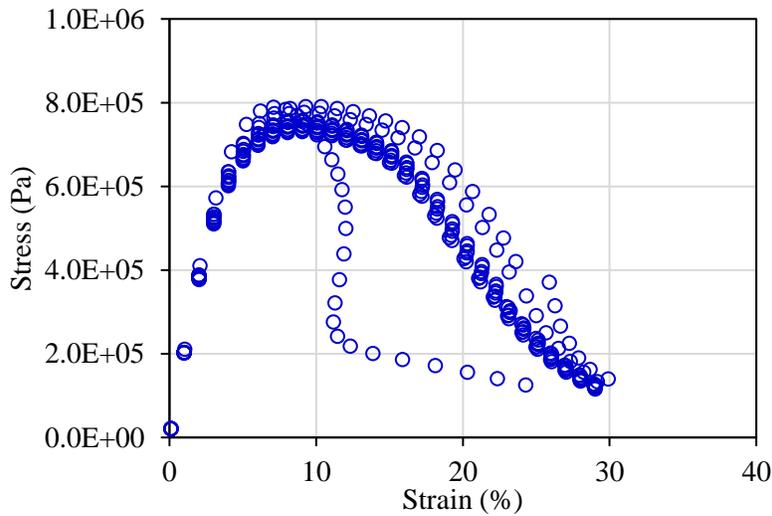
Figure 3-8. Stress-strain curve of the PG 76-22 PMA binder

31
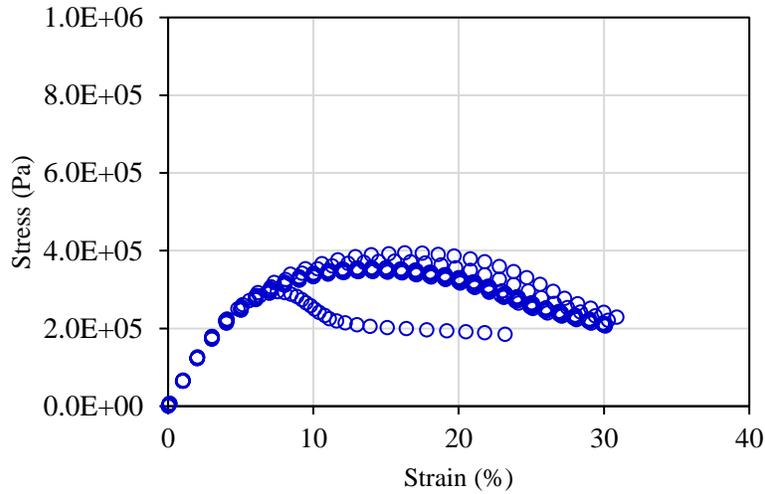
Figure 3-9. Stress-strain curve of the HP binder

Attempts were also made to apply a continuous loading scheme, which was employed in TP 101 (2014). Standard rheometers supposedly can make small, continuous adjustments in loading amplitude. However, two types of erratic trends in strain output were observed when employing the standard rheometers at SMO to apply a continuous amplitude sweep, as shown in Figure 3-10 and Figure 3-11. The former curve exhibits a concave upward direction at a strain level of approximately 15%, whereas a discontinuity at a similar strain level was observed for the latter.

After consulting a product specialist from the rheometer manufacturer, it appears that for purposes of performing the revised LAS tests, it is necessary to install a software feature named "TruStrain" on the standard rheometers at SMO. The "TruStrain", which is basically the same as the previously mentioned "DSO" module, would allow for precise strain control to match the target loading sequence.
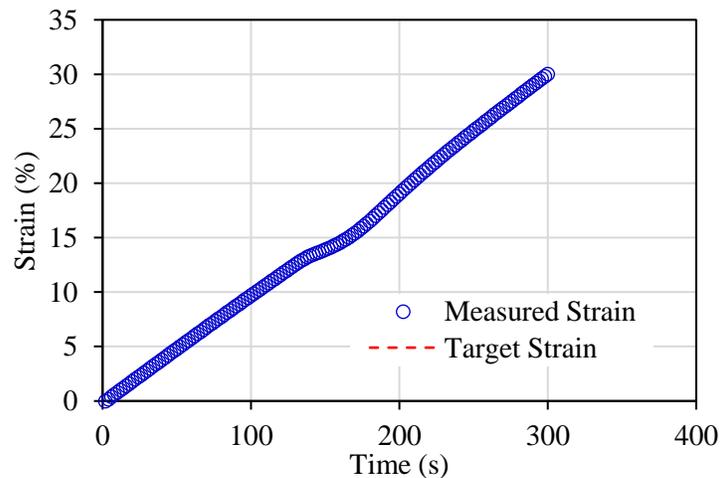
Figure 3-10. Erratic trend in actual loading scheme: a concavity
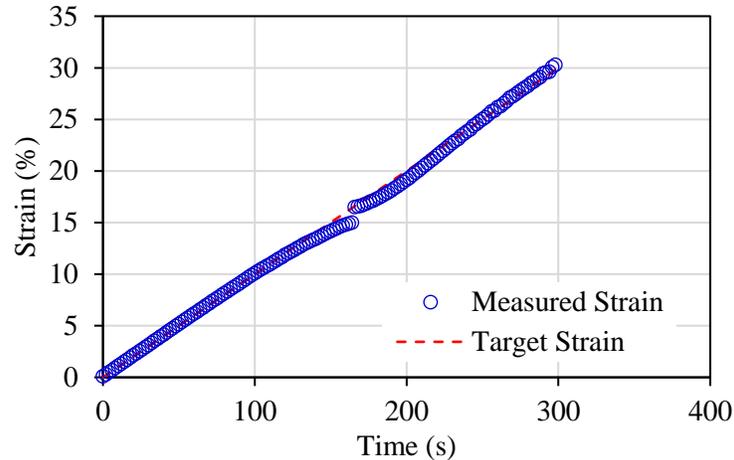
Figure 3-11. Erratic trend in actual loading scheme: a discontinuity

3.3 Binder Fracture Energy Test

The BFE test was developed to determine the binder failure limit (i.e., FED) at intermediate temperatures. This test employs a unique specimen geometry to introduce a sufficient stress concentration in the middle section of the specimen, where fracture is expected. This ensures accurate determination of stress and strain on the fracture plane, which in turn ensures accurate fracture energy density determination.

The BFE test is performed by pulling the upper loading head (the lower one remains fixed) at a constant displacement rate until fracture. Time, force, and displacement data are collected by the data acquisition system. The measured force and displacement are then transformed to true stress and true strain in the central cross-sectional area of the specimen where fracture occurs. The BFE test can be used to determine binder fracture energy density (FED) for any binder, including any neat binder, modified binders (e.g., rubber or polymer-modified), and asphalt binder extracted and recovered from pavement. This test now has an AASHTO provisional standard (TP 127), entitled *Standard Method of Test for Determining the Fracture Energy Density of Asphalt Binder Using the Binder Fracture Energy (BFE) Test.*

3.3.1 Fracture energy density

FED is defined as the energy per unit volume required to initiate fracture (i.e., local failure). Binder FED is calculated as the area under the true stress-true strain curve up to the stress peak. The post peak energy is not included in the determination of FED since it is used to split the specimen in half after local fracture initiates. True stress and true strain, which refer to the local stress and strain on the failure plane, can be determined based on global force and displacement using the data analysis procedure developed by Niu et al. (2014) and revised by Yan et al. (2017). FED describes the damage tolerance before material fractures, and in this study, the binder FED was used along with binder damage rate to provide a complete assessment of binder cracking performance at intermediate temperatures.

3.3.2 Preliminary BFE testing results

BFE tests were performed on the same six binder types previously evaluated using the LAS tests. Testing was performed at 500 mm/min and 15°C except for HP binder, which required 5°C for successful fracture. Three replicates of each binder type were tested, and all specimens were conditioned through the RTFO plus PAV protocol, which simulates long-term field aging.

Figure 3-12, Figure 3-13, and Figure 3-14 present the true stress-true strain curves of the PG 52-28, PG 58-28 and the PG 67-22 binders, respectively. Great consistency between the three replicates was observed for the three binder types. All binders exhibited one true peak stress with the peak strain close to 1.0, which is a unique characteristic specified in the TP 127-17 for unmodified binders. A reduction in stress at failure and an increase in strain at failure were observed as binder became softer, i.e., high PG grade decreased from 67 to 52°C.
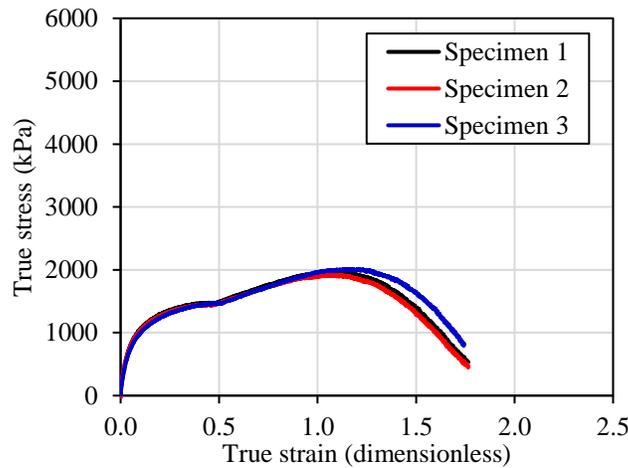
Figure 3-12. True stress-true strain curve of PG 52-28 binder
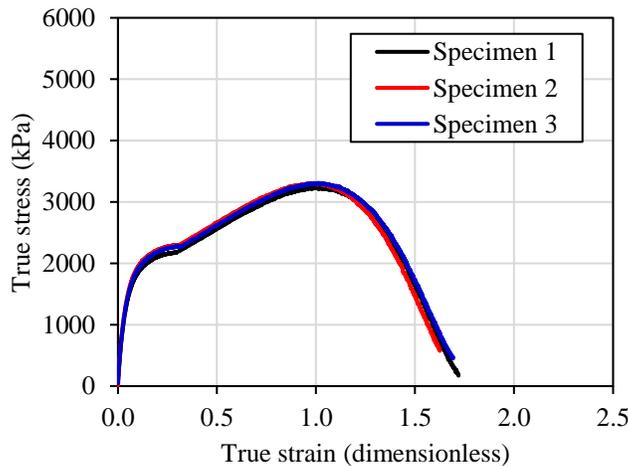
Figure 3-13. True stress-true strain curve of PG 58-28 binder
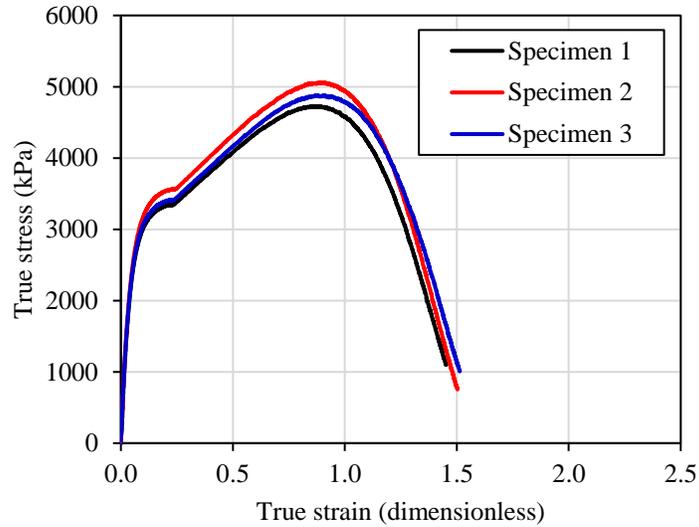
Figure 3-14. True stress-true strain curve of PG 67-22 binder

Figure 3-15, Figure 3-16 and Figure 3-17 present the true stress-true strain curves of the PG 76-22 ARB, the PG 76-22 PMA and the HP binders, respectively. Consistent results were obtained for the two binders modified with SBS polymer only (i.e., PG 76-22 PMA and HP). One specimen of PG 76-22 ARB binder, which is a hybrid binder containing a minimum of 7% rubber and an optional amount of SBS polymer, exhibited a notably higher peak stress than the other two specimens. This could be attributed to the presence of rubber that is not completely digested in the PG 76-22 ARB. This indicates that better mixing before pouring the specimens may be needed for future testing. All modified binders were characterized by a steady increase in true stress. Compared to unmodified binders, modified binders showed a higher stress and strain values at failure, particularly for the HP binder, which is contains approximately 7% SBS polymer.
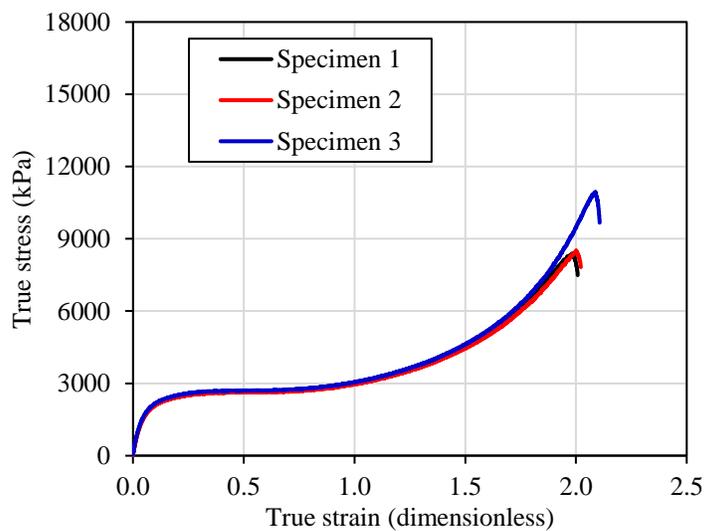
Figure 3-15. True stress-true strain curve of PG 76-22 ARB binder

35
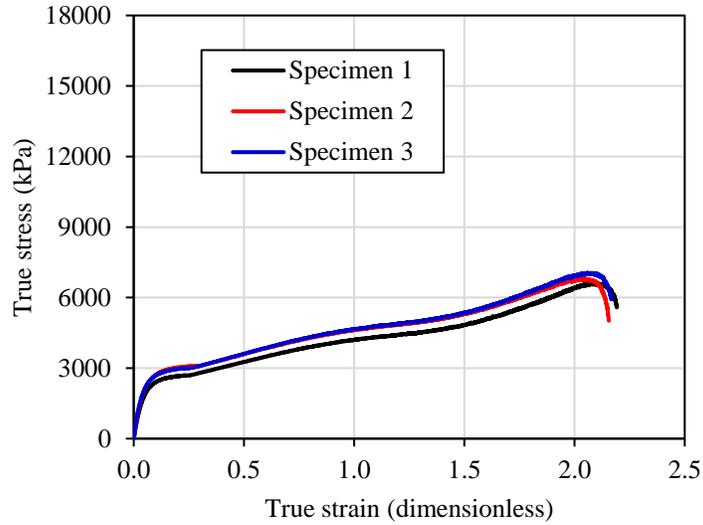
Figure 3-16. True stress-true strain curve of PG 76-22 PMA binder
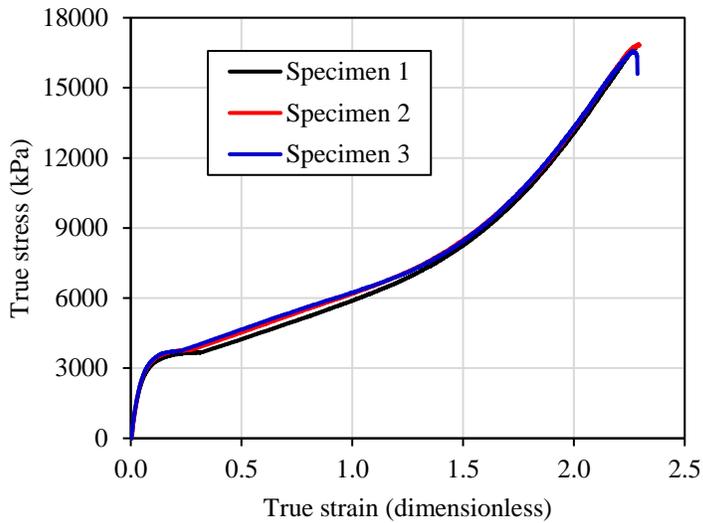
Figure 3-17. True stress-true strain curve of HP binder

Figure 3-18 summarizes binder FED values obtained as the average of three replicates. As the figure shows, FED quantitatively distinguished different binder types. Unmodified binders had lower FED values (below 4,000 kJ/m^3) than modified binders, and the PG 58-28 binder exhibited a lower FED than the PG 67-22 binder. The hybrid binder, (PG 76-22 ARB) had a FED value lower than that of the PG 76-22 PMA binder. The heavily polymer modified binder (HP) had the highest FED value, which exceeded 15,000 kJ/m^3. The average FED values obtained agreed with typical values recommended by the AASHTO TP 127-17.
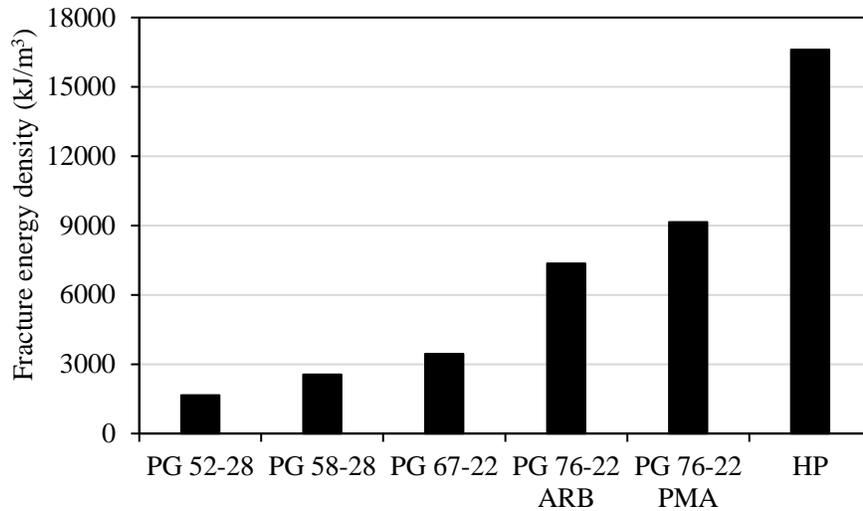
Figure 3-18. Average FED values of five asphalt binders obtained from the BFE tests

3.4 Candidate Approaches

Three proposals were identified and two of them were selected for further evaluation in this study. The first proposal is to adopt the LAS test recently revised by Wang et al. (2015, 2017) to evaluate binder fatigue cracking performance. More specifically, the revised LAS test employs an energy-based definition of binder fatigue failure, which supposedly is more fundamental than the failure definition in the TP 101. The second and third proposals were to obtain binder damage rate by using the BFE test with either an alternative interpretation of the true stress-true strain curve of the BFE test or a further developed version of the BFE test. Once the binder FED and damage rate were determined, a method analogous to the HMA-FM model was followed to integrate the two binder properties for a complete assessment on binder cracking performance. Details about these three proposals are presented as below.

3.4.1 Revised LAS Test

Wang et al. (2015) revised the standard LAS testing protocol and applied recent advances in the simplified viscoelastic continuum damage (S-VECD) modeling of asphalt mixtures to the LAS data analysis procedure. Table 2-3 summarizes the framework of the revised LAS test, which contains three material-dependent functions, in terms of linear viscoelasticity, damage property, and failure mechanism. Time-dependent effect of viscoelasticity (i.e., delayed elastic energy) can be separated from damage associated energy by replacing physical strain with equivalent pseudo strain. The revised LAS test is currently being evaluated by the ongoing NCHRP 9-59 project, *Relating Asphalt Binder Fatigue Properties to Asphalt Mixture Fatigue Performance*.

Table 3-3. Application of S-VECD in the revised LAS test

Material behaviors	Laboratory experiments	Material characteristics
Linear viscoelasticity in undamaged domain	Frequency sweep test	Dynamic modulus master curve Shift factors
Fatigue behavior in damaged domain	Amplitude sweep test	Damage characteristic curve Failure criterion

3.4.1.1 S-VECD model

VECD-based frameworks have been used extensively to characterize the complex behavior of asphalt mixtures (Kim and Little, 1990; Chehab et al., 2002; Underwood et al., 2006), and more recently have been applied to binders (Hintz et al., 2011). However, the VECD model was reported to have limited applications due to certain faults in the rigor of the theoretical application. Underwood et al. (2009a, 2009b and 2009c) proposed a more rigorously accurate simplified model (i.e., S-VECD) to address the deficiencies associated with VECD. Key aspects of the S-VECD modelling approach are presented below (i.e., Equations 11 to 19).

Damage evolution is based on Schapery's work potential theory (Schapery, 1984), which follows Equation 11 to define rate-dependent damage evolution rate.

$$\frac{dS}{dt} = (-\frac{\partial W^R}{\partial S})^\alpha \tag{11}$$

where, S is the internal state variable representing damage; W^R is the work performed; α is the undamaged material-dependent constant, determined by using Equation 12; and t is time.

$$\alpha = 1/m \tag{12}$$

where, m is the fitting slope parameter of the linear viscoelastic dynamic shear modulus ($|G^*|_{LVE}$) mastercurve.

The work performed (W^R) can be quantified using pseudo-strain energy (Equation 13).

$$W^R = \frac{1}{2} C(S)(\gamma^R)^2 \tag{13}$$

where, γ^R is pseudo-strain; $C(S)$ is pseudo-stiffness; determined by Equation 14:

$$C(S) = \frac{\tau_p}{\gamma_p^R \times DMR} \tag{14}$$

where, τ_p is the measured peak shear stress in a given cycle; γ_p^R is the peak pseudo-strain for that given cycle, which can be obtained following Equation 15; and DMR is dynamic modulus ratio, which is introduced to eliminate sample variability and can be determined using Equation 16.

$$\gamma_{pi}^R = \frac{1}{G_R}\gamma_{pi} \times |G^*|_{LVE} \tag{15}$$

where, γ_{pi} is the measured peak strain in the given cycle; γ_{pi}^R is the peak pseudo-strain for that given cycle; G_R is the arbitrary reference modulus, selected to be 1, which implies that the pseudo-strain is equivalent to the linear viscoelastic stress response to a given loading input; and $|G^*|_{LVE}$ is the linear viscoelastic dynamic shear modulus at a given temperature and loading frequency.

$$DMR = \frac{|G^*|_{fingerprint}}{|G^*|_{LVE}} \tag{16}$$

where, $|G^*|_{fingerprint}$ is obtained by subjecting the specimen to several cycles of loading within the linear viscoelastic range at small strain (e.g., 0.1%).

Equations 11 through 16 are combined, and Equation 6 is numerically integrated to solve for damage (S) as a function of time (Equation 17).

$$S = \sum_{i=1}^{N} \left[\frac{DMR}{2}(\gamma^R)^2(C_{j-1} - C_j)\right]^{(\frac{\alpha}{1+\alpha})} \left[(t_j - t_{j-1})\right]^{(\frac{1}{1+\alpha})} \tag{17}$$

where, j is the time steps.

Data collected from the fatigue test are used to calculate pseudo-stiffness ($C(S)$) and damage (S), which are then fitted in the function expressed in Equation 18. Figure 3-19 shows a comparison between actual data and the fitted results.

$$C = 1 - C_1(S)^{C_2} \tag{18}$$

where, C_1 and C_2 are the parameters that best fit the damage and pseudo-stiffness curve.
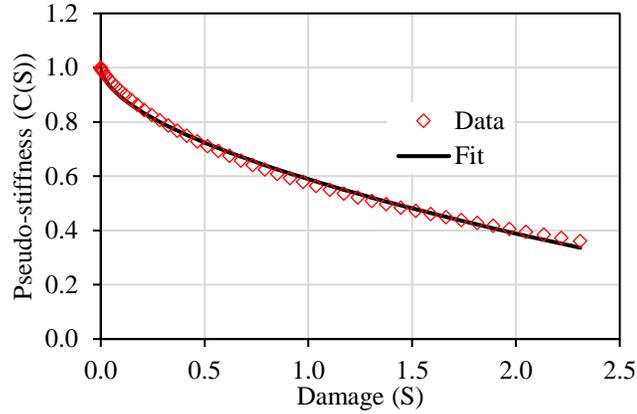
Figure 3-19. Damage characteristic curve of S-VECD binder fatigue modeling

Combining Equation 11, 13, 15 and 18 allows for the derivation of a model between loading cycles (N) and measured strain amplitude (γ_p) (Equation 14). Equation 19 can be used to predict fatigue life in terms of number of cycles to failure (N_f) at any strain amplitude by setting damage (S) to damage at failure (S_f).

$$N = \frac{f \cdot 2^\alpha \cdot S^{1-\alpha C_2 + \alpha}}{(1 - \alpha C_2 + \alpha)(C_1 C_2)^\alpha (|G^*|_{LVE} \cdot \gamma_p)^{2\alpha}} \tag{19}$$

where, f is the loading frequency and t is the loading time.

3.4.1.2 Failure definition

The definition of fatigue failure in the LAS test is a crucial component of binder fatigue performance evaluation and prediction. The peak stress on the stress-strain curve, which has been used as an indicator of failure in the current standard (i.e., TP 101-16), was recognized by Wang et al. (2015) only as a binder yielding threshold under increased loading. Alternatively, they introduced a failure analysis based on pseudo-strain energy (PSE) for the LAS test. Two types of failure definition were proposed for binder purchase specification and complete characterization of binder fatigue performance, respectively.

Binder purchase specification

According to Wang et al. (2015), the total PSE input (W^R_{total}) is the total amount of PSE that goes into the material, which can be separated into stored PSE (W^R_s), and released PSE (W^R_r). Equations 20, 21, and 22 were followed to determine the total PSE, stored PSE and released PSE, respectively.

$$W^R_{total} = \frac{1}{2} \cdot (\gamma^R_p)^2 \tag{20}$$

$$W_s^R = \frac{1}{2} \cdot C \cdot (\gamma_p^R)^2 \tag{21}$$

$$W_r^R = \frac{1}{2} \cdot (1 - C) \cdot (\gamma_p^R)^2 \tag{22}$$

where C is pseudo-stiffness and γ_p^R is the peak pseudo-strain for a given cycle.

Moreover, a parameter named stored PSE (W_s^R) was proposed, whose maximum value can be used to define failure and to determine corresponding binder fatigue life (number of cycles to failure, N_f), as shown in Figure 3-20. This definition is based on logical trends in energy evolution. An increasing W_s^R indicates that the material retains the ability to store additional energy as the loading amplitude (and hence energy input) increases in the LAS test. Conversely, a decrease in W_s^R indicates that the material is losing the ability to store PSE as the loading input increases, indicating that failure has occurred. Wang et al. (2015) reported that fatigue life (N_f) results of six different binders determined based on the maximum W_s^R are comparable to those based on the phase angle drop criterion, which has been used extensively in defining asphalt mixture fatigue failure.
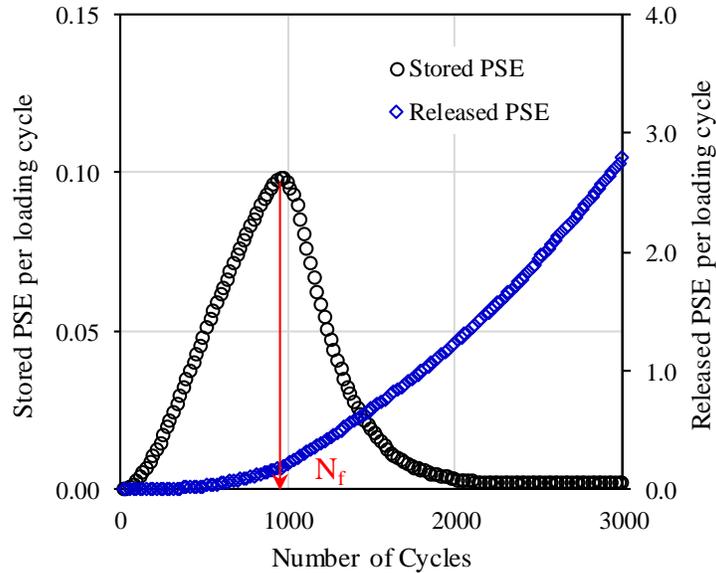
Figure 3-20. Pseudo-strain energy PSE-based failure analysis

<u>Full fatigue characterization of asphalt binder</u>

The relationship between averaged PSE release rate (G^R), which is the rate of change of the average released PSE per cycle, and the number of cycles to failure (N_f) was found to be unique, independent of loading history, as shown in Figure 3-21. This relationship can be derived by performing the LAS tests (i.e., amplitude sweep tests) at three amplitude-strain rates (0.1, 0.05 and 0.033 percent strain increase per second) on

three replicates of a given binder type. Equation 23 can be applied to determine the average PSE release rate (G^R).

$$G^R = \frac{\overline{W_r^R}}{N_f} = \frac{A/N_f}{N_f} = \frac{A}{(N_f)^2} \tag{23}$$

where, A is total released PSE, which is the area under the released PSE curve in Figure 3-20 and can be determined by using Equation 24; and N_f is the number of cycles to failure determined by the maximum stored PSE.

$$A = \int_0^{N_f} W_r^R \, dN$$

$$= \left[\frac{1}{2} \cdot C_1 \cdot (|G^*|_{LVE})^2 \cdot q^{\left(-\left(\frac{C_2}{p}\right)\right)} \cdot \frac{1}{\left(\frac{C_2}{p}\right)+1} \right] \cdot (\gamma)^{2+2\alpha\left(\frac{C_2}{p}\right)}(N_f)^{\left(\frac{C_2}{p}\right)+1}$$

$$= k \cdot (\gamma)^{2+2\alpha\left(\frac{C_2}{P}\right)}(N_f)^{\left(\frac{C_2}{P}\right)+1} \tag{24}$$

where, C_1 and C_2 are the parameters that best fit the data of damage and pseudo-stiffness (Equation 18), p, q, and k are combined constants expressed as:

$$p = 1 - \alpha \cdot C_2 + \alpha \tag{25}$$

$$q = \frac{f \cdot 2^\alpha}{(1-\alpha \cdot C_2+\alpha)(C_1 \cdot C_2)^\alpha(|G^*|_{LVE})^{2\alpha}} \tag{26}$$

$$k = \frac{1}{2} \cdot (|G^*|_{LVE})^2 \cdot q^{\left(-\left(\frac{C_2}{p}\right)\right)} \cdot \frac{1}{\left(\frac{C_2}{p}\right)+1} \tag{27}$$

where, α is the undamaged material-dependent constant (Equation 12), f is the loading frequency (10 Hz), $|G^*|_{LVE}$ is the linear viscoelastic dynamic shear modulus at a given temperature (e.g., 20°C).
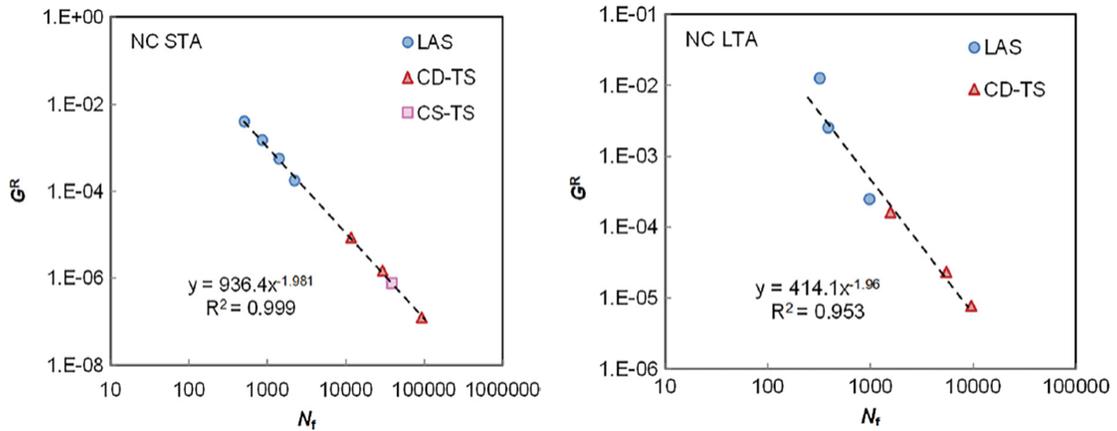
Figure 3-21. Correlation between G^R and N_f: (a) short-term aged; (b) long-term aged binders (Note: CD-TS refers to the time sweep test under displacement control, CS-TS is the time sweep test under stress control, and LAS stands for the linear amplitude sweep test)

The power law model is fit to the relationship between G^R and N_f, as shown in Equation 28. The G^R failure criterion is then incorporated into the S-VECD model, which enables predictions of binder fatigue life.

$$G^R = a \cdot (N_f)^b \tag{28}$$

Substituting Equation 24 into Equation 23, and then combining with Equation 28 derives the solution of N_f in terms of the applied shear strain (γ), as shown in Equation 29.

$$N_f = \left[\frac{k}{a} \cdot (\gamma)^{2+2\alpha\left(\frac{C_2}{p}\right)} \right]^{\left(\frac{1}{b+1-\left(\frac{C_2}{p}\right)}\right)} \tag{29}$$

Equation 29 can now be used to predict the fatigue cracking performance of asphalt binders at given applied shear strain (γ), which is a pavement structure indicator.

The DSR is one of the most commonly used binder testing devices and therefore, it is of great interest to determine whether the revised LAS test can be adopted to predict binder fatigue life. The PSE-based failure analysis, which is based on logical trends in energy evolution, improves the existing definition of fatigue failure in the LAS test. In the meantime, it must be emphasized that the S-VECD model, which was adopted to analyze the DSR collected binder properties, is not totally consistent with the physical phenomenon occurring during the LAS tests. More specifically, damage is not uniformly distributed in the DSR specimen and fracture manifests as an edge crack, which initiates at the periphery of the sample and propagates inward as loading cycles increase.

Evaluation of the revised LAS test focused on 1) investigating the correlation between binder FED as determined from the BFE test and the total released pseudo-strain energy obtained from the revised LAS test and 2) determining whether binder fatigue life (N_f) determined based on the revised LAS test is consistent with mixture fatigue life predicted by the HMA-FM model. Note that it may still be necessary to modify the data analysis procedure of the revised LAS test to obtain binder damage rate.

3.4.2 Further Developed BFE Test

In this section, two approaches were presented to use the BFE test to obtain binder damage rate. This included an alternative interpretation of the true stress-true strain curve of the BFE test and a further developed version of the BFE test to perform a creep test.

3.4.2.1 Alternative interpretation

The true stress-true strain curve has been used to determine the binder FED, which is the area under the curve until the stress peak. Also, the characteristics of the curve have been employed to differentiate between binders with and without additives (e.g., rubber and SBS polymer). The present goal was to derive a parameter (i.e., creep strain rate per unit stress) from the true stress-true strain curve to calculate the DCSE per cycle, which can be used to characterize damage in the binder and to predict crack initiation and growth.

As shown in Figure 3-22, the true stress-true strain curve obtained from the BFE test can be conceptually divided into two parts: DCSE and EE. A key assumption was made that there is very little or no delayed elastic energy because the BFE test was conducted at a very rapid displacement rate (e.g., 500 mm/min), which also does not allow for binder healing. The DCSE is the FED minus the EE at the time of fracture. Resilient modulus (M_R) has been used to determine the EE of asphalt mixtures, while elastic modulus was employed to obtain the EE of asphalt binder. The elastic modulus of asphalt binder was estimated by using Equation 30 and the shear modulus was determined by performing DSR tests.

$$B = \frac{E}{3(1-2\gamma)} \tag{30}$$

where, B is elastic modulus; E is shear modulus, which was determined from the DSR data; and γ is poison ration, equal to 0.5.
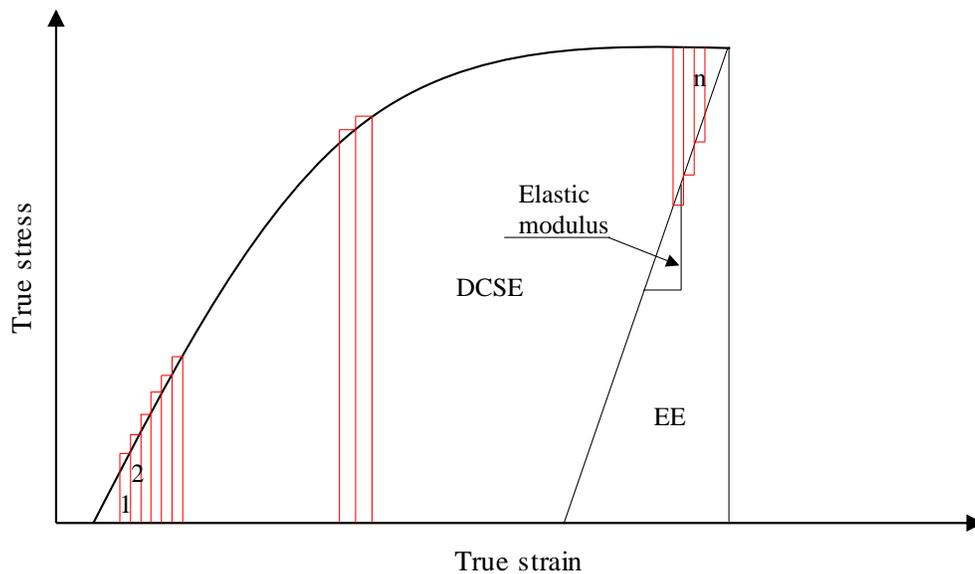
Figure 3-22. An alternative interpretation of the true stress-true strain curve

It has been assumed in the HMA-FM model that damage is associated with the viscous response (creep). Therefore, the DCSE can be obtained by using Equation 31.

44

Thus, the creep strain rate per unit stress (CSR/S), which is assumed to be a constant of a given binder, can be determined following Equation 32. This parameter, which is directly related to the DCSE, can be used to characterize the binder damage rate.

$$DCSE = FED - EE = \sum_{i=1}^{n} fnc(\sigma_i) \cdot \dot{\varepsilon}_{cr(i)} \tag{31}$$

where, σ_i is the average stress in step i, which was determined by fitting a step function to the stress versus time data; $\dot{\varepsilon}_{cr(i)}$ is the creep strain rate at step i; and n is the last step of the fitted function.

$$\frac{\dot{\varepsilon}}{\sigma} = \frac{DCSE}{\sum_{i=1}^{n} f(\sigma_i)^2} \tag{32}$$

where, $\frac{\dot{\varepsilon}}{\sigma}$ is creep strain rate per unit stress (CSR/S), which is assumed to be a material constant.

Whereas the CSR/S is believed to be a material constant, the binder DCSE/cycle depends on the loading function. A haversine load consisting of a 0.1-s loading period followed by a 0.9-s rest period has been used to determine mixture DCSE/cycle. In this study, the same loading scenario was adopted for asphalt binder, and Equation 33 can be used to determine binder DCSE/cycle.

$$DCSE/cycle = \frac{1}{20} \cdot \sigma^2 \cdot CSR/S \tag{33}$$

where, σ represents the tensile stress in the pavement structure and 1 MPa (150 psi), which has been used to determine the energy ratio of asphalt mixtures, is employed in this study. Note that the same tensile stress value shall be used for all binders. It can be observed that binder DCSE/cycle is governed by the CSR/S parameter.

3.4.2.2 Further test development

A binder creep test based on the BFE test would require precise control of very small loads over long periods of time, e.g., a static load of 3 lbs force for 1,000 s, which cannot be achieved using the standard equipment required to obtain binder FED. A possible solution is to add inert fine aggregates to the asphalt binder, which increases the specimen stiffness without changing the binder properties. The approach would involve three major steps: 1) determination of specimen composition including aggregate type and size, and the relative proportion of aggregate and binder, 2) development of the testing protocol, including the loading magnitude, function and duration, and 3) development of the data analysis procedure, which would follow that of the mixture creep test. Note that the BFE test also needs to be conducted on composite specimens to obtain the failure limit (i.e., FED).

Although further development of the BFE test may potentially provide accurate measurement of binder damage rate, the amount of anticipated work would far exceed the scope of the current study. In consultation with research panel of this project, the decision

was made to employ the approach of alternative interpretation of the true stress-true strain curve to derive the binder damage rate parameter.

3.5 SUMMARY

The LAS test and BFE test were identified as candidate tests, which are currently standardized to characterize the fatigue damage resistance and fracture tolerance of asphalt binders, respectively. Furthermore, preliminary tests were performed on six asphalt binders following the provisional standards. Finally, three proposals were presented, including the revised LAS test with a new definition of binder failure and two modifications of the BFE test, both of which potentially allow for the determination of properties relevant to binder damage rate.

It was determined that the standard rheometer available at SMO was incapable of providing accurate strain control as required in the provisional standard of the LAS test. The erratic trend in strain output was found to be more pronounced for modified binders than for unmodified binders. Regardless of the strain errors, the stress peak that has been specified as an indicator of binder fatigue failure may not appropriate, because modified binders including PMA, hybrid and HP exhibited a stress plateau instead of a clear stress peak. Consequently, a revised LAS test that employs an energy-based definition of fatigue failure was proposed for further evaluation in this study. Two types of erratic trend were observed when employing the continuous loading scheme of the revised LAS test. After consulting a product specialist from the rheometer manufacturer, a software upgrade was necessary for performing the revised LAS test.

The BFE test provided accurate and consistent determination of the FED of the same six binders previously tested with the LAS test. As expected, FED results differentiated between unmodified, polymer-modified, hybrid and heavily polymer-modified binders. Two approaches were presented, both of which have great potential in obtaining properties relevant to binder damage rate. The alternative interpretation of the true stress-true strain curve would only require additional information on binder elastic modulus. Conversely, the idea of performing a creep test on binder specimens that contains fine inert aggregates would require a significant additional amount of research effort beyond the current scope of this study. Therefore, the former approach was proposed for further development.

CHAPTER 4 EXPERIMENTAL PLAN

4.1 Introduction

This chapter summarized the completed experimental design. Six binders, including three unmodified and three modified, were included in this study. A total of twelve asphalt mixtures were evaluated, corresponding to two aggregate types and six binder types. Two versions of the LAS test with three different failure definitions were conducted to characterize binder resistance to fatigue damage using the LAS binder-N_f parameter. Moreover, BFE tests were performed to obtain binder FED and damage rate (i.e., DCSE/cycle). A new binder parameter (i.e., BFE binder N_f parameter) that integrates the two properties was derived by following the principles of HMA-FM model. This parameter was employed to evaluate the relative cracking performance of asphalt binders.

Mixture fracture properties (e.g., failure strain, FED, resilient modulus, etc.,) were determined using Superpave IDT tests. The relative cracking performance of mixtures was evaluated by using the mixture N_f parameter. The mixture FED and damage rate values, as well as cracking performance were compared with respect to the binder types. The comparison results were used to evaluate the relative effect of binder FED and rate of damage on binder cracking performance as predicted by the proposed BFE binder N_f parameter. Figure 4-1 shows the experimental design. Details were described in following sections.
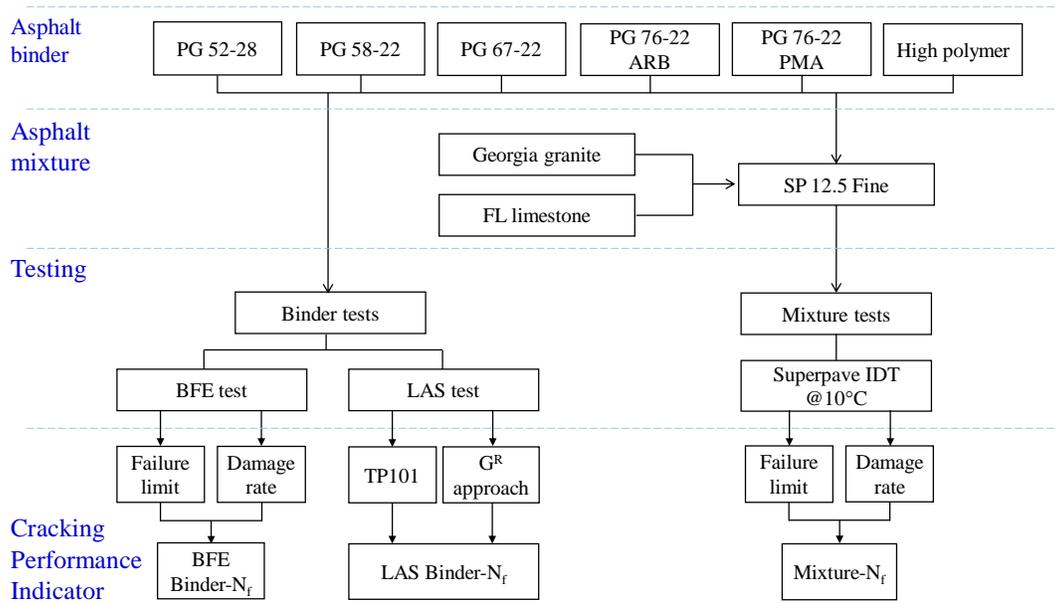
Figure 4-1. Experimental design

4.2 Materials

4.2.1 Aggregate

Aggregates used throughout this research were Georgia granite and Florida limestone. These aggregates have been widely used in Florida and are approved by the FDOT for road

construction and rehabilitation projects. Table 4-1 presents aggregate source information and Figure 4-2 shows the aggregate gradations.

Table 4-1. Aggregate sources

Type of Material		FDOT Code	Producer	Pit	Terminal
FL Limestone	#67	42	Rinker Master Corp.	87090	TM-447
	S1B	C55		87090	TM447
	Med. Screening	21		87090	TM447
Georgia Granite	#78	43	Junction City Mining	GA-553	TM-561
	#89	51		GA-553	TM-561
	W-10 Screenings	20		GA-553	TM-561
Local Sand		-	V.E. Whitehurst & Sons	Starvation Hill	
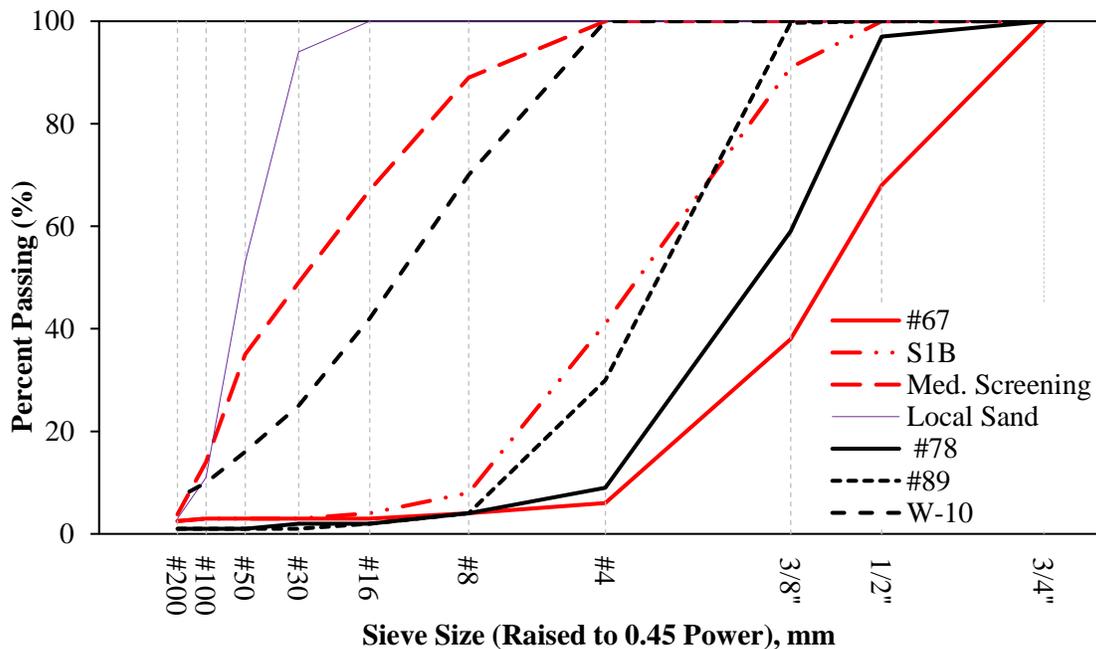
Figure 4-2. Aggregate gradations

4.2.2 Asphalt binder

Six asphalt binders commonly used in Florida were evaluated in this study, including three unmodified binders (i.e., PG 52-28, PG 58-22, PG 67-22), one polymer-modified binder (PG 76-22 PMA), one hybrid binder (PG 76-22 ARB) that contains a minimum of 7% asphalt rubber and optional content of SBS polymer, and one high polymer-modified (HP) binder. In addition to Superpave Performance Grade (PG), continuous/true grades of each binder were determined by interpolating between test results obtained at two adjacent specification

48

temperatures. The two temperatures are chosen so that the test result at one temperature is greater than the specification requirement and the test result at the other temperature is less than the specification requirement. Table 4-2 summarizes the true grade of these six binders.

Table 4-2. High-, intermediate- and low-temperature true grades of six binders

Superpave binder true grades (°C)						
Binder type	High Temp.		Intermediate temp.	Low Temp.		
	Original	RTFO		Stiffness-based	Relaxation-based	Delta Tc
PG 52-28	57.2	58.0	15.0	-33.6	-33.7	0.1
PG 58-22	62.1	62.0	19.1	-29.5	-28.4	-1.1
PG 67-22	69.6	69.8	22.9	-26.1	-25.4	-0.7
PG 76-22 ARB	82.2	82.2	19.3	-28.3	-26.9	-1.4
PG 76-22 PMA	80.9	79.9	22.1	-27.2	-25.3	-1.9
High Polymer	92.2	92.1	14.3	-32.9	-31.8	-1.1

Delta Tc (ΔTc) parameter, which is the difference between the stiffness-based and relaxation-based low temperature true grades, was also determined for these six binders. This parameter has been proposed as a relatively simple method for measuring the loss of relaxation properties of asphalt binders. All six binders met the minimum Delta Tc requirement of -5°C, which has been shown to differentiate between mixtures exhibited non-load related cracking and those that did not (Anderson, 2011).

4.3 Binder Testing

Superpave PG binder tests such as dynamic shear rheometer test and bending beam rheometer test were performed to evaluate specification compliance of selected binders. Two versions of the LAS test were employed to predict binder fatigue resistance. The BFE tests in the current form were performed to determine binder failure limit and FED results were presented in section 3.3.2. An alternative interpretation of the true stress-true strain obtained from the BFE test was selected, and this approach was applied to determine creep strain rate per unit stress, which is directly related to binder damage rate (i.e., dissipated creep strain energy per loading cycle). Superpave binder tests and the LAS test were performed at SMO bituminous laboratory, whereas the BFE test was conducted at the UF bituminous laboratory.

4.3.1 Linear amplitude sweep test

The LAS test consists two main steps: 1) a frequency sweep to determine undamaged binder properties and 2) an amplitude sweep to measure the resistance of asphalt binder to fatigue damage. Two versions of the LAS test have been previously discussed in Task 2, including the standardized LAS test following AASHTO provisional standard TP 101 and a revised LAS test by Wang et al. (2015). The revised LAS test applies recent advances in the simplified viscoelastic continuum damage (S-VECD) modeling of asphalt mixtures to the LAS

data analysis procedure. The major difference between the two versions is that TP 101 uses the peak shear stress as the failure indicator, whereas Wang et al. (2015) recommended the maximum stored pseudo-strain energy (max W_S^R) failure definition. Moreover, Wang et al. (2015) identified a unique relationship between pseudo-strain energy release rate and fatigue life (i.e., number of cycles to failure), which is independent of loading mode and history. Wang et al. (2015) incorporated the relationship between strain energy release rate and fatigue life in the S-VECD model to enable fatigue life prediction for one asphalt binder material at any strain amplitude. For the purpose of performing the revised LAS test, it was necessary to install a software feature named "TruStrain" on the standard rheometers at SMO, which allowed for precise strain control to match the target loading sequence.

Both versions of LAS test were performed to evaluate fatigue resistance of selected binders. The conditioned state was rolling thin film oven (RTFO) plus pressure aging vessel (PAV) to simulate the long-term field aging. For each binder type, two replicates were used and average values of each result (e.g., number of cycles to failure) were reported. Note that the relationship used in the revised LAS test needs to be derived by differing rates of increase in strain amplitudes (i.e., 0.001, 0.0005, and 0.00033 corresponding to 5, 10 and 15 minutes of sweep time, respectively). Therefore, a complete set of the revised LAS test required four specimens: one for the frequency test and the other three for the amplitude tests. Figure 4-3 shows that ten specimens per binder type are needed for the two versions of LAS test. At a minimum, a total of 24 LAS tests, requiring 60 binder specimens, were performed to meet the objective of this study.
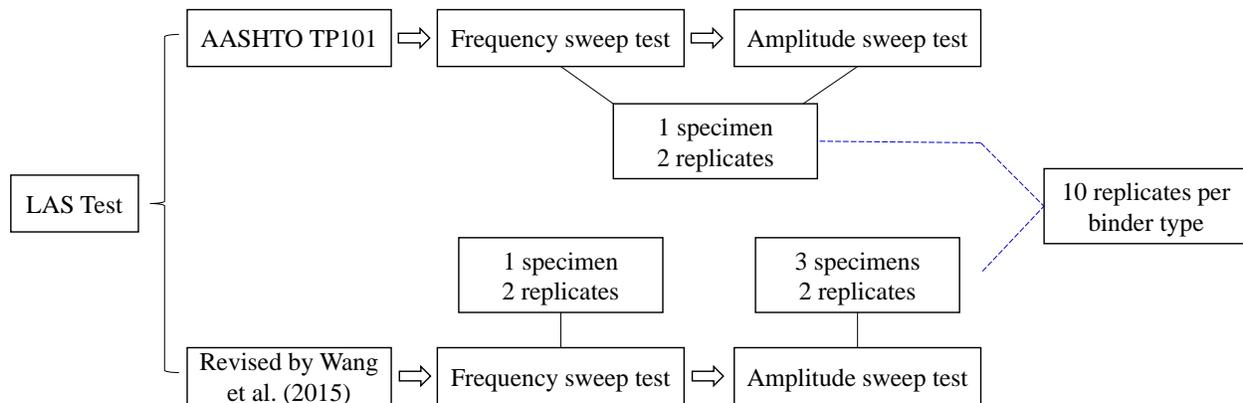
Figure 4-3. LAS testing plan

4.3.2 Binder fracture energy test

The BFE test was developed to determine the binder fracture energy density (FED) at intermediate temperatures. FED describes the damage tolerance before fracture occurs, and it is also a component associated with crack propagation. The BFE test can be used to identify the presence of various modifiers, such as styrene-butadiene-styrene polymer and ground tire rubber. Importantly, binder FED measured by the BFE test has been shown to correlate well with mixture FED, validating the relevance of binder FED in characterizing mixture cracking performance.

FED values of the six selected binders were determined following AASHTO provisional standard TP 127. Section 3.3.2 presented the detailed BFE testing results including the binder FED values and the true stress-true strain curves. Binder damage rate was obtained by performing an alternative interpretation of the true stress-true strain curve of the BFE test. More specifically, the approach was to derive a parameter (i.e., creep strain rate per unit stress) from the true stress-true strain curve to calculate the dissipated creep strain energy per cycle (DCSE/cycle), which can be used to characterize damage accumulation in the binder. Note that DSR tests were necessary to obtain binder elastic modulus for determination of binder creep strain rate per unit stress. Detailed procedure to obtain binder creep strain rate per unit stress was documented in Chapter 3.

A new binder parameter combining binder FED and damage rate (i.e., DCSE/cycle) was used to predict binder crack initiation and growth, providing a complete assessment of binder cracking performance at intermediate temperatures. The BFE binder N_f parameter was determined by using the binder FED divided by the damage rate. Figure 4-4 shows the general steps to obtain the BFE binder N_f parameter.
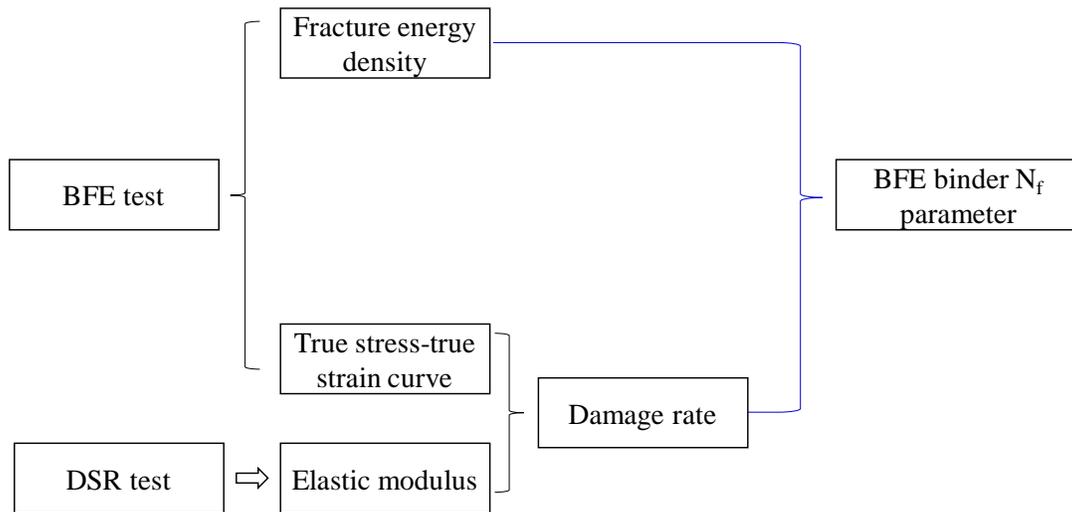
Figure 4-4. Development of a new binder cracking parameter

4.4 Mixture Testing

4.4.1 Mixture design

A total of 12 dense-graded Superpave mixtures were evaluated, corresponding to two mixture gradations and six virgin binders. Figure 4-5 shows the gradations of two control mixtures, one for Georgia granite and the other one for Florida limestone, which coincidently to be very similar to each other. All mixtures were designed using the Superpave system with 12.5 Nominal Maximum Aggregate Size gradation and traffic level C, which corresponds to 3-10 million Equivalent Single Axle Loads over 20 years. The PG 67-22 unmodified binder was used to determine optimum asphalt content, which was fixed for other mixtures with four different binders. This helped to isolate the effect of binder type and minimize effect of mixture (e.g., air void structure) that may confound the effect of binder alone.
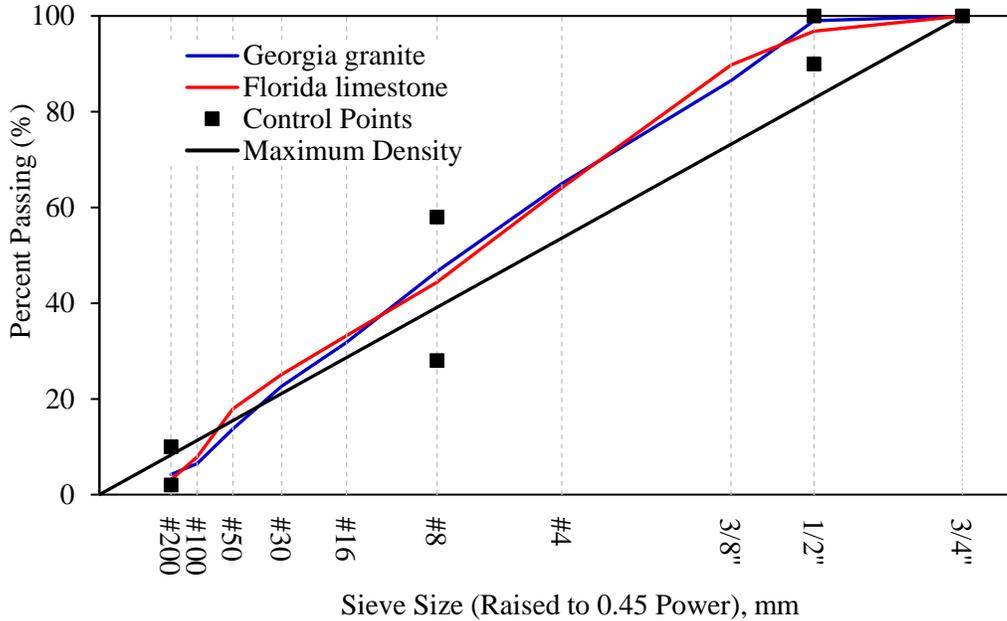
Figure 4-5. Gradation design of granite and limestone mixtures

Table 4-3 summarizes the Superpave volumetric parameters of the two reference mixtures, including maximum specific gravity (G_{mm}), bulk specific gravity (G_{sb}), design binder content (P_b), air voids content (V_a), voids in mineral aggregate (VMA), voids filled with asphalt (VFA) and dust proportion (DP). Superpave mix design procedure were followed to validate the volumetric parameters of the two reference mixtures.

Table 4-3. Superpave volumetric parameters for two reference mixtures

Mixture type	G_{mm}	G_{sb}	P_b (%)	V_a (%)	VMA (%)	VFA (%)	DP
Granite Mixture	2.579	2.770	4.8	4.0	14.9	73.2	0.93
Limestone Mixture	2.311	2.400	6.6	4.0	13.6	70.6	0.69

In addition to Superpave volumetrics, the dominant aggregate size range—interstitial component (DASR-IC) model, which provides a framework of gradation-based parameters and associated criteria to characterize mixture structural characteristics and to link gradation and volumetric properties to field performance, was also adopted in this study. The DASR model uses: (a) DASR porosity to ensure contact between larger particles within the mixture to provide suitable resistance to deformation; (b) disruption factor (DF) to evaluate the degree of disruption of the interstitial component on the DASR structure; (c) effective film thickness to characterize binder distribution within the interstitial volume; and (d) fine aggregate ratio (FAR) to estimate the relative coarseness of interstitial component particles. This model was applied to make sure that the two reference mixtures are not deficient in some aspect of their gradation, such that the effects of the deficiency may overwhelm or mask the effects of asphalt binder. Table 4-4 shows that DASR-IC parameters of both mixtures are all within the allowable ranges.

Table 4-4. DASR-IC parameters for two mixtures

Parameters	Acceptable ranges	Granite mixture	Limestone mixture
DASR (mm)		9.5-1.18	4.75-1.18
Porosity (%)	38-48	42.3	46.4
Disruption factor	0.50-0.95	0.77	0.74
FAR	0.28-0.36	0.41	0.32
EFT	12.5-25	21.7	22.3

4.4.2 Superpave IDT test

Superpave IDT tests were performed at 10°C to obtain HMA fracture properties for each mixture. A set of Superpave IDT test consists of three tests (i.e., resilient modulus, creep and strength tests), from which damage and fracture related mixture properties are determined. The three tests can be performed in a sequence on the same specimen to obtain resilient modulus, creep compliance rate and fracture energy density, respectively. Superpave gyratory compacted (SGC) pills were prepared using the materials described in previous sections. Two Superpave IDT specimens with standard dimension of 150 mm (6 inches) diameter and 38 mm (1.5 inches) thickness can be obtained from a SGC pill, as shown in Figure 4-6.

Figure 4-6. Superpave IDT specimen: (a) masonry saw; (b) cutting from an SGC pill

One of the main advantages of Superpave IDT test is that the failure plane is known a priori, hence properties including failure limits (e.g., FED) can be accurately determined from measurements obtained on the failure plane. This can be obtained by gluing four stainless gauge points to the center area of each specimen face and attaching two strain gauges to measure the vertical and horizontal deformations, as shown in Figure 4-7. The point of macrocrack initiation can be identified based on the comparative evaluation of the change in the vertical and horizontal deformation in the center region of the specimen.

Figure 4-7. Use of strain gauges for accurate determination of fracture properties: (a) stainless steel gauge points attachment; (b) a specimen on the load frame with strain gauges

The resilient modulus test is a nondestructive test used to determine the resilient modulus (M_R) of asphalt mixtures. The resilient modulus is defined as the ratio of the applied stress to the recoverable strain when repeated loads are applied. A haversine waveform load is repeatedly applied to the specimen for 0.1 second followed by a rest period of 0.9 second. The load is selected to restrict the horizontal resilient deformations between 100 to 180 micro-inches to stay within the linear viscoelastic range. Figure 4-8 shows the haversine load applied and typical deformation response for a resilient modulus test.
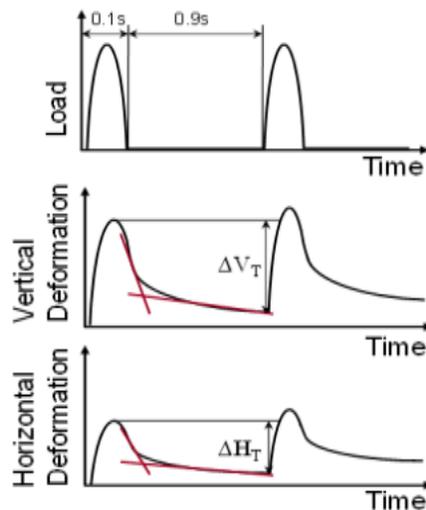
Figure 4-8. Typical load, deformation versus time relationships in a resilient modulus test

Creep compliance, which is defined as the ratio of the time-dependent strain over stress, has been used to evaluate the rate of damage accumulation of asphalt mixture. The creep test is a nondestructive test conducted in a load-controlled mode by applying a static load in the form of a step function to the specimen and then holding it for a period. Typically, a 1,000-s creep test has been considered to enough to isolate the viscous response of asphalt mixture for intermediate temperatures associated with fatigue cracking (0-25°C). Horizontal and vertical deformations are

recorded during the load applications to determine creep compliance and Poisson's ratio. A power law fitting function is used to express the compliance curve (creep compliance versus time), and the three fitting parameters (D_0, D_1 and m-value) can be obtained by presenting the compliance curve in the logarithm scale, as shown in Figure 4-9.
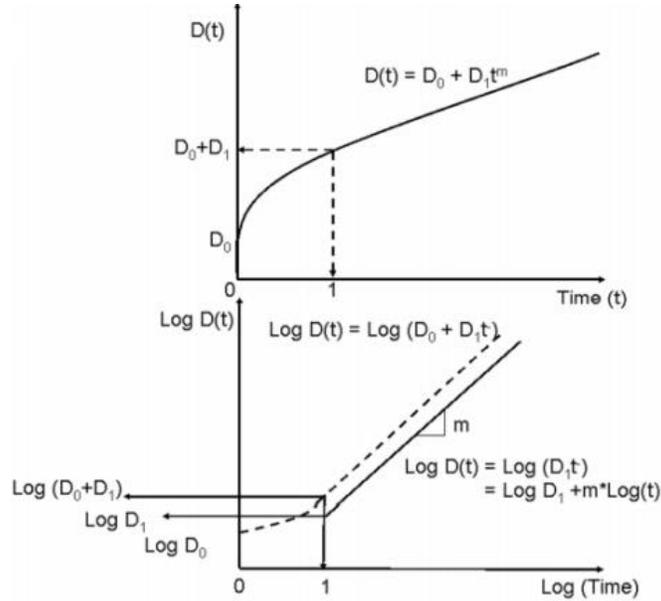
Figure 4-9. Power model of creep compliance curve

Creep compliance rate, which is the rate of change of the creep compliance curve at 1,000 seconds, can be determined using Equation 34. This parameter has been shown in prior work to be directly related to the rate of damage accumulation of a mixture (i.e., DCSE/cycle), as indicated by Equation 35. The specific relationship between damage rate and creep compliance rate depends on the loading function, and Equation 35 shall only be used when a haversine load is applied.

$$\dot{D}(t) = m \cdot D_1 \cdot (t)^{m-1} \tag{34}$$

where, $\dot{D}(t)$ is creep compliance rate; t is time (s) equals 1,000; m and D_1 are fitting parameters.

$$DCSE/cycle = \frac{1}{20} \cdot (\sigma_{ave})^2 \cdot m \cdot D_1 \cdot (t)^{m-1} \tag{35}$$

where, DCSE/cycle is dissipated creep strain energy per cycle referring to damage accumulation rate; σ_{ave} represents the average peak stress.

Strength test is a destructive test performed in a displacement-controlled mode by applying a constant rate of displacement of 50 mm/min until failure. The purpose of strength test is to determine the failure limit parameters of the asphalt mixtures, including tensile strength (S_t), failure strain (ε_f) and FED, which is the total energy necessary to induce fracture. FED can be determined by integrating the area under the stress-strain curve until failure, as shown in Figure

4-10. Another important failure limit is dissipated creep strain energy (DCSE), which is the absorbed energy that damages the specimen. Dissipated creep strain energy to failure, referring to the absorbed energy to fracture ($DCSE_f$), can be obtained by subtracting elastic energy (EE) from the FED once the resilient modulus is known.
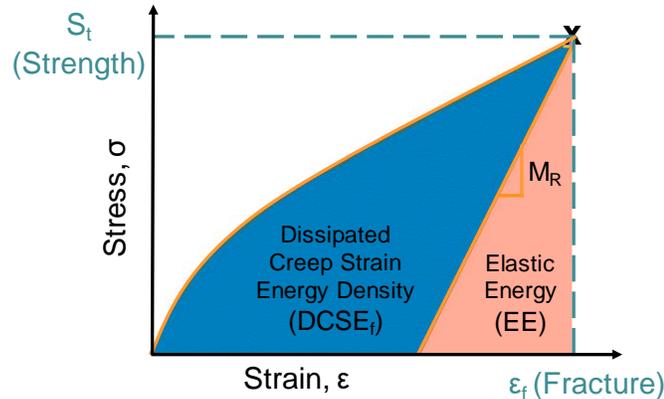
Figure 4-10. Determination of failure limits from a stress-strain curve

A total of 12 mixtures (two gradations and six asphalt types) were encompassed and three replicates per mixture type were tested, for a total of 36 Superpave IDT specimens. The main objective of this study was to derive a binder cracking parameter and therefore, all mixtures were tested in the unconditioned state (i.e., short-term oven aging only). This minimizes the effect of mixture factors such as air void structure on mixture fracture properties and performance. A software program was used to analyze the load and deformation data to determine resilient modulus, creep compliance rate and FED of the mixtures. More details regarding testing procedures of the Superpave IDT tests (resilient modulus test, creep test and strength test) can be found in Roque and Buttlar (1992), Buttlar and Roque (1994), and Kim and Roque (2006).

The relative cracking performance of mixtures with the same aggregate type, gradation and Superpave volumetrics but different binder type was evaluated by using the number of cycles to failure parameter, which is defined as the mixture failure limit (i.e., dissipated creep strain energy at failure) divided by the mixture damage rate (i.e., dissipated creep strain energy per loading cycle). Generally, the higher the value of the mixture N_f at a given condition, the better the expected mixture cracking performance at that condition, i.e., should not compare N_f from different conditions. The mixture FED and damage rate values, as well as cracking performance as determined by the mixture N_f, were compared with respect to the binder types. Then the results were used to calibrate the relative effect of binder FED and rate of damage on binder cracking performance as predicted by the proposed binder parameter.

4.5 Summary

An experimental plan was summarized in this chapter. Six asphalt binders including three unmodified and three modified binders were included in this study. Two versions of the LAS test with three different failure definitions would be employed to characterize the binder fatigue resistance using the number of cycles to failure (N_f) parameter. The BFE test has been used to

determine the binder failure limit (i.e., FED). An alternative analysis of the true stress-true strain curve would be performed to derive a parameter (i.e., creep strain rate per unit stress) that can be used to compute binder damage rate (i.e., DCSE/cycle). The BFE binder N_f parameter that integrates binder failure limit and damage rate would be derived by following principles of the HMA-FM model. This parameter would be used to characterize the relative cracking performance of selected binders.

A total of twelve dense-grade Superpave mixtures would be evaluated, corresponding to the two aggregate types and six virgin binders. Mixture design parameters for each aggregate type were held constant, so the only variable was binder type. This helped to isolate the effect of binder type and minimize effect of mixture that may confound the effect of binder alone. Superpave IDT tests would be conducted to obtain mixture fracture properties and mixture relative cracking performance would be evaluated by using the mixture N_f parameter. Comparisons in mixture fracture properties and performance would be made and results would be employed to evaluate the relative effect of binder FED and damage rate on binder relative cracking performance as predicted by the proposed binder parameter.

CHAPTER 5 BINDER EVALUATION

5.1 Introduction

The linear amplitude sweep (LAS) test and binder fracture energy (BFE) test were identified in chapter 3 and employed in the current chapter as laboratory tools to evaluate the cracking performance of asphalt binders at intermediate temperatures. Six asphalt binders commonly used in Florida were included in this study: PG 52-28, PG 58-22, PG 67-22, PG 76-22 ARB, PG 76-22 PMA and high polymer (HP). All binders were conditioned using rolling thin film oven plus pressure aging vessel to simulate long-term field aging.

Three versions of the LAS test, including the standardized LAS test procedure described in AASHTO TP 101-12 (published in 2012, 2016 and 2018), AASHTO TP 101-14 (published in 2014)[1] and a revised version proposed by Wang et al. (2015), were performed to determine the binder resistance to fatigue damage. Table 5-1 summarizes the differences between the three LAS test procedures, including loading scheme, failure definition and prediction model of fatigue life. The previously identified issue with a standard dynamic shear rheometer (DSR) when performing the LAS test is discussed in detail in Appendix I. The results associated with the stepwise strain load presented in the current chapter were determined based on the corrected raw data (e.g., trimmed shear stress, shear strain and complex shear modulus, refer to Appendix I for trimming process). The other two testing procedures with linearly increased strain load were performed using a DSR with the software feature named TruStrain.

Table 5-1. Similarities and differences between the three versions of LAS test

LAS tests	Loading scheme of amplitude sweep	Indicator of fatigue failure	Fatigue prediction model
AASHTO TP 101-12	Stepwise	35% reduction in undamaged $|G^*| \cdot \sin\delta$	VECD (physical strain)
AASHTO TP 101-14	Linear	Peak shear stress	VECD (physical strain)
GR approach	Linear	Peak stored pseudo-strain energy	SVECD (pseudo strain)

BFE tests were performed following AASHTO TP 127-17 to determine binder fracture energy density (FED) and the results were presented in chapter 3. The current chapter focused on the determination of binder damage rate by performing an alternative interpretation of the binder true stress-true strain curve. The binder damage rate parameter, i.e., dissipated creep strain energy per loading cycle, is fully governed by the binder creep strain rate per unit stress (CSR/S) parameter, referring to Equation 33 in section 3.4.2. To avoid being lengthy, only the CSR/S results of the selected six binders were summarized and reported in this chapter. There were mainly four steps

---

[1] During an email conversation with researchers at the University of Wisconsin (UW)—Madison, who developed the LAS test and drafted the provisional standard, researchers of this study were informed that AASHTO TP 101-14 should be followed as the correct provisional standard and AASHTO would be informed by the test developers to make proper changes as well.

to obtain the binder CSR/S parameter: 1) determining binder complex shear modulus, 2) obtaining the binder elastic energy (EE), 3) deriving the binder dissipated creep strain energy to failure, 4) computing the binder CSR/S parameter that governs the binder DCSE/cycle parameter.

5.2 Linear Amplitude Sweep Test Results

LAS tests were performed on all binders at 20°C using DSR specimens with 8-mm-diameter parallel plate geometry. The provisional standards do not specify how many replicates should be used; however, Hintz et al. (2011) indicated that results of two replicates should be within 15% of each other and if not, a third replicate should be tested. Average values of the fatigue model parameters A (intercept) and B (slope), and fatigue life (N_f) were determined for each binder type. Figure 5-1 illustrates the binder fatigue performance model, which can be used to predict the allowable binder fatigue life for different strain amplitudes. In general, a larger value of A indicates greater fatigue life while a higher magnitude of B decreases fatigue life (at a constant A). The strain amplitude used to predict binder fatigue performance is 5.0%, corresponding to a mixture strain of approximate 1,000με, which is typically considered to be high strain in pavements (Johnson, 2010). A lower strain amplitude of 2.5%, which has been used by some researchers, was also employed for data analysis in this study.
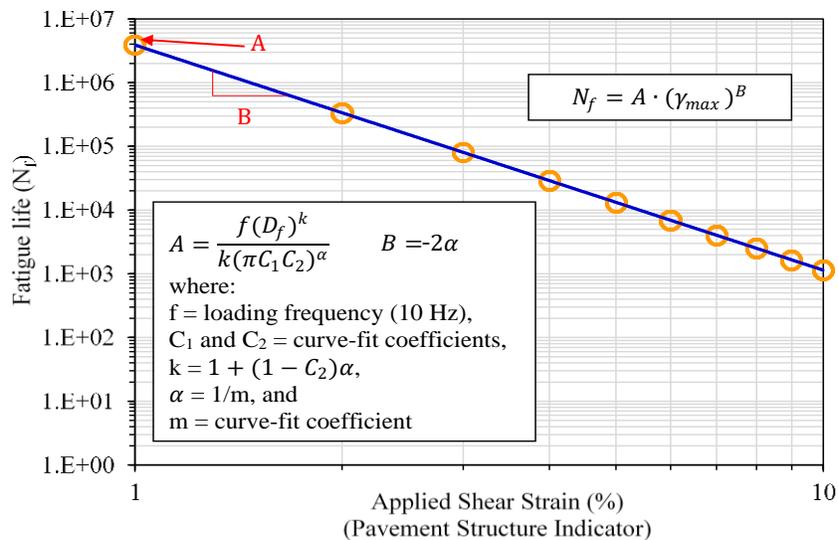
Figure 5-1. Fatigue life versus applied shear strain on a log-log scale

5.2.1 AASHTO TP 101-12

AASHTO TP 101-12 employs a stepwise load strain from 0 to 30% to introduce damage in DSR samples. Figure 5-2a illustrates the stepwise strain load and Figure 5-2b shows the corresponding shear stress versus shear strain curve of the PG 52-28 binder. The level of damage at failure (D_f) was defined as the damage ($D_{(t)}$) that corresponds to a 35 percent reduction in undamaged $|G^*|·\sin\delta$. As discussed in chapter 2, this is an arbitrary failure criterion without theoretical or phenomenological justification.
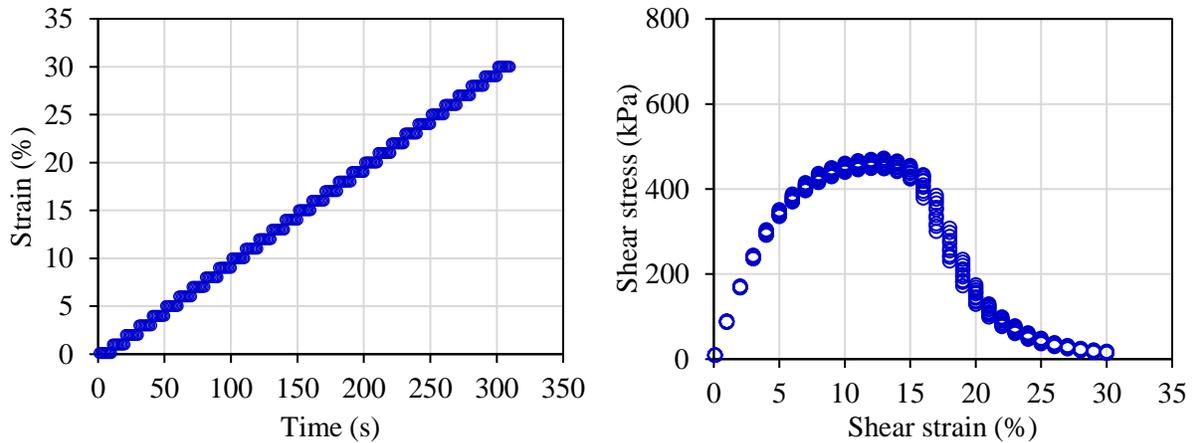
Figure 5-2. Illustration of (a) stepwise strain load; (b) shear stress versus shear strain curve

Figure 5-3 plots the fatigue life versus shear strain curves of all binders. Results of fatigue model parameters and N_f are summarized in Table 5-2. The A_{35} parameter (intercept) differentiated between unmodified binders, whereas the two SBS binders yielded comparable A_{35} values. In terms of the B parameter (slope), the three unmodified binders and the PG 76-22 PMA binder exhibited similar values within the range of 3.9-4.4, while the HP binder had a lower value of 3.5 compared to 4.4 for PG 76-22 PMA. As a combined result, the HP binder yielded the greatest fatigue life (N_f) and the relative benefit increased as the applied shear strain increased. The improvement caused by adding SBS polymer can be seen from the comparisons between HP and PG 52-28 binders, as well as between PG 76-22 PMA and PG 67-22 binder. However, it was also observed that the hybrid binder (PG 76-22 ARB) which contains both SBS polymer and rubber did not exhibit improvement in terms of A_{35} and N_f values. Nonetheless, based on the 35% reduction criterion, it appears that the use of a softer unmodified binder can result in predicted N_f value similar to or even better than that of SBS binders, e.g., PG 52-28 outperformed PG 76-22 ARB and PG 76-22 PMA.
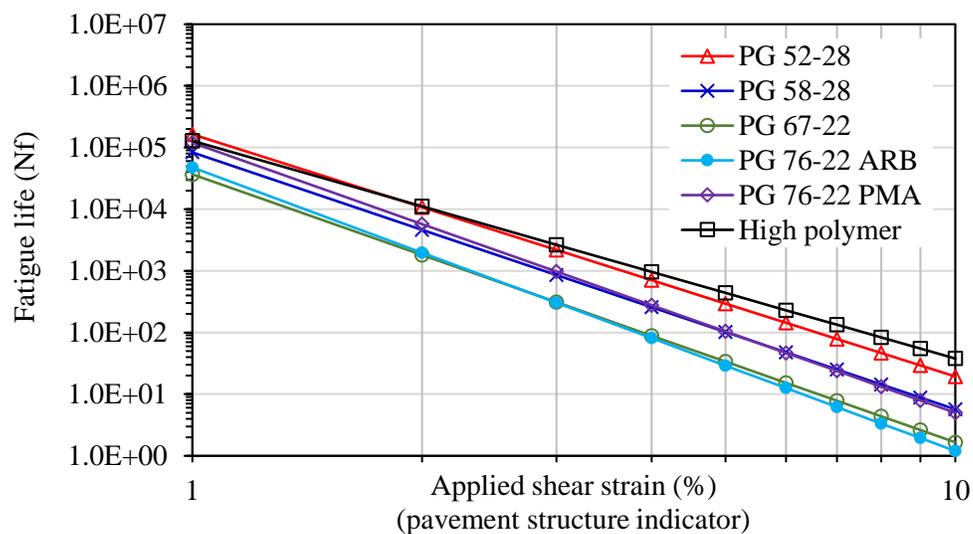
Figure 5-3. Fatigue life versus applied shear strain following the AASHTO TP 101-12

Table 5-2. Fatigue model parameters and fatigue life of six binders following TP 101-12

Binder type	A_{35}	B	N_f	
			2.5%	5.0%
PG 52-28	1.64E+05	-3.9	4481	294
PG 58-22	8.35E+04	-4.2	1791	102
PG 67-22	3.67E+04	-4.3	685	34
PG 76-22 ARB	4.76E+04	-4.4	845	40
PG 76-22 PMA	1.20E+05	-4.4	2164	104
High polymer	1.28E+05	-3.5	5053	437

5.2.2 AASHTO TP 101-14

AASHTO TP 101-14 introduced two major changes: a gradually increasing linear strain load and use of maximum shear stress as the indicator of failure. The linear strain load has the same amplitude range (0-30%) and the same total testing time (300 s) as the stepwise strain load. However, it increases from 0 to 30% at a constant rate of 0.1% strain per second until 30% strain is reached, as shown in Figure 5-4a. Figure 5-4b shows shear stress versus shear strain curve of the PG 52-28 binder obtained from a DSR with the TruStrain feature active. The level of damage corresponding to the maximum shear stress (marked with a red circle in Figure 5-4b) is used as the damage at failure (D_f) to predict binder fatigue life.
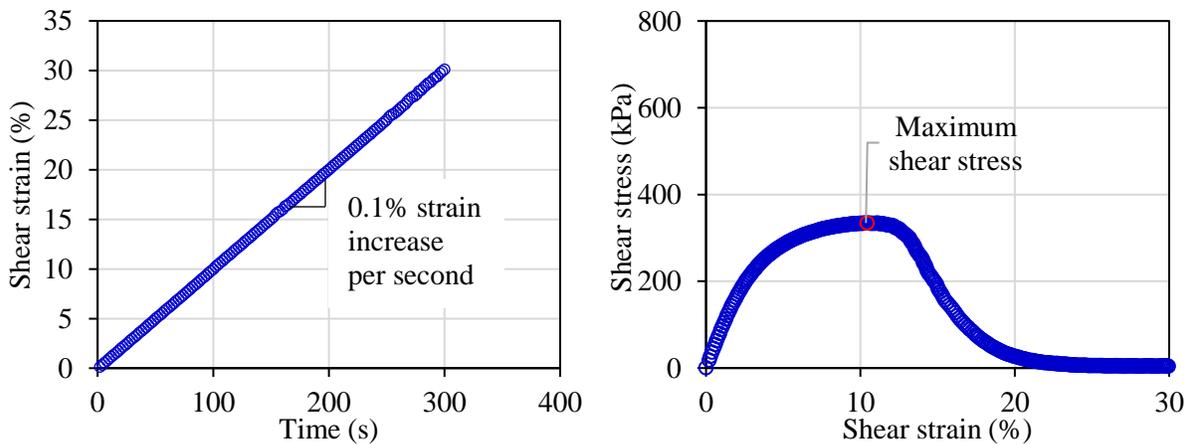
Figure 5-4. Illustration of (a) linear strain load; (b) shear stress versus shear strain curve (PG 52-28)

Figure 5-5 shows the shear stress versus shear strain curves of all six binders. Instead of a distinct shear stress peak, almost all binders except the PG 58-22 exhibited a plateau where the shear stress barely changed as the shear strain increased. This curve characteristic appears to negate the idea of using the shear stress peak for failure indication. More specifically, existence of a plateau challenges the accuracy of using the shear stress peak to determine damage at failure (D_f), which is used to predict binder fatigue life.
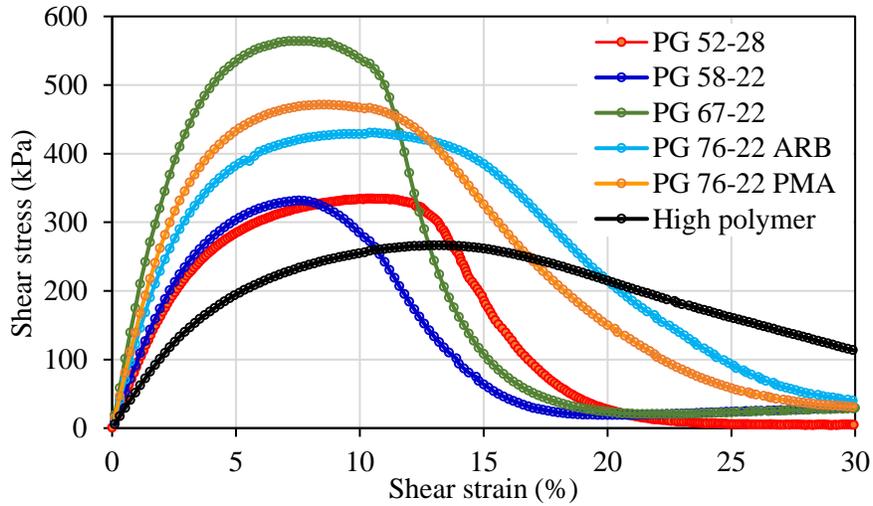
Figure 5-5. Shear stress versus shear strain curves of six binders using a DSR with TruStrain

Figure 5-6 plots the fatigue life predictions of the six binders. Detailed results in terms of fatigue model parameters, and fatigue life at 2.5% and 5.0% strain are summarized in Table 5-3. Fatigue life of HP and PG 76-22 PMA binders were comparable initially but the former, which had significantly higher content of SBS polymer, immediately outperformed the latter as the shear strain increased. PG 76-22 PMA exhibited greater fatigue life than PG 52-28 at strain levels below 4.3%; however, the trend reversed at higher strain levels. Interestingly, the PG 76-22 ARB outperformed all binders at low strain levels and exhibited second greater Nf values at high strain levels. This reveals the importance of failure definition/indicator in determining binder fatigue life. Once again, it appears that both soft binder and polymer modification are beneficial for binder cracking performance based on LAS test results. The other two unmodified binders ranked last: PG 67-22 had greater fatigue life than PG 58-22, but the gap narrowed as the shear strain increased.
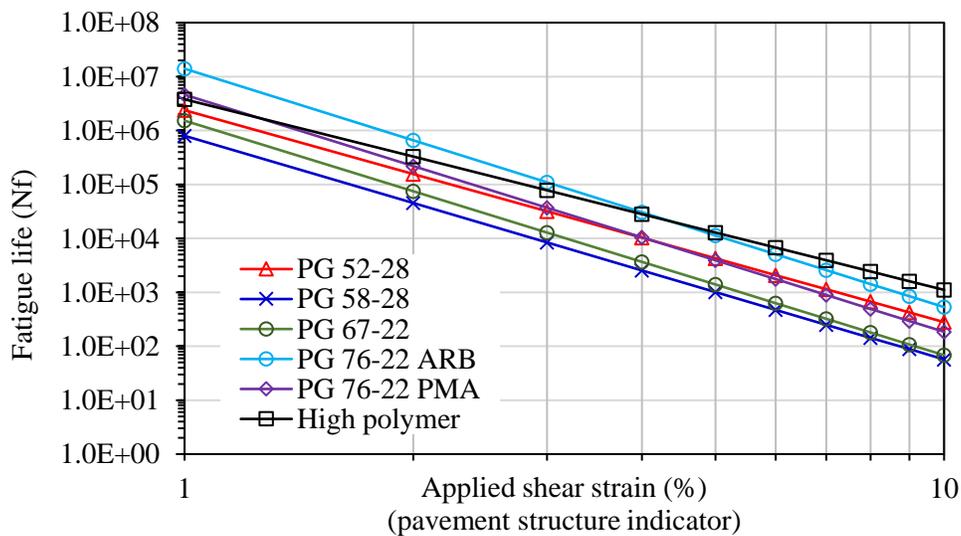

Figure 5-6. Fatigue life versus applied shear strain following TP 101-14

Table 5-3. Fatigue model parameters and fatigue life of six binders following TP 101-14

Binder type	A	B	N_f	
			2.5%	5.0%
PG 52-28	2.38E+06	-3.9	65,100	4,276
PG 58-22	7.98E+05	-4.2	17,508	974
PG 67-22	1.52E+06	-4.3	28,416	1,398
PG 76-22 ARB	1.40E+07	-4.4	244,000	11,400
PG 76-22 PMA	4.61E+06	-4.4	83,437	4,009
High polymer	3.79E+06	-3.5	149,249	12,911

5.2.3 LAS-G^R approach

Wang et al. (2015) proposed analyzing LAS test results in the pseudo-strain domain which eliminates the time-dependent effect of viscoelasticity (i.e., delayed elastic energy) from energy associated with damage, by replacing physical strain with equivalent pseudo strain. For a given loading cycle, the total pseudo strain energy (PSE) can be separated into two parts: the released PSE and the stored PSE. A peak in stored PSE indicates that the material lost its ability to store more PSE with increasing strain, indicating failure occurred. Thus, the maximum stored PSE is used as an energy-based failure criterion and the corresponding number of loading cycles is reported as the binder fatigue life (N_f), as depicted in Figure 5-7. Note that the N_f parameter in this approach was determined from the LAS amplitude sweep test at a linear amplitude rate of 0.1% strain per second.
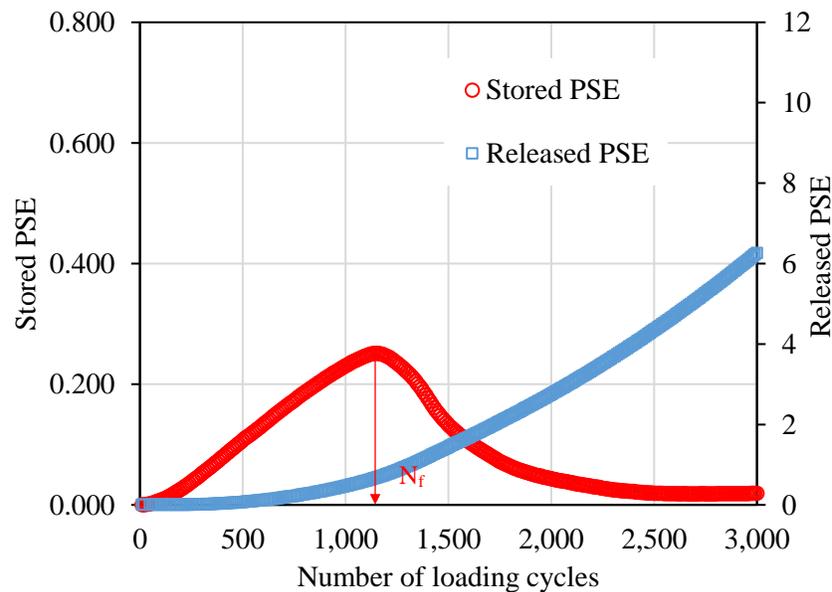
Figure 5-7. Illustration of stored and released PSE of a PG 52-28 specimen

The characteristics of the stored PSE versus number of loading cycles curve separated the six binders into three groups, as shown in Figure 5-8. PG 52-28 and PG 58-22 had similar curve shapes with a peak stored PSE value of approximately 0.25. PG 67-22, PG 76-22 ARB and PG 76-22 PMA yielded peak stored PSE values approximately twice those of the other three binders. HP binder exhibited a plateau where stored PSE remained relatively unchanged as loading cycles increased.
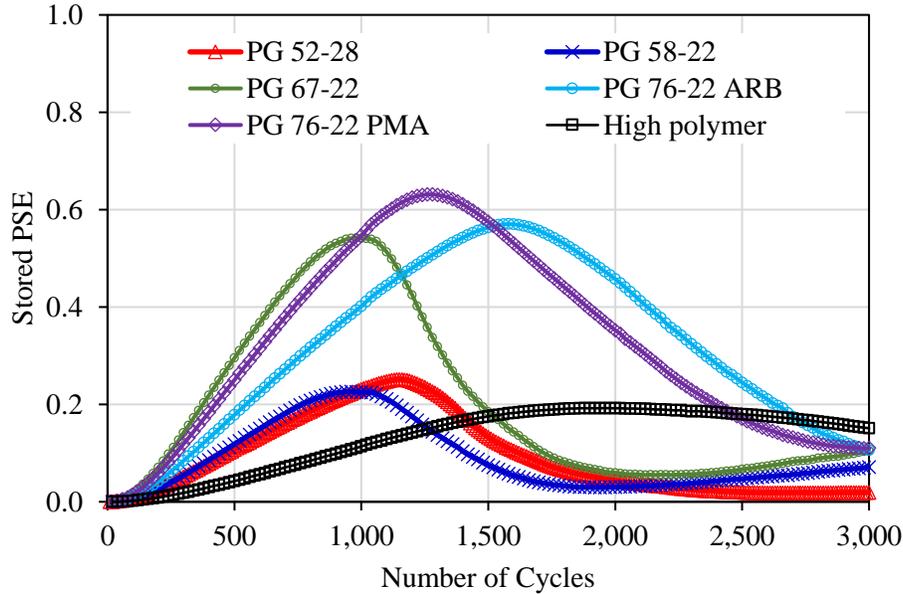
Figure 5-8. Stored PSE versus number of loading cycles of six binders

Table 5-4 summarizes the peak stored PSE and the corresponding N_f values of the six binders. The store PSE peak, which implies a specimen has lost its ability to store more energy with increased input strain, only serves as the indicator of failure. Although PG 76-22 PMA had notably higher stored PSE values than PG 52-28, the N_f value of the former was only approximately 150 cycles more than that of the latter. HP binder, which has a very soft base binder, exhibits the lowest stored PSE at small strain levels. However, the benefit of SBS polymer became evident at higher strain levels and HP binder yielded the greatest N_f value of 1840 cycles, indicating the best resistance to fatigue damage.

Table 5-4. Stored PSE peak and the corresponding N_f values of six binders

Binder type	Stored PSE peak	Number of cycles to failure
PG 52-28	0.251	1,150
PG 58-22	0.221	950
PG 67-22	0.547	1,020
PG 76-22 ARB	0.570	1,560
PG 76-22 PMA	0.620	1,300
High polymer	0.186	1,840

Wang et al. (2015) also conducted the LAS amplitude sweep tests at three different constant strain amplitude rates of 0.1, 0.05 and 0.033 percent strain increase per second, which corresponds to a loading time of 5, 10 and 15 minutes, respectively. The average rate of total released PSE (G^R) can be determined from LAS amplitude sweep tests at each strain amplitude rate by the following two steps:

Step 1. Calculate the averaged total released PSE ($\overline{W_r^R}$) during the test until failure

Step 2. Calculate G^R using Equation 36, where A is the area under the $\overline{W_r^R}$ curve until failure, as shown in Figure 5-7.

$$G^R = \frac{\overline{W_r^R}}{N_f} = \frac{A/N_f}{N_f} = \frac{A}{(N_f)^2} \tag{36}$$

The relationship between the averaged G^R and predicted binder fatigue life (N_f) of a given binder has been found to be independent of loading history.

Figure 5-9 shows the relationship between G^R and number of loading cycles based on data collected from PG 52-28 at three constant strain amplitude rates. This relationship can be incorporated into the simplified viscoelastic continuum damage model by fitting a power law model between G^R and N_f, which allows for prediction of N_f at any strain amplitude in a way similar to that in the AASHTO TP 101 (i.e., Figure 5-1). Additional details about the LAS-G^R approach can be found in Chapter 2.
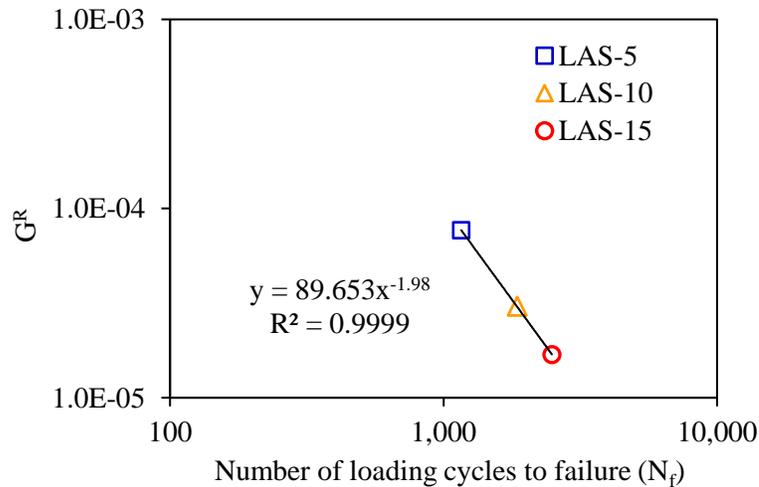
Figure 5-9. Correlation between G^R and N_f of the PG 52-28 binder on a log-log scale

Figure 5-10 shows that different strain amplitude rates (or loading time) resulted in different N_f values of a given binder. Smaller strain amplitude rates (or longer loading time) result in less damage per loading cycle, which requires more loading cycles to failure for a DSR specimen and vice versa. The relative ranking of the six binders in terms of the N_f values is shown in Figure 5-10. The best performer was HP, followed by PG 76-22 PMA, and lastly, unmodified binders in the order of PG 52-28, PG 67-22, and PG 58-22.

The N_f results of the six binders were normalized with respect to the greatest values obtained from HP binder. Figure 5-11 reveals that the relative ranking of the six binders was unaffected by employing different strain amplitude rates. A single rate appears to be sufficient when the goal is to perform a relative comparison between different binders. This would reduce testing time from approximately 4 hours per binder type to one and a half hours, assuming two replicates per constant strain-amplitude rate were tested. At the same time, it was worth mentioning that differences in N_f of the six binders were relatively small (e.g., the fatigue life of PG 76-22 PMA was only about 25% greater than PG 67-22).
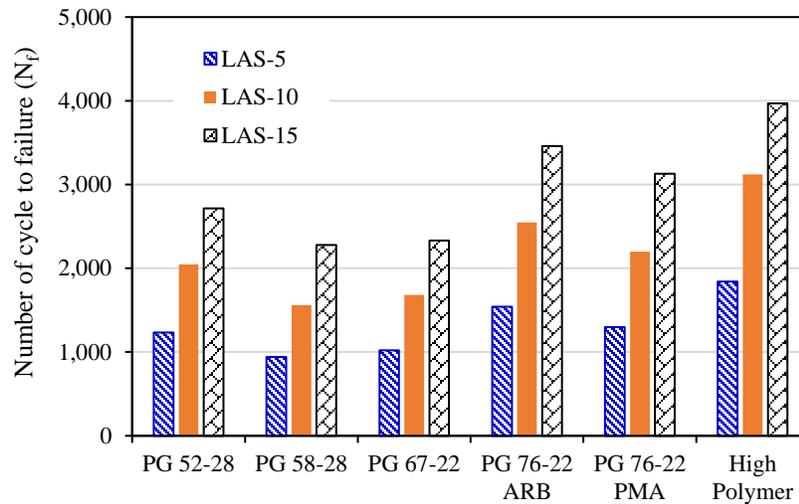
Figure 5-10. N_f values obtained at three constant strain-amplitude rates
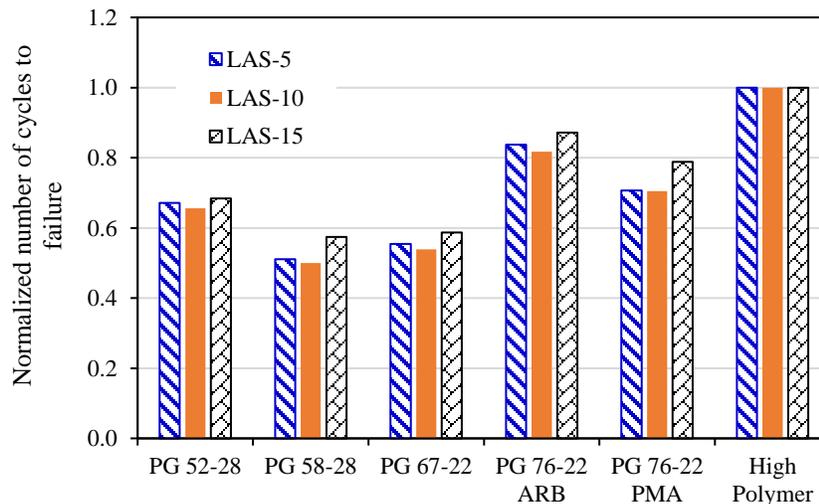
Figure 5-11. N_f normalized with respect to the largest values obtained from HP binder

Figure 5-12 shows the predictions of binder fatigue life using the G^R approach, while Table 5-5 summarizes the fatigue model parameters and N_f values of the six binders. The benefit of SBS polymer seemed evident: all three modified binders exhibited notably greater N_f values

66

than that of the three unmodified binders at any strain level. The HP binder exhibited the best performance, surprisingly followed by the PG 76-22 ARB, which has the N_f value almost doubled that of the PG 76-22 PMA. Nevertheless, N_f value of the PG 76-22 PMA binder was over 60 percent greater than that of PG 52-28 binder at any strain level. Similar to the observation made from Figure 5-6, PG 67-22 outperformed PG 58-22 and the relative benefit decreased with increased shear strain. Figure 5-12 also indicates that soft unmodified binders cannot be used as alternatives to SBS polymer binders to provide enhanced resistance to fatigue damage. This does not agree with observations made from test results obtained following the AASHTO TP 101 provisional standards.
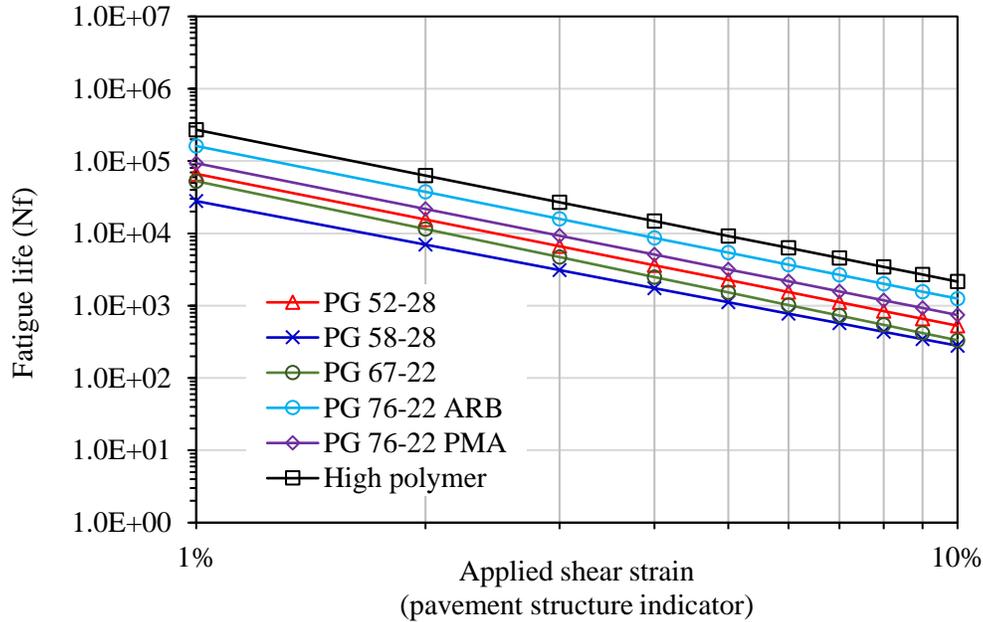
Figure 5-12. N_f versus applied shear strain on a log-log scale based on the G^R approach

Table 5-5. Fatigue model parameters and fatigue life of six binders following the G^R approach

Binder type	A	B	N_f	
			2.5%	5.0%
PG 52-28	4.2	-2.1	9185	2163
PG 58-22	2.8	-2.0	4646	1153
PG 67-22	2.1	-2.2	6728	1475
PG 76-22 ARB	9.7	-2.1	23400	5420
PG 76-22 PMA	5.9	-2.1	15541	3541
High polymer	17.1	-2.1	40675	9435

Note that fatigue model parameters A and B, which are intercept and slope of the line associated with the G^R approach, were calculated using equations that are different from those in AASHTO TP 101, even though both methods employ a power function to predict binder fatigue

67

life. Considering the complexity of the calculation, an excel spreadsheet template was developed in the present study to perform data analysis for the LAS-G^R approach.

5.3 Binder Fracture Energy Test Results

The true stress-true strain curve obtained from the BFE test was used to determine binder failure limit, i.e., FED, and the results were summarized in Section 3.3.2. This section presented an alternative interpretation of the true stress-true strain curve to derive a parameter named CSR/S, which could be used to determine the binder damage rate, i.e., DCSE/cycle and consequently, the binder N_f parameter that combined binder failure limit and damage rate.

5.3.1 Complex shear modulus

The true stress-true strain curve from the BFE test can be conceptually divided into two parts: dissipated creep strain energy to failure ($DCSE_f$) and elastic energy (EE), as shown in Figure 5-13. $DCSE_f$ is the dissipated energy that damages a specimen to failure and it can be determined by subtracting EE from FED. Resilient modulus has been traditionally used in the HMA-FM model to determine the EE of asphalt mixtures; however, any predicted or measured modulus such as dynamic modulus, tangent modulus at the testing temperature and a frequency of 10 Hz is considered appropriate to calculate the EE of asphalt mixtures. In this study, the complex shear modulus ($|G^*|$) available from LAS frequency tests was employed as a substitute for elastic modulus to obtain the binder EE (Figure 5-13), following Equation 37.

$$\text{Elastic energy (EE)} = \frac{1}{2} \cdot \frac{S_t^2}{|G^*|} \tag{37}$$

where, S_t is tensile strength and $|G^*|$ is complex shear modulus.
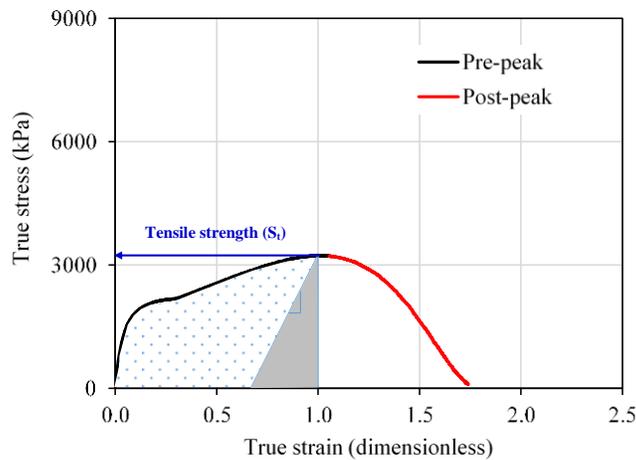
Figure 5-13. Illustration of the DCSE, EE, and FED of the PG 52-28 binder

Asphalt binder is a viscoelastic material and its complex shear modulus changes with testing temperature and loading frequency. In this study, binder complex shear modulus value obtained at its corresponding BFE testing temperatures (5°C for HP binder and 15°C for the

other four binders) and a loading frequency of 10 Hz (the same frequency used for the mixture M_R test), was employed to determine binder EE.

The G^R approach requires the frequency sweep tests of a given binder to be conducted at three different temperatures (5, 20 and 35°C) to construct a binder master curve. Figure 5-14 plots the complex shear modulus values of the PG 52-28 binder obtained at the three temperatures over a range of frequencies from 0.0159 to 15.9 Hz (0.1-100 rad/s). Although binder master curves were not used in this section, the complex shear modulus values at 10 Hz were employed to interpolate the value at the desired testing temperature (e.g., 15°C), as shown in Figure 5-15.
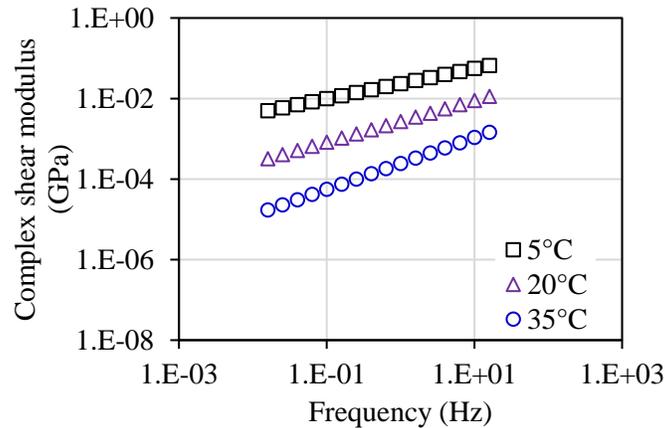
Figure 5-14. Complex shear modulus of PG 52-28 at three temperatures
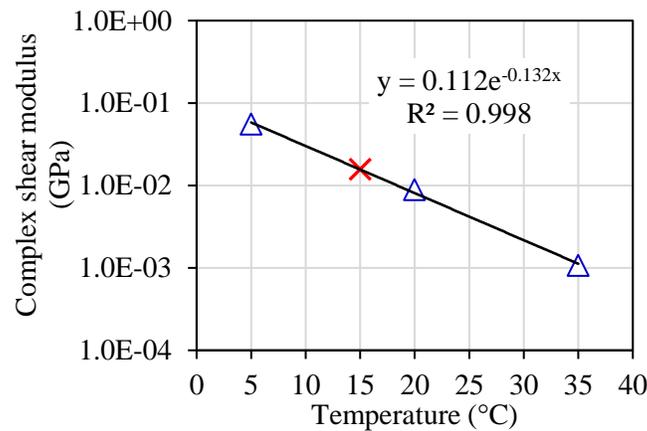
Figure 5-15. Interpolation of |G*| of PG 52-28 at 15°C and a frequency of 10 Hz

Figure 5-16 summarizes the interpolated complex shear modulus values of the six binders at 15°C and 10 Hz. Two replicates per binder type were tested and the average values were reported. As expected, stiffer unmodified binders had higher complex shear modulus. Note that PG 76-22 ARB and PG 76-22 PMA were slightly less stiff than PG 67-22, which was unexpected given that the latter is typically used as a base binder for the former. Also, the BFE

testing temperature used for HP binder was 5°C because it did not fracture at higher temperatures (10 and 15°C), so the complex shear modulus was obtained at 5°C instead of 15°C.
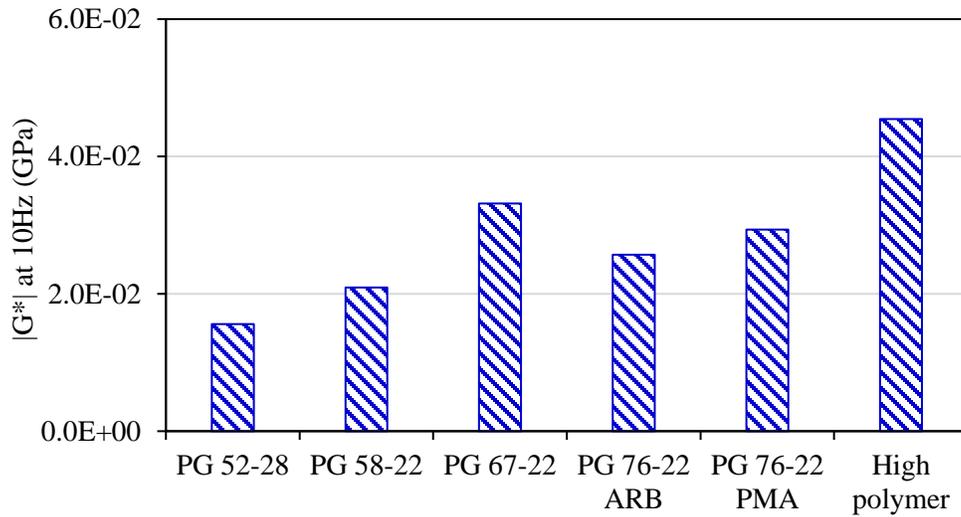
Figure 5-16. Complex shear modulus of the six binders at desired temperature conditions (5°C was used for the HP binder and the other five binder were tested at 15°C)

5.3.2 Dissipated creep strain energy to failure

Figure 5-17 plots binder tensile strength obtained as the peak true stress on the true tress-true strain curve. Four BFE specimens per binder type were tested and the average values were reported. Unmodified binders with higher performance grade exhibited greater tensile strength but they were all lower than that of PG 76-22 PMA binder. The HP binder yielded the greatest tensile strength partially due to the fact that it was tested at a lower temperature.
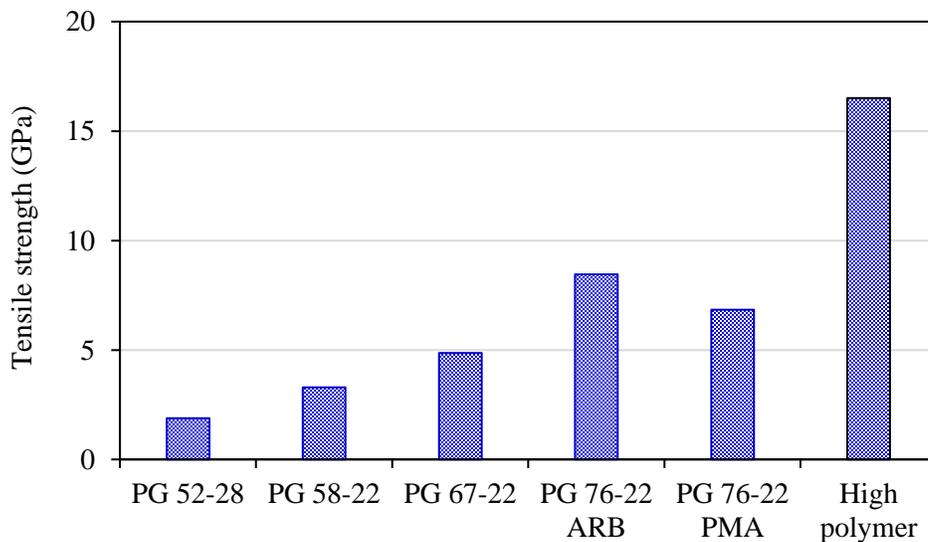
Figure 5-17. Tensile strength of six binders (standard deviation as error bar)

The elastic energy of the six binders presented in Figure 5-18 was determined following Equation 37. The lowest value was 114 kJ/m^3 for PG 52-28 whereas the greatest value was 2997 kJ/m^3 for HP binder. The effect of SBS polymer on binder EE was evident: PG 76-22 PMA has more than twice the EE of PG 67-22 binder.
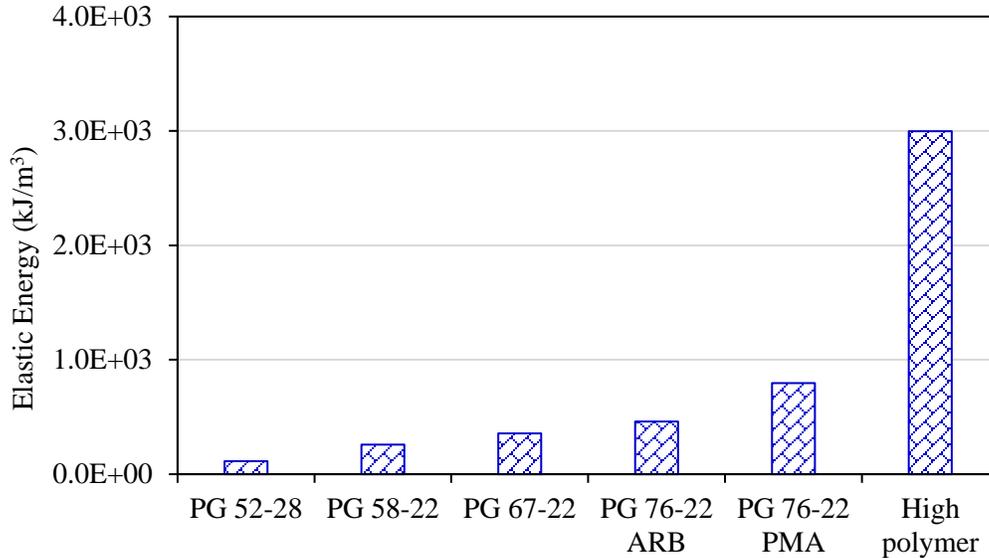
Figure 5-18. Elastic energy of six binders

DCSE$_f$ was determined by subtracting EE from FED. Figure 5-19 compares the FED and DCSE$_f$ values of the six binders. It appears that EE was almost negligible for the unmodified binders but not for the SBS polymer-modified binders, especially for HP binder with higher content of SBS polymer.
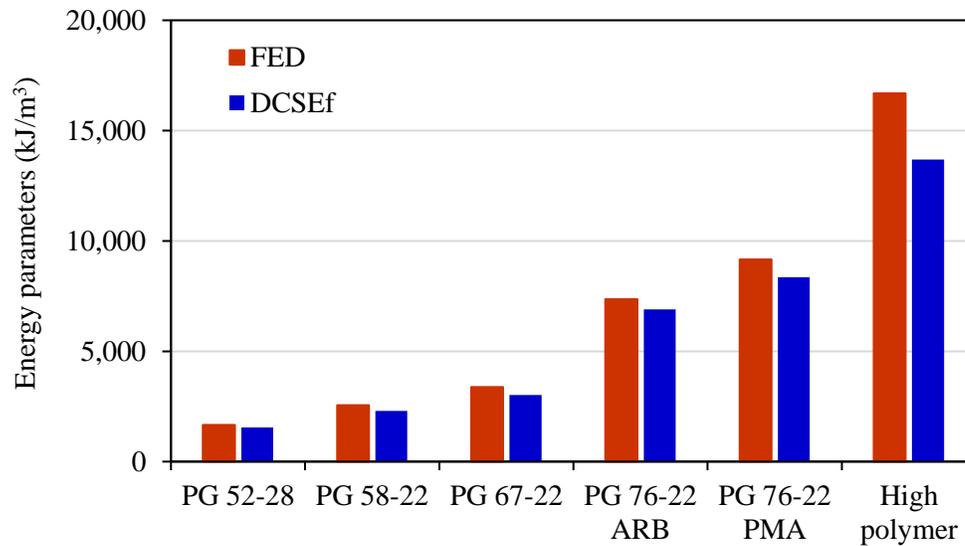
Figure 5-19. FED and DCSE$_f$ of six binders

5.3.3 Creep strain rate per unit stress

The creep strain rate per unit stress (CSR/S) parameter can be determined by using Equation 32, where the numerator $DCSE_f$ is dissipated creep strain energy to failure and the denominator is the square of the area under a fitted function to describe true stress over time (t) until failure. A sixth-order polynomial trend line was used to fit the true stress and time data (up to the true stress peak), so the area under the curve can be determined using trapezoids of equal width, as illustrated in Figure 5-20.

The plot shows true stress (kPa) versus time (s) with the polynomial fit:

$$y = 24{,}527x^6 - 94{,}009x^5 + 123{,}886x^4 - 57{,}278x^3 - 4{,}615x^2 + 10{,}591x$$
$$R^2 = 0.99$$

and the area term $\sum_{t=0}^{n} f(\sigma_t)$
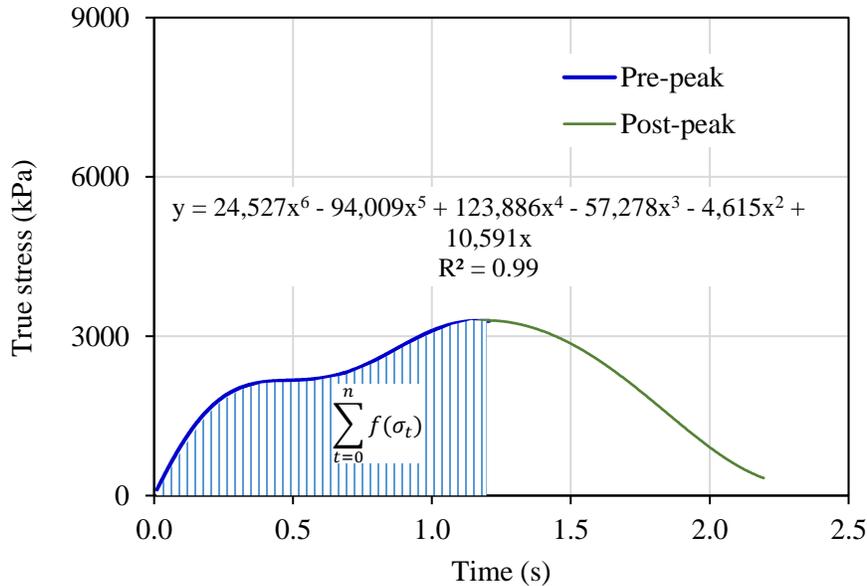
Figure 5-20. True stress versus time curve of the PG 52-28 binder

Figure 5-21 presents the CSR/S of the six binders determined following Equation 35. A greater CSR/S value indicates a faster rate of damage accumulation and vice versa. The three unmodified binders yielded comparable values with a trend of slightly lower CSR/S with increasing high temperature PG grade (stiffer binder). At the same time, there was a clear distinction between unmodified and SBS polymer-modified binders, which exhibited significantly lower CSR/S values. This general trend agrees with previous observations in asphalt mixtures: mixes with PG 76-22 ARB and 76-22 PMA yielded notably lower damage accumulation rate than mixes with PG 67-22 unmodified binder. As expected, the HP binder exhibited the lowest CSR/S value of all binders.

CSR/S values of the six binders were also calculated using binder FED instead of $DCSE_f$ as the numerator in Equation 32. The use of binder FED resulted in higher CSR/S values, with the difference being 7%, 5%, 7%, 6%, 4%, and 15% for PG 52-28, PG 58-22, PG 67-22, PG 76-22 ARB, PG 76-22 PMA, and HP binders, respectively. Nevertheless, Figure 5-22 reveals that whether binder EE was excluded or not does not change the relative ranking between the six binders. This indicates that binder EE may not be necessary for purpose of performing a relative

comparison, and thus, the BFE test alone can be used to determine both failure limit (FED) and damage rate (CSR/S) of asphalt binders at intermediate temperatures.
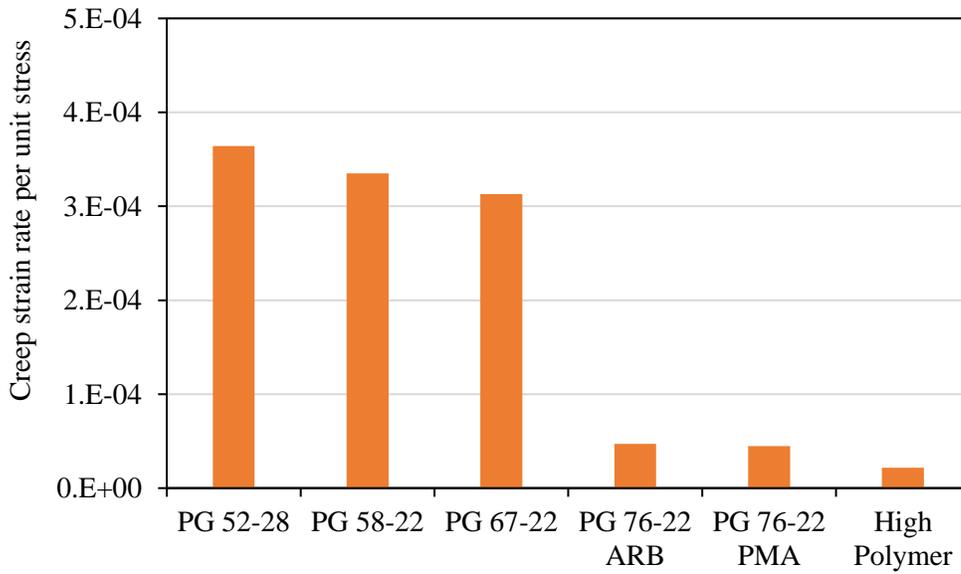
Figure 5-21. Creep strain rate per unit stress of six binders based on binder $DCSE_f$
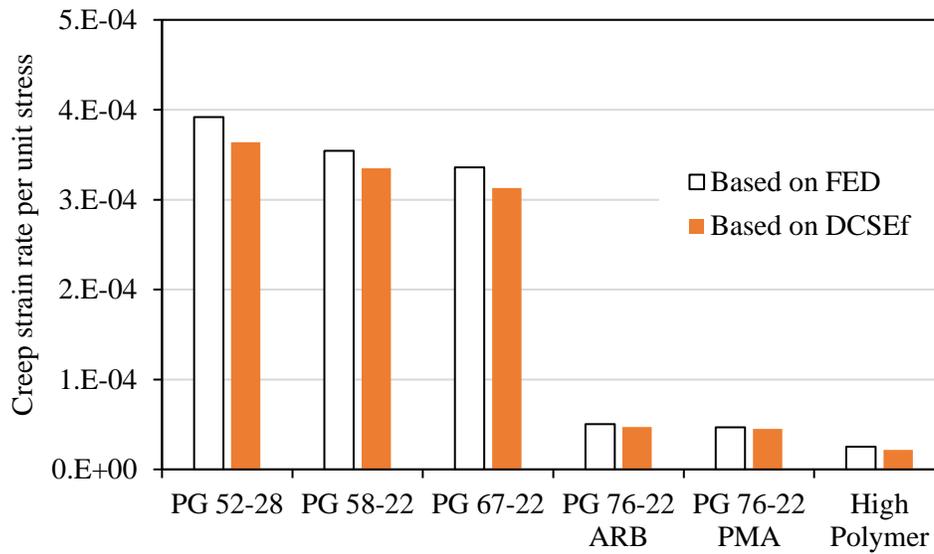
Figure 5-22. Creep strain rate per unit stress of six binders based on FED and $DCSE_f$

5.4 SUMMARY

Three versions of the LAS test (AASHTO TP 101-12, AASHTO TP 101-14, and the G^R approach) were performed to characterize binder fatigue resistance using the N_f parameter. Table

5-6 summarizes the relative ranking of the six binders based on N_f values obtained at 5% shear strain.

LAS test results following AASHTO TP 101-12, which employs a 35% reduction in $|G^*|$ as the failure indicator, does not appear to be reasonable. Florida's standard modified binder, PG 76-22 PMA, was found to be comparable to PG 58-22 and even worse than PG 52-28. The G^R approach distinguished between unmodified and SBS polymer-modified binders. Moreover, the six binders were ranked in a way that meets general expectations. The failure indicator (i.e., maximum shear stress) in AASHTO TP 101-14 also appears to be inappropriate because a plateau instead of a clear shear stress peak was observed for most binders. This may contribute to the equivalent N_f predictions for PG 76-22 PMA and PG 52-28. However, the TP 101-14 and the G^R-approach would result in the same binder ranking when the PG 52-28 was excluded. This indicates the failure indicator in AASHTO TP 101-14 may be clear enough for its data analysis.

Table 5-6. Relative ranking of six binders in terms of N_f value at 5% shear strain

Binder type	AASHTO TP 101-12		AASHTO TP 101-14		G^R approach	
	N_f at 5% strain	Relative ranking	N_f at 5% strain	Relative ranking	N_f at 5% strain	Relative ranking
PG 52-28	294	2	4276	3	2163	4
PG 58-22	102	3	974	6	1153	6
PG 67-22	34	6	1398	5	1475	5
PG 76-22 ARB	40	5	11400	2	5420	2
PG 76-22 PMA	104	4	4009	4	3541	3
High polymer	437	1	12911	1	9435	1

An alternative interpolation of the BFE true stress-true strain curve was conducted to derive a binder parameter named CSR/S. Four steps were identified and followed: 1) obtain $|G^*|$ at 15°C and a frequency of 10 Hz, 2) obtain binder EE, 3) determine binder $DCSE_f$, 4) compute CSR/S, which governs the binder DCSE/cycle. Three unmodified binders yielded comparable values with a trend of slightly lower CSR/S with increasing high temperature PG grade (stiffer binder). Moreover, a clear distinction was observed between unmodified and modified binders, which exhibited significantly lower CSR/S values. Both observations agree with previous findings on mixture studies. Finally, the relative ranking of the six binders in terms of the CSR/S was not changed when binder FED was used as a substitute for $DCSE_f$. This indicates that the aforementioned steps 1, 2 and 3 can be eliminated and the BFE test alone may be sufficient to determine both binder failure limit and damage rate.

CHAPTER 6 MIXTURE EVALUATION

6.1 Introduction

This chapter summarized the fracture properties of asphalt mixtures obtained by performing Superpave IDT tests. Twelve dense-grade Superpave mixtures were evaluated, corresponding to two mixture designs (one for GA granite and one for FL limestone) and six asphalt binders (PG 52-28, PG 58-22, PG 67-22, PG 76-22 ARB, PG 76-22 PMA, and HP). Mixtures of the same aggregate type were designed to have the same gradation and Superpave volumetrics but different binder types. A complete set of Superpave IDT tests includes the resilient modulus test, the tensile creep test, and the tensile fracture test. Fracture energy density (FED), damage rate (dissipated creep strain energy per loading cycle, DCSE/cycle) and a cracking performance indicator (i.e., number of cycles to failure, N_f) that considers both mixture FED and damage rate, were compared for different binder types.

The correlation between binder and mixture cracking performance at intermediate temperatures was also evaluated. Two binder tests were used for this purpose: the linear amplitude sweep (LAS) test and the binder fracture energy (BFE) test, which were identified in Chapter 3 as candidates to characterize binder cracking performance.

Three variants of the LAS test with different failure definition were conducted in Task IV. The AASHTO provisional standard (TP 101-14) and the G^R approach by Wang et al. (2015) were found to provide the similar ranking of binder cracking performance based on N_f results. For research purpose, binder N_f results obtained from the LAS-G^R approach were used to evaluate correlation with mixture N_f results.

Two binder parameters obtained from the BFE test were reported in Chapter 5, including binder FED and damage rate. Binder FED values were determined by performing the BFE test following the AASHTO provisional standard (TP 127-17), whereas binder damage rate results were determined by performing an alternative analysis of the binder true stress-true strain curves obtained from BFE tests. Binder cracking performance was quantified by using BFE binder N_f parameter, which combines the binder FED and damage rate. This chapter examined the correlations between asphalt binder and mixture results in terms of fracture properties and relative cracking performance. More details about the BFE binder N_f parameter can be found in Appendix II.

6.2 Mixture Results

For convenience, mixtures in the following paragraphs were named after the binder type, e.g., a mixture with PG 67-22 binder was called PG 67-22 mixture. The thickness and air void content of Superpave IDT specimens were within the target range of 1.5±0.1 inch and 7±0.5%, respectively. A total of 36 mixture specimens were tested, which comprised three replicates for each set of Superpave IDT tests. Raw data from Superpave IDT tests were analyzed using software named ITLT to determine mixture properties. Information on Superpave IDT specimens can be found in Appendix III and the analyzed mixture results can be found in Appendix IV.

6.2.1 Georgia granite mixtures

Tensile strength and failure strain of granite mixtures obtained from Superpave IDT tensile fracture tests are presented in Figure 6-1 and Figure 6-2, respectively. Among the three unmodified binders, the softer binder resulted in a more ductile mixture with lower tensile strength but greater failure strain. Mixtures with PG 67-22 and PG 76-22 PMA exhibited similar tensile strength and failure strain. Note that PG 67-22 binder is commonly used as the base binder for the two modified binders in Florida. This indicates that relatively low content (i.e., less than 3%) of SBS polymer has negligible effect on tensile strength and failure strain of granite mixtures. Conversely, the HP binder, which contains more than 7% SBS polymer, notably increased mixture tensile strength with respect to PG 52-28, which is commonly used as the base binder in the production of HP binder.
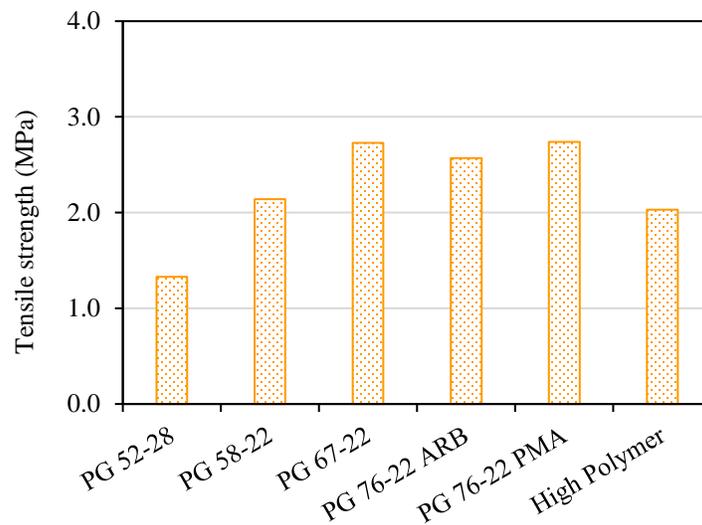
Figure 6-1. Tensile strength of granite mixtures
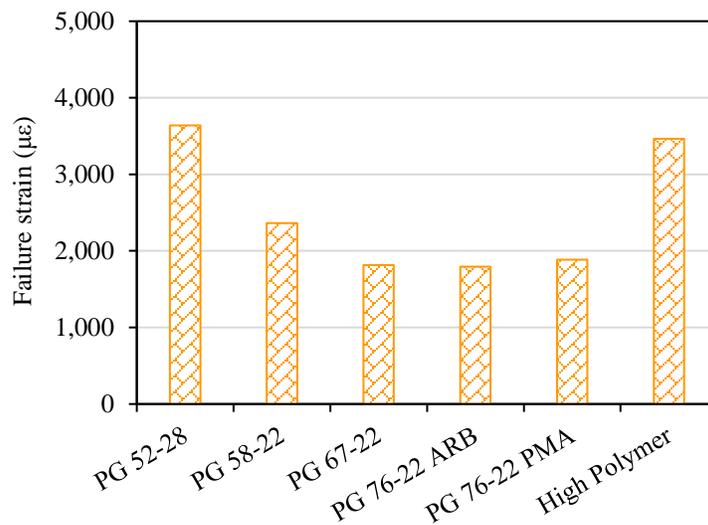
Figure 6-2. Failure strain of granite mixtures

Figure 6-3 depicts the FED values of six granite mixtures obtained from the Superpave IDT tensile fracture test. FED describes the damage tolerance of a mixture before fracture occurs and is employed as an energy threshold or failure limit in the hot mix asphalt-fracture mechanics (HMA-FM) model. Mixtures with the three unmodified binders and the two modified binders exhibited similar FED values of approximately 3.5 kJ/m^3, indicating the FED parameter is not sensitive to the change in binder stiffness or to the use of lower SBS polymer content included in this study. The HP binder, which has higher SBS polymer content, yielded the greatest mixture FED value of 5.0 kJ/m^3.
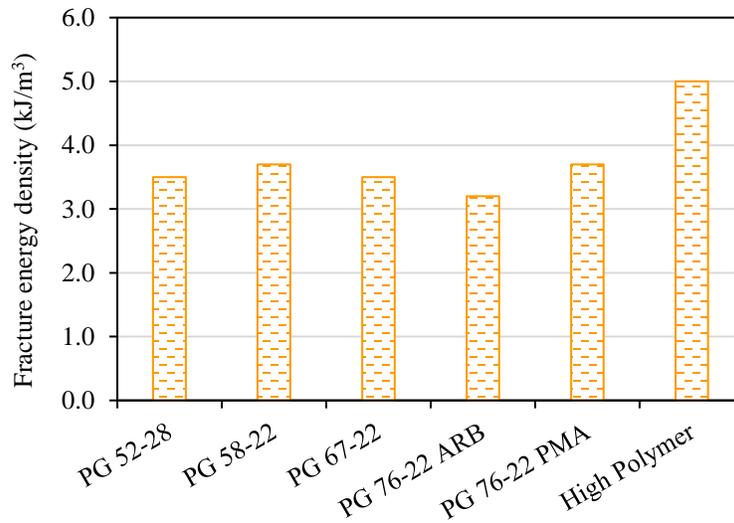
Figure 6-3. Fracture energy density of granite mixtures

The damage rate of an asphalt mixture under repeated load applications is defined as the dissipated creep strain energy density accumulated per load cycle (DCSE/cycle). The input parameters for determination of mixture DCSE/cycle can be estimated from a 1,000-s Superpave IDT tensile creep test. However, a longer testing time was found to be necessary to isolate the viscous response of HP mixtures. A 7,000-s tensile creep test was found sufficient to accurately obtain the damage rate of HP mixtures. More details are provided in Appendix V.

Figure 6-4 presents the damage rate of six granite mixtures. The softest binder (i.e., PG 52-28) resulted in the highest mixture damage rate (7.8 E-03 kJ/m^3), which is two orders of magnitude greater than that of the HP mixture. This value appears to be excessively high, indicating that the current testing protocol may not applicable to extremely soft unmodified binders. It is emphasized that PG 52-28 is used in Florida only in mixtures with high content (≥30% by weight of aggregate) of reclaimed asphalt pavement. In other words, evaluating the cracking performance of a virgin mixture with PG 52-28 binder at intermediate temperatures may not have a practical value in Florida.

Therefore, the PG 52-28 mixture was excluded from Figure 6-4 to better compare damage rate results of the other five granite mixtures. Figure 6-5 shows the DCSE/cycle parameter differentiates between the other six binders: regular modified binders resulted in lower mixture damage rates than unmodified binders and the use of a higher SBS polymer content (i.e.,

the HP binder) further reduced the mixture damage rate. It appears that the main benefit of using SBS polymer modified binder in a mixture is reduction in mixture damage rate.
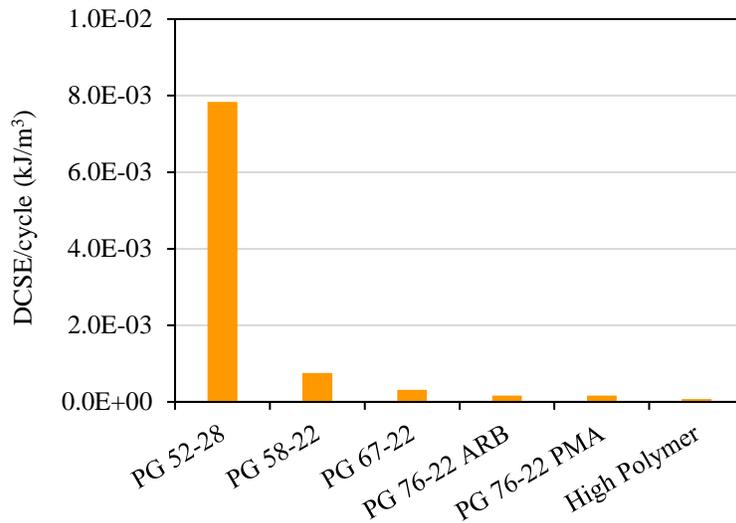
Figure 6-4. Damage rate of granite mixtures
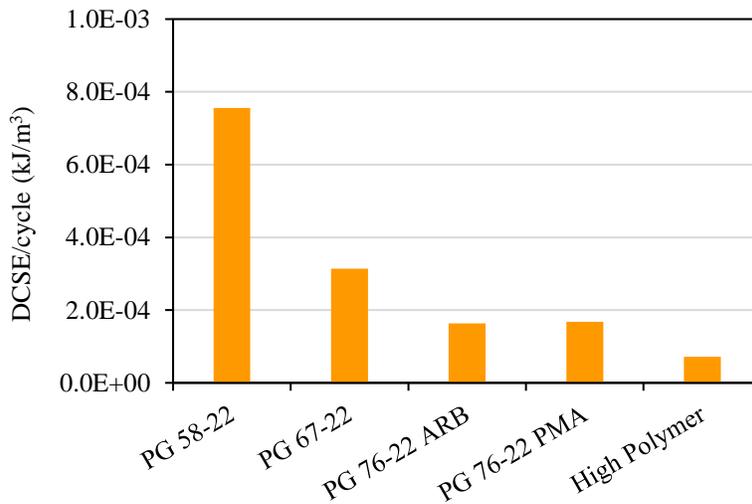
Figure 6-5. Damage rate of granite mixtures excluding PG 52-28 mixture

Figure 6-6 presents the number of cycles to failure (N_f) results of the six granite mixtures obtained by dividing FED by damage rate. In general, the greater the N_f values the better mixture relative cracking performance. The N_f value of PG 52-28 mixture was excessively low (almost invisible on the chart), mainly due to its unreasonably high damage rate. The N_f value of the PG 76-22 PMA mixture was about 15% greater than that of the PG 76-22 ARB mixture, and importantly, both were at least twice that of the mixtures with unmodified binders. The HP mixture had the greatest N_f value (almost three times that of the two conventional modified binders), indicating superior mixture cracking performance.
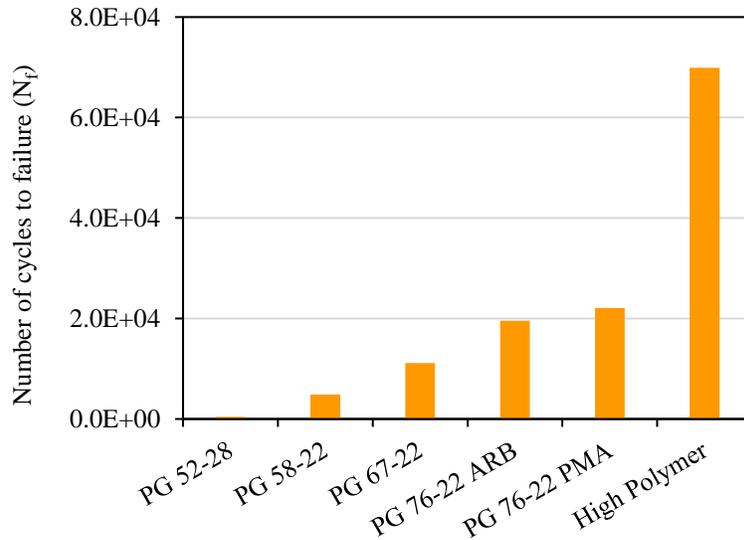
Figure 6-6. Number of cycles to failure for granite mixtures

6.2.2 Florida limestone mixtures

Figure 6-7 and Figure 6-8 show tensile strength and failure strain of Florida limestone mixtures, respectively. As expected, the use of softer unmodified binders resulted in mixtures with lower tensile strength but higher failure strain values. Among the three unmodified binders, the PG 52-28 yielded slightly higher FED than the other two binders, as shown in Figure 6-9. Compared to PG 67-22 mixture, PG 76-22 PMA and PG 76-22 ARB mixtures showed improvement in mixture tensile strength and failure strain. As a result, FED values were higher than that of the PG 67-22 mixture. The HP mixture exhibited the greatest FED value (3.5 kJ/m^3), substantiating the effectiveness of using higher content of SBS polymer in improving mixture fracture tolerance.
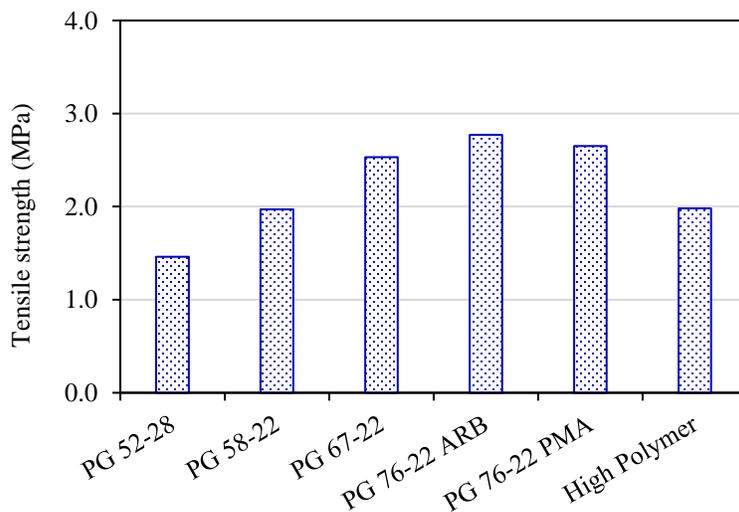
Figure 6-7. Tensile strength of limestone mixtures

79
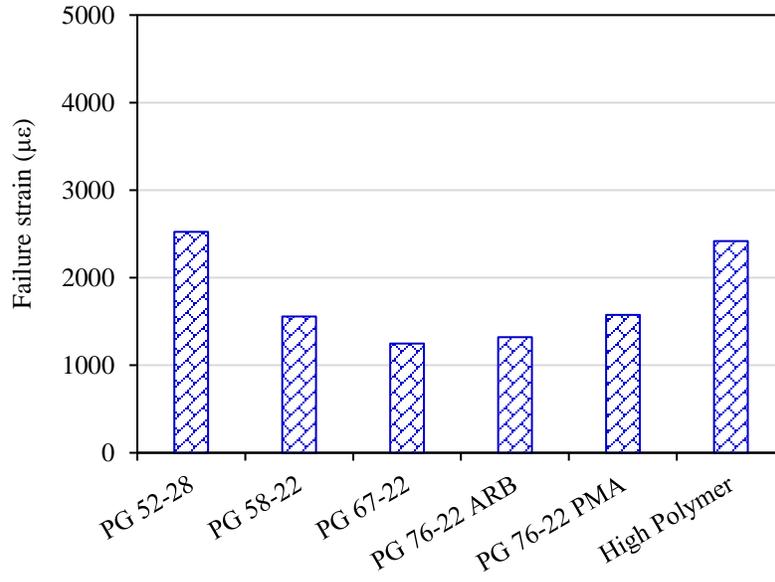
Figure 6-8. Failure strain of limestone mixtures

Figure 6-9 also reveals that limestone mixtures yielded lower failure limit (i.e., equivalent tensile strength, lower failure strain and consequently, lower FED) than granite mixtures regardless of binder type. This is primarily due to the weaker Florida limestone, which is often manifested as fracture through the coarse limestone aggregates instead of through the mastic as in the case of granite mixtures. The three modified binders, particularly HP binder, yielded greater FED than mixtures with unmodified binders.
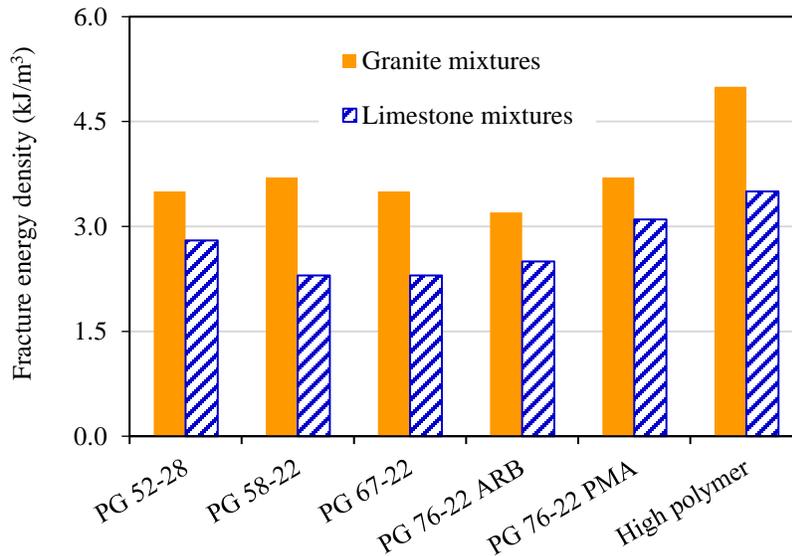
Figure 6-9. Fracture energy density of limestone and granite mixtures

Figure 6-10 shows DCSE/cycle values of five limestone mixtures as well as the results of granite mixtures. In general, mixtures with modified binders had notably lower damage rate than mixtures with unmodified binder. The PG 76-22 PMA mixture had the DCSE/cycle value of 6.4E-05 kJ/m^3, which is the highest value among the three modified mixtures. Nevertheless, the value is only about 20% and 60% of the value for PG 58-22 and PG 67-22 mixtures, respectively. The PG 52-28 mixture had a DCSE/cycle value of 1.3E-03 kJ/m^3, which is about 20 times greater than that of the HP mixture. This value is believed to be unreasonably high, so it was excluded from the mixture damage rate comparison.
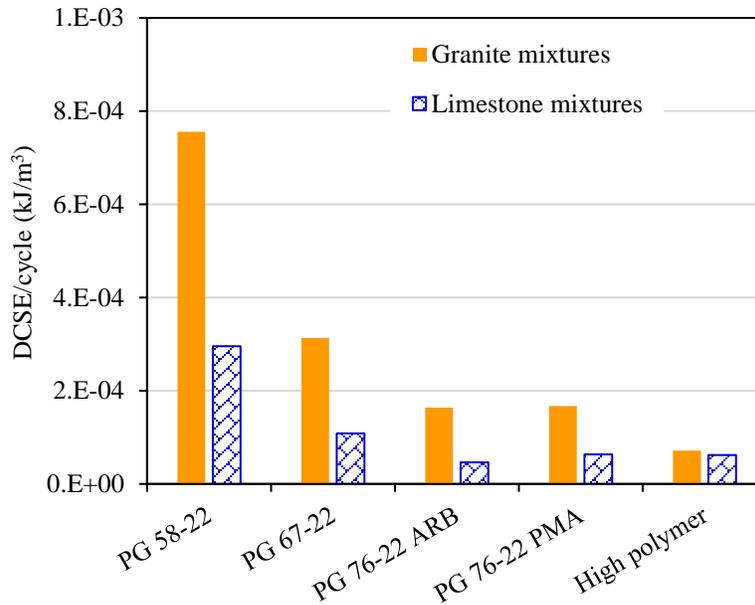
Figure 6-10. DCSE/cycle of limestone and granite mixtures (excluding the PG 52-28 mixture)

Surprisingly, the damage rate of the HP mixture was about the same as that of the PG 76-22 PMA mixture. Regardless of binder type, FL limestone mixture had lower damage rate than granite mixture, as shown in Figure 6-10. This may be explained by the fact that limestone aggregates have much rougher surface texture and are more porous than granite aggregates, which reduces creep compliance relative to smoother, less porous granite aggregate (Roque et al. 2015). Also, there appeared to be a lower limit of mixture damage rate (i.e., approximately 6E-05 kJ/m^3/cycle), where no further reduction was achieved by increasing the SBS polymer content.

Figure 6-11 shows N_f values of the six limestone mixtures. Mixtures with unmodified binder had notably lower N_f values than modified mixtures, mainly due to their relatively high damage rates. Stiffer binder yielded less fracture tolerant mixture (i.e., higher tensile strength, lower failure strain and lower fracture energy) but also resulted in lower mixture damage rate. As a result, PG 67-22 outperformed PG 58-22, and the worst performer was the PG 52-28 mixture. The three modified binders yield similar mixture N_f values. The N_f value of HP limestone mixture, despite being three times greater than that of the best unmodified performer, was only about 4% and 15% greater than that of the mixtures with the PG 76-22 ARB and PG 76-22 PMA binders, respectively.
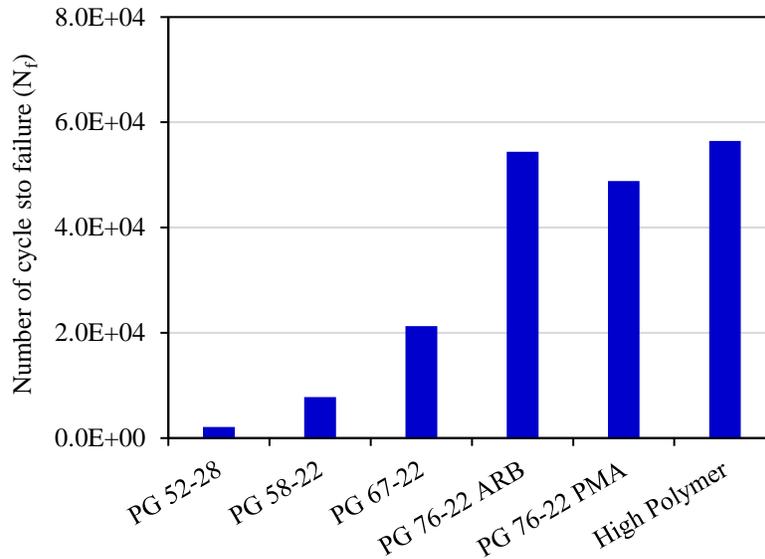
Figure 6-11. Number of cycles to failure for six limestone mixtures

6.3 Correlations between Binder and Mixture Results

Comparisons between properties and performance of binders and mixtures were made at equivalent specimen conditioning levels. All binders went through the rolling thin film oven test and the pressure aging vessel test, which simulate plant and field aging, respectively. Meanwhile, all mixtures were subjected to oxidative aging only, i.e., short-term oven aging plus long-term oven aging. Moisture and micro-damage effects, which can be simulated by using the cyclic pore pressure conditioning (CPPC) system, are considered mixture effects related to the air void structure of a mixture, so it cannot be captured by binder test. Therefore, the CPPC test was not performed on mixture specimens in this study.

Binder results obtained from the LAS test and BFE test were normalized with respect to that of PG 67-22 binder, and similarly, mixture results from Superpave IDT results were normalized with respect to that of PG 67-22 mixture. The PG 67-22 binder was selected as the benchmark because: 1) mixture results associated with PG 67-22 and PG 76-22 PMA have been validated by field performance data in Florida and 2) the relative improvement in mixture N_f values achieved by using PG 76-22 PMA with respect to PG 67-22 can be used as a scale to evaluate the effectiveness of the two binder N_f parameters obtained from the LAS and BFE tests.

6.3.1 Linear amplitude sweep test – G^R approach

Figure 6-12 displays the normalized N_f values of asphalt binder and granite mixture. There was generally good agreement between PG 58-22, PG 76-22 PMA and HP binder and corresponding granite mixture. PG 76-22 ARB outperformed PG 76-22 PMA at binder level but not at mixture level. PG 76-22 ARB is a hybrid binder containing low (or none) SBS polymer content plus more than 7% rubber. Of note, binder tests with the parallel plate geometry like the

LAS test are known to be problematic in characterizing rubber modified binder, making the relatively high N_f value of the PG 76-22 ARB binder questionable.
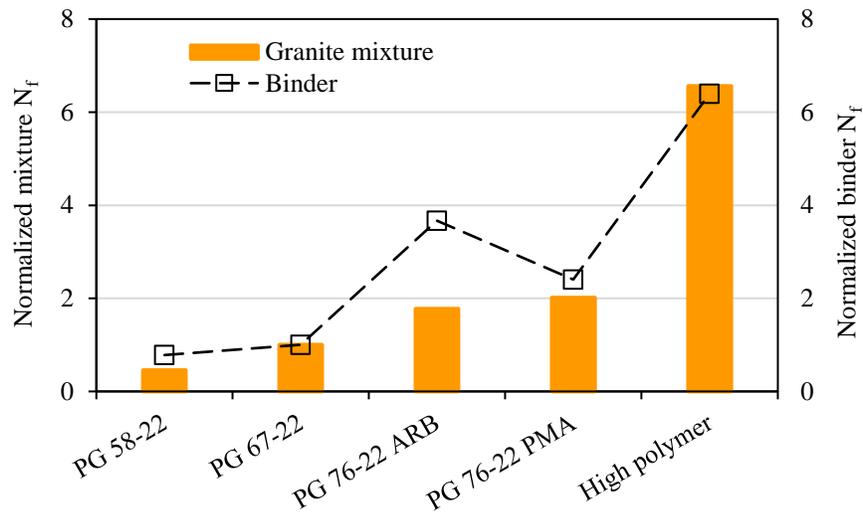
Figure 6-12. Correlation in normalized N_f values between binder and granite mixtures

Figure 6-13 compares normalized N_f for asphalt binder and limestone mixture. The ranking established by the LAS-G^R approach agreed with Superpave IDT mixture results. However, the difference in relative N_f of the three modified mixtures is not as significant as that of the three modified binders. This indicates that characterizing binder alone may not be sufficient to predict mixture cracking performance. Effects of aggregate type (e.g., rough porous nature of the FL limestone aggregate) on mixture cracking performance may sometimes overwhelm effect of asphalt binder type.
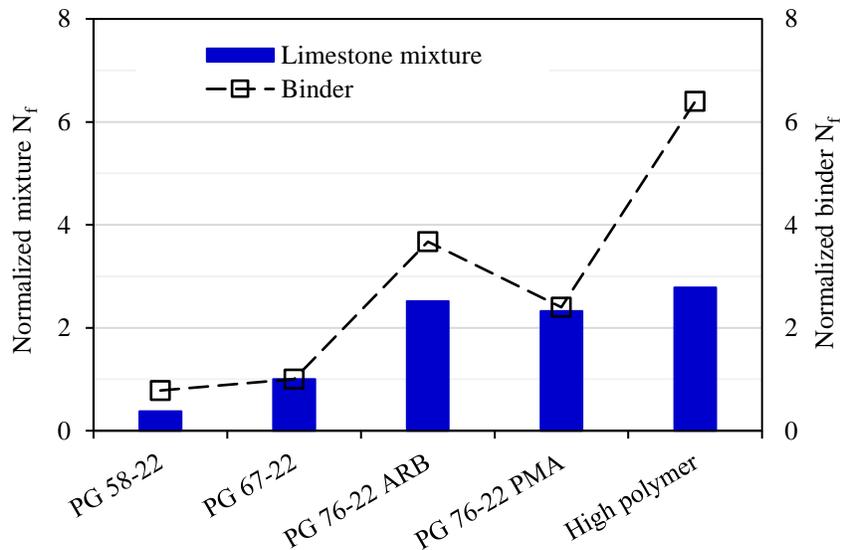
Figure 6-13. Correlation in normalized N_f values between binder and limestone mixtures

6.3.2 Binder fracture energy test

Binder FED values obtained from the BFE test were normalized with respect to that of PG 67-22 binder. Similarly, mixture FED results determined by performing the Superpave IDT tensile fracture test were normalized with respect to that of the PG 67-22 mixture. Figure 6-14 shows that the FED parameter differentiates asphalt binders: softer binders exhibited lower FED values and polymer modification notably increased binder FED. More specifically, the higher the polymer content, the greater the binder FED value. However, the rise in binder FED associated with the presence of SBS polymer was not proportionally reflected in mixture FED results. FED values of the PG 76-22 ARB mixture and PG 76-22 PMA mixture were about the same as that of the PG 67-22 mixture. HP binder, with a binder FED almost 5 times greater than that of PG 67-22 binder, yielded only a 40% increase in mixture FED value. It appears that mixture factors such as aggregate type, gradation characteristics, and air void structure overwhelmed the impact of asphalt binder on mixture FED. The same observation was made when correlating normalized binder FED with the normalized FED of limestone mixtures, as shown in Figure 6-15.

The damage rate of asphalt binders and mixtures was also normalized with respect to that of the PG 67-22 binder and mixture, respectively. Figure 6-16 plots the normalized damage rate values of five asphalt binders and the associated granite mixtures. The impact of SBS polymer is manifested as a reduction in damage rate, both at binder and mixture levels. HP binder, which contains the highest content of SBS polymer among the three modified binders, exhibited the lowest binder damage rate and yielded the lowest mixture damage. Results of PG 52-28 binder were not included due to the uncertainty about the significance of its damage rate.
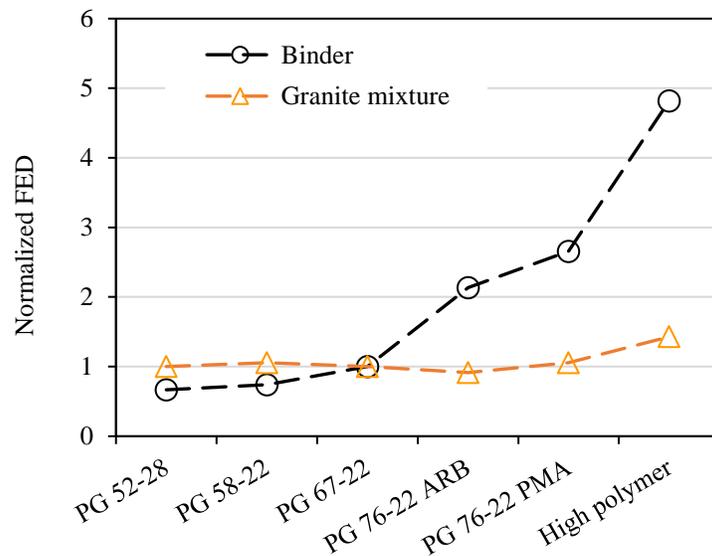
Figure 6-14. Correlation between normalized binder FED and granite mixture FED results
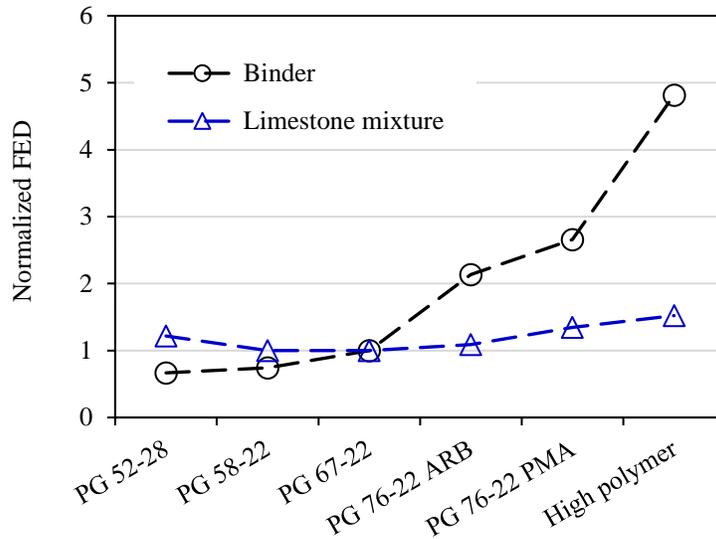
Figure 6-15. Correlation between normalized binder FED and limestone mixture FED results
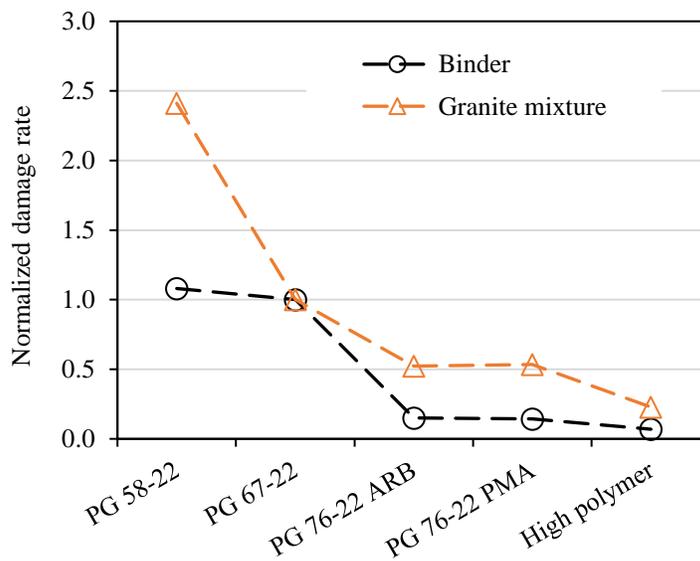
Figure 6-16. Correlation in normalized damage rate of binders and granite mixtures

Figure 6-17 plots the normalized damage rate of five asphalt binders and the associated limestone mixtures. There is generally good agreement in damage rate between asphalt binders and limestone mixtures. The three modified limestone mixtures exhibited similar rate of damage accumulation and importantly, they were all notably lower than that of the unmodified limestone mixtures.
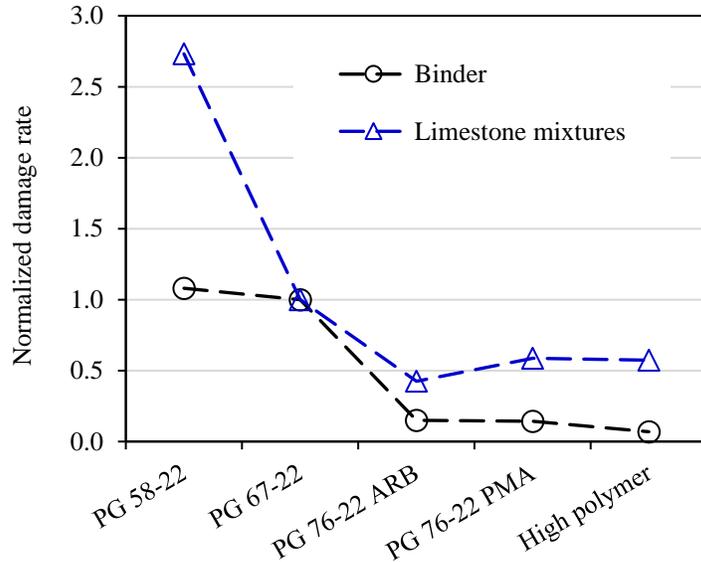
Figure 6-17. Correlation in normalized damage rate of binders and limestone mixtures

Relative cracking performance of asphalt binder and mixture was characterized using the BFE binder N_f and mixture N_f parameters, respectively. Both N_f parameters were determined following the principles of the HMA-FM model that failure limit (FED) and damage rate (DCSE/cycle) shall be considered together to predict fracture.

Figure 6-18 shows that BFE binder N_f parameter accurately captured the effect of SBS polymer modification on mixture cracking performance. However, the difference in Nf between unmodified and modified binders was significantly greater (almost 10 times) than the difference between the unmodified and modified mixtures. For example, the N_f of HP mixture was 6.5 times greater than the PG 67-22 mixture but the same ratio between the HP and PG 67-22 binder was 65. In other words, the BFE binder N_f parameter either underestimates effects of unmodified binder or overestimates effect of modified binder.
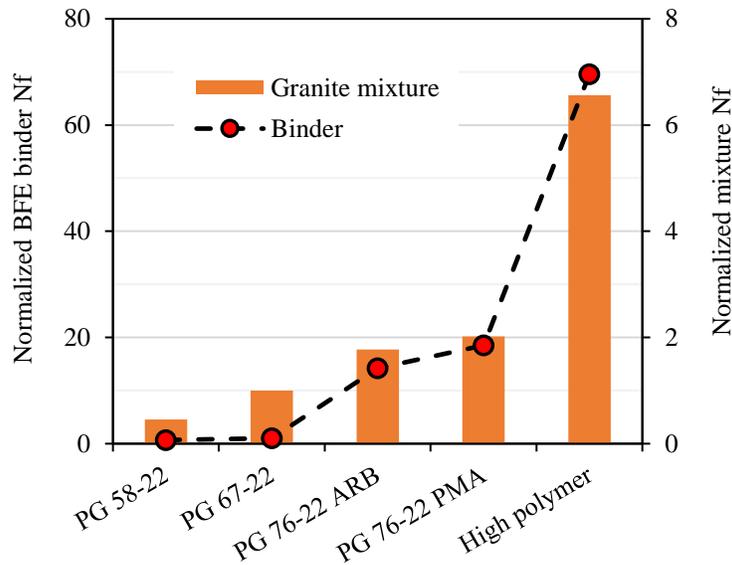
Figure 6-18. Comparison of normalized BFE binder N_f and normalized granite mixture N_f results
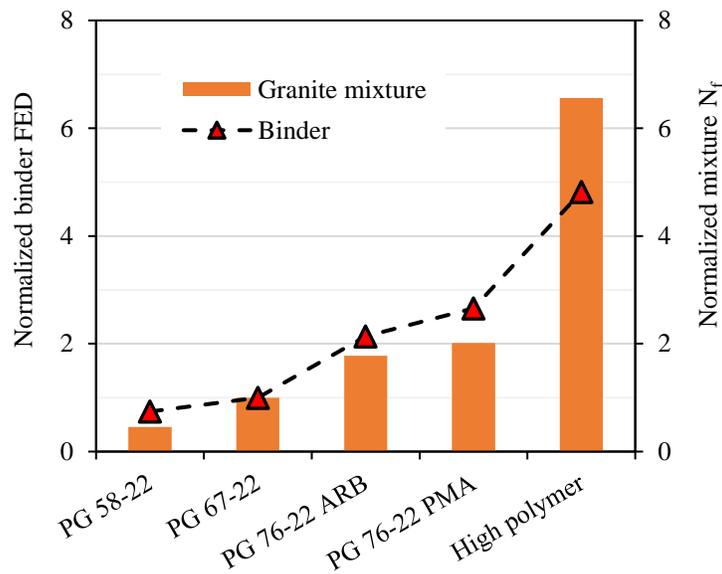
Figure 6-19. Comparison of normalized binder FED and normalized granite mixture N_f results

Figure 6-19 presents normalized binder FED values and normalized N_f results of granite mixtures. Interestingly, binder FED appears to be as good or better parameter than BFE binder N_f in correlating binder and mixtures cracking performance. Of note, SBS polymer, which improved both binder failure limit and damage rate, was found to only affect mixture damage rate. Therefore, binder FED parameter, which is inversely related to the binder damage rate, appeared to be at least as good an indicator of mixture cracking performance as BFE binder N_f.

Evaluation of correlation between binders and limestone mixtures was performed. Figure 6-20 shows a relatively weak correlation between the normalized BFE binder N_f and normalized mixture N_f values. This is because the effect of limestone aggregate overwhelms the impact of SBS polymer on mixture damage rate as well as the mixture cracking performance. An improved correlation was observed between binder FED and mixture N_f results, as shown in Figure 6-21.
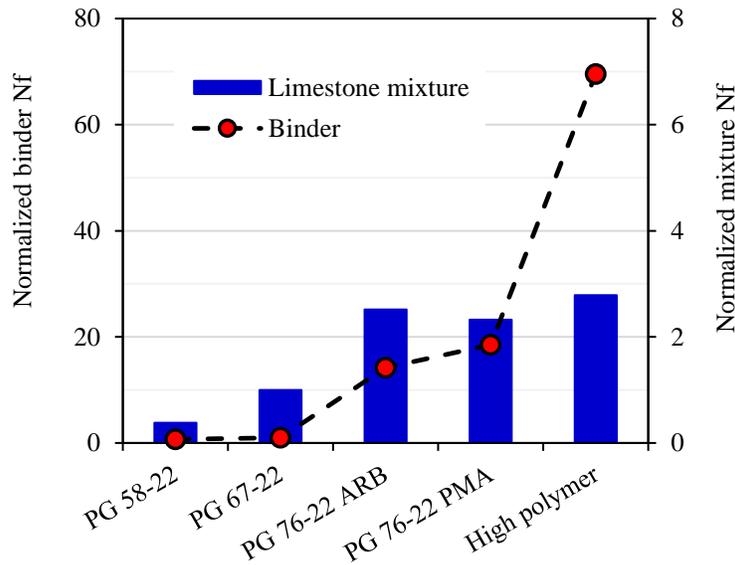
Figure 6-20. Comparison of normalized BFE binder N_f and normalized limestone mixture N_f results
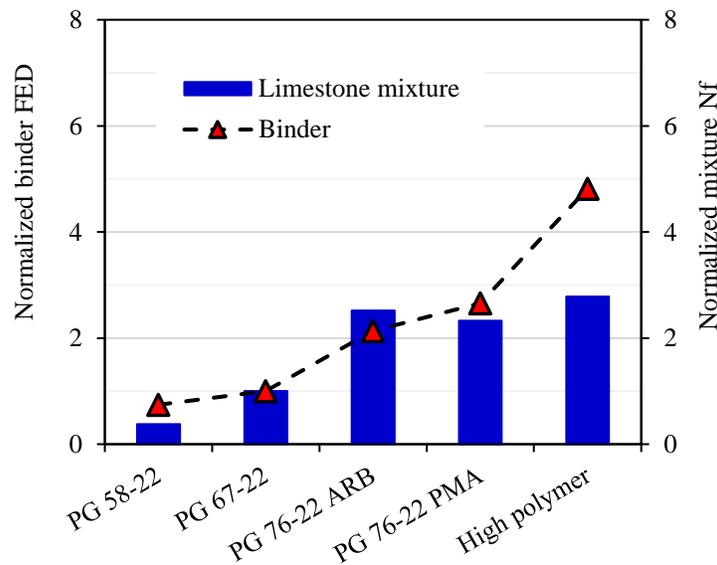
Figure 6-21. Comparison of normalized binder FED and normalized limestone mixture N_f results

6.4 Summary

In summary, this chapter documented the fracture properties and performance of asphalt mixtures as determined from Superpave IDT tests. FL limestone mixtures were found to have both lower failure limit and damage rate than GA granite mixtures, resulting in better relative cracking performance as indicated by the mixture N_f parameter. Relatively little difference was observed in FED between mixtures with unmodified and modified binders. However, significant reduction in mixture damage rate was achieved by the modified binders, especially the HP binder. Consequently, mixtures with modified binders had greater N_f values than mixtures with unmodified binders, regardless of the aggregate types.

There is a good correlation between binder N_f parameter obtained from the LAS test-G^R approach and mixture N_f parameter determined based on Superpave IDT tests, except for PG 76-22 ARB. This discrepancy may be associated with the inadequacy of parallel plate binder tests (e.g., the LAS test) in characterizing asphalt binders containing rubber particles.

SBS polymer modification appeared to increase binder FED but had no influence on mixture FED. However, SBS polymer reduced the damage rate of both asphalt binder and mixture. As a result, the difference in cracking performance of unmodified and modified binders depicted by the BFE binder N_f parameter were not proportionally reflected on the corresponding mixture N_f results. The binder FED, which was found to be inversely related to binder damage rate, more accurately captured the effect of binder type on mixture cracking performance.

CHAPTER 7 CLOSURE

7.1 Summary and Findings

The major objective of this research was to identify a binder parameter to effectively characterize binder cracking performance at intermediate temperatures. Based on literature review, the LAS test and the BFE test were identified as candidate binder tests. A laboratory experimental plan was developed, including six asphalt binders and twelve asphalt mixtures of two aggregate types. Two versions of the LAS with three different failure definitions were employed to characterize the binder resistance to fatigue damage. Moreover, the BFE test in its existing form was performed to determine the binder failure limit (FED) and additionally, an alternative interpretation of the true stress-true strain curve was proposed in this study to obtain the binder damage rate. The BFE binder N_f parameter that integrates binder FED and damage rate was used to evaluate the relative cracking performance of asphalt binders. Fracture properties of the twelve mixtures were determined by performing the Superpave IDT tests. The relative cracking performance of asphalt mixtures was evaluated by using the mixture N_f parameter, which was determined based on mixture failure limit and damage rate. Correlations between binder and mixture results were examined in terms of fracture properties and relative cracking performance. The main findings based on results of laboratory testing are listed below:

7.1.1 Binder testing results

- The standard rheometer was incapable of providing accurate strain control (either stepwise or linearly increased strain load) as required for the LAS test.

    o The erratic trend in strain output was more pronounced for modified binders than for unmodified binders.

    o A software upgrade (i.e., TruStrain for Anton Parr Rheometer) was necessary for performing the LAS test.

- Fatigue failure indicator (i.e., 35% reduction rule) in the LAS provisional standard TP 101-12,16,18 is not appropriate.

    o The 35% reduction rule was empirical, and it was listed in the TP 101 by mistake. A call for correction was made by researchers of this study to the preparers of TP 101.

- Fatigue failure indicator (i.e., maximum shear stress) in the LAS provisional standard TP 101-14 was found to be unclear on the shear strain versus shear stress curve.

    o Most binders in this study exhibited a stress plateau instead of a clear stress peak. As a result, the PG 52-28 had greater N_f value to that of the PG 76-22 PMA binder.

- A revised LAS test that employs an energy-based definition of fatigue failure (i.e., the maximum PSE) appeared to suitably characterize the binder damage resistance.

- The failure indicator (stored PSE peak) of the HP binder was less clear than the other five binders but may be clear enough to determine the N_f parameter.
- The revised LAS differentiated between unmodified and modified binders, and five of the six binders (excluding the PG 76-22 ARB) were ranked in a way that meets general expectations.

- The LAS test with the maximum shear as the failure indicator ranked the six binders in a way similar to that by the LAS-G^R approach, especially when PG 52-28 was excluded.

- The BFE test provided accurate and consistent determination of the FED of the same six binders previously tested with the LAS test.

  - Binder FED results differentiated between unmodified, polymer-modified, hybrid and heavily polymer-modified binders.

- An alternative interpolation of the BFE true stress-true strain curve was proposed and performed to derive a binder parameter (CSR/S) that is directly related to binder damage rate (DCSE/cycle).

  - The three unmodified binders yielded comparable values with a trend of slightly lower CSR/S with increasing high temperature PG grade (stiffer binder).
  - A clear distinction in CSR/S was observed between unmodified and SBS modified binders, which exhibited significantly lower CSR/S values.
  - The relative ranking of the six binders in terms of the CSR/S was not changed when binder FED was used as a substitute for the $DCSE_f$, which indicated the BFE test alone may be sufficient to determine both binder failure limit and damage rate.

- Binder FED was found to be inversely related to binder damage rate.

  - A binder with higher FED also exhibited lower damage rate.
  - SBS polymer not only increased binder FED but also reduced binder damage rate.

7.1.2 Mixture testing results

- FL limestone mixtures were found to outperform the GA granite mixtures in terms of relative cracking performance.

  - FL limestone mixtures exhibited similar tensile strength but lower failure strain than those of GA granite mixtures, resulting in lower FED values.
  - Conversely, FL limestone mixtures yielded notably lower damage rate values than those of GA granite mixtures, potentially due to the fact that limestone aggregate had much rougher surface texture and are more porous than granite aggregate.
  - Overall, FL limestone mixtures exhibited greater mixture N_f values than those of GA granite mixtures, indicating better relative cracking performance.

- Regardless of aggregate type, mixtures with modified binders had greater N_f values than mixtures with unmodified binders, indicating better cracking performance.

  o Relatively little difference in FED was observed between mixtures with unmodified and modified binders, except that the HP binder which had the greatest binder FED value also resulted in the greatest mixture FED value.

  o Damage rate parameter appeared to be the factor that dominates the crack performance of mixtures with different binders: modified binders resulted in lower mixture damage rates than unmodified binders, and the use of a higher SBS polymer content (i.e., the HP binder) further reduced the mixture damage rate.

- The 1,000-s Superpave IDT tensile creep test was found to inadequately characterize the damage accumulation of mixtures with an extremely soft unmodified binder (PG 52-28) and the heavily polymer-modified (HP) binder.

  o The 1,000-s creep test was found to be sufficient to isolate the viscous response of common asphalt mixture at intermediate temperatures associated with fatigue cracking; however, longer testing time of 7,000-s was found to be necessary to separate the viscous response and delayed elastic response of the HP mixture.

  o Mixture with the PG 52-28 binder exhibited excessively high damage rate. More research is needed to further explain this observation, although evaluating the cracking performance of a virgin mixture with PG 52-28 binder at intermediate temperatures may not have a practical value in Florida.

7.1.3 Correlation between binder and mixture results

- There is a fairly good correlation between binder N_f parameter obtained from the LAS-G^R approach and mixture N_f determined based on Superpave IDT tests.

  o The only exception was the PG 76-22 ARB which outperformed the PG 76-22 PMA at binder level but not at mixture level. This discrepancy may be associated with the inadequacy of parallel plate binder tests including the LAS test in characterizing asphalt binders containing rubber particles.

- The BFE binder N_f parameter satisfactorily ranked the six binders; however, in terms of quantitatively evaluation, the binder FED, which was found to be inversely related to binder damage rate, more accurately captured the effect of binder type on mixture cracking performance.

  o SBS polymer modification was found to increase binder FED but have almost no impact on mixture FED. Conversely, it reduced the damage rate of both asphalt binder and the corresponding mixtures.

  o As a result, the difference in cracking performance of unmodified and modified binders depicted by the BFE binder N_f parameter seemed to be exaggerated and was not proportionally reflected on the corresponding mixture N_f results.

7.2 Conclusions and Recommendations

Based on the findings of this study, the following conclusions and recommendations were made:

- The BFE test can be used to accurately determine the binder FED, which is recommended to be used to characterize the relative cracking performance of asphalt binders at intermediate temperatures.

- The LAS test either TP 101-14 or the G^R approach can also be used to evaluate the relative cracking performance of asphalt binders excluding the one modified with rubber and possibly also the extremely soft unmodified binder. The TP 101-14 is recommended because it requires significantly less amount of testing effort than the G^R approach.

- More research is needed to look into evaluating the cracking performance of soft unmodified binders and mixtures with soft unmodified binders.

LIST OF REFERENCES

AASHTO Provisional Standard TP 101-12. (2012). Standard method of test for estimating fatigue resistance of asphalt binders using the linear amplitude sweep, American Association of State Highway and Transportation Officials, Washington, D.C.

AASHTO Provisional Standard TP 101-14. (2014). Standard method of test for estimating damage tolerance of asphalt binders using the linear amplitude sweep, American Association of State Highway and Transportation Officials, Washington, D.C.

AASHTO Provisional Standard TP113-15. (2015). Standard method of test for determination of asphalt binder resistance to ductile failure using double-edge-notched (DENT) test, American Association of State Highway and Transportation Officials, Washington, D.C.

AASHTO Provisional Standard TP 127-17. (2017). Standard method of test for determining the fracture energy density of asphalt binder using the binder fracture energy (BFE) test, American Association of State Highway and Transportation Officials, Washington, D.C.

Aboutorabi, H., Ebbot, T. and Gent, A.N. (1998). Crack growth in twisted rubber disks. Part I: fracture energy calculation, Rubber Chemistry and Technology, Vol.71, Issue. 1, pp. 76–83.

Anderson, D.A., Hir, Y., Marasteanu, M., Planche, J.P., Martin, D. and Gauthier, G. (2001). Evaluation of fatigue criteria for asphalt binders, In Transportation Research Record: Journal of the Transportation Research Board, No.1766, TRB, National Research Council, Washington, D.C., pp. 48–56.

Andriescu, A., Hesp, S.A.M. and Youtcheff, J.S. (2004). Essential and plastic works of ductile fracture in asphalt binders, Transportation Research Record: Journal of the Transportation Research Board, No.1875, TRB, National Research Council, Washington, D.C., pp. 1–8.

Anderson, R. M. (2011). Evaluation of the Relationship between Asphalt Binder Properties and Non-Load Related Cracking. Association of Asphalt Paving Technologists, 2011 Volume 80, pp. 615-663.

Bahia, H.U., Hanson, D.I., Zeng, M., Zhai, H., Khatri, M.A. and Anderson, R.M. (2001). Characterization of modified asphalt binders in Superpave mix design, NCHRP Report 459, National Cooperative Highway Research Program, Transportation Research Board — National Research Council, Washington, D.C.

Birgisson, B., Montepara, A., Romeo, R., Roque, R., Roncella, R. and Tebaldi, G. (2007). Determination of fundamental tensile failure limits of mixtures, Journal of the Association of Asphalt Paving Technologists, Vol.76, pp. 303–344.

Buttlar, W.G. and Roque, R. (1994). Development and evaluation of the Strategic Highway Research Program measurement and analysis system for indirect tensile testing at low

temperatures, In Transportation Research Record: Journal of the Transportation Research Board, No. 1454, Transportation Research Board of the National Academies, Washington, D.C., pp. 163–171.

Chehab, G., Kim, Y.R., Schapery, R.A., Witczack, M. and Bonaquist, R. (2002). Time-temperature Superposition principle for asphalt concrete mixtures with growing damage in tension state, Journal of Association of Asphalt Paving Technologists, Vol. 71, pp. 559–593.

Carpenter, S.H., Ghuzlan, K. and Shen, S. (2003). A fatigue endurance limit for highway and airport pavement, Transportation Research Record: Journal of the Transportation Research Board, No.3428, TRB, National Research Council, Washington, D.C., pp. 131–138.

Ghuzlan and Carpenter. (2000). Energy-derived, damage-based failure criterion for fatigue testing, Transportation Research Record: Journal of the Transportation Research Board, No.1723, TRB, National Research Council, Washington, D.C., pp. 141–149.

Gibson, N., Qi, X., Shenoy, A., Al-Khateeb, G., Kutay, M.E., Andriescu, A., Stuart, K., Youtcheff, J. and Harman, T. (2012). Performance testing for Superpave and structural validation, FHWA Final Report HRT-11-045, Office of Infrastructure Research and Development, Washington, D.C.

Hintz, C., Velasquez, R., Tabatabaee, H. and Bahia, H. (2011). Fatigue characterization of asphalt binders with the linear amplitude sweep (LAS), Modified Asphalt Research Center, University of Wisconsin-Madison, available at https://uwmarc.wisc.edu/linear-amplitude-sweep, Accessed on August 24, 2018.

Hintz, C., Velasquez, R., Johnson, C. and Bahia, H. U. (2011). Modification and Validation of the Linear Amplitude Sweep Test for Binder Fatigue Specification, In Transportation Research Record: Journal of the Transportation Research Board, No. 2207, Transportation Research Board of the National Academies, Washington, D.C., pp. 99–106.

Hintz, C. and Bahia, H.U. (2013a). Understanding mechanisms leading to asphalt binder fatigue in the dynamic shear rheometer, Road Materials and Pavement Design, Vol. 14, Issue S2, pp. 231–251.

Hintz, C. and Bahia, H.U. (2013b). Simplification of linear amplitude sweep test and specification parameter, Transportation Research Record: Journal of the Transportation Research Board, No. 2370, Washington, D.C., pp. 10–16.

Johnson, C. and Bahia, H. U. Evaluation of an accelerated procedure for fatigue characterization of asphalt binders, available at: https://uwmarc.wisc.edu/files/linearamplitudesweep/RMPD10_LAS_CMJ_HB-100321.pdf, Accessed on April 11th, 2020.

Johnson, C. M., Wen, H. and Bahia, H. U. (2009). Practical application of viscoelastic continuum damage theory to asphalt binder fatigue characterization. Journal of the Association of Asphalt Paving Technologists, Vol. 78, pp. 597–638.

Johnson, C.M. (2010). Estimating asphalt binder fatigue resistance using an accelerated test method, Ph.D. dissertation, University of Wisconsin-Madison, Madison, WI.

Kim, Y. R., and D. N. Little (1990). One-dimensional constitutive modeling of asphalt concrete, ASCE Journal of Engineering Mechanics, Vol. 116, No.4, pp. 751–772.

Kim, Y.R., Lee, H.J. and Little, D.N. (1997). Fatigue characterization of asphalt concrete using viscoelasticity and continuum damage theory, Journal of the Association of Asphalt Paving Technologists, Vol. 66, pp. 520–569.

Kim, Y., Lee, H. J. Little, D. N. and Kim, Y. R. (2006). A simple testing method to evaluate fatigue fracture and damage performance of asphalt mixtures, Journal of the Association of Asphalt Paving Technologists, Vol. 75, pp. 755–788.

Kim, B. and Roque, R. (2006). Evaluation of healing property of asphalt mixtures, In Transportation Research Record: Journal of the Transportation Research Board, No. 1970, Washington, D.C., pp. 84–91.

Niu, T., Roque, R. and Lopp, G. (2014). Development of a binder fracture test to determine fracture energy. Road Materials and Pavement Design, Vol. 15, Supplement 1, pp. 219–238.

Pronk, A.C. (1995). Evaluation of the dissipated energy concept for the interpretation of fatigue measurements in the crack initiation phase, Road and Hydraulic Engineering Division, Amsterdam, Netherlands.

Pronk, A.C. (1997). Fatigue lives of asphalt beams in 2 and 4-point dynamic bending tests based on a "new" fatigue life definition using the "dissipated energy concept". Proc., Eighth International Conference on Asphalt Pavements, Seattle, Wash., pp. 987–994.

Roque, R. and Buttlar, W.G. (1992). The development of a measurement and analysis system to accurately determine asphalt concrete properties using the indirect tensile mode, Journal of the Association of Asphalt Paving Technologists, Vol. 61, pp. 304–332.

Roque, R., Buttlar, W.G., Ruth, B.E., Tia, M., Dickson, S.W. and Reid, B. (1997). Evaluation of SHRP indirect tension tester to mitigate cracking in asphalt pavements and overlayers, FDOT final report No. BA-546, University of Florida, Gainesville

Roque, R., Birgisson, B., Sangpetngam, B. and Zhang, Z. (2002). Hot mix asphalt fracture mechanics: a fundamental crack growth law for asphalt mixtures, Journal of the Association of Asphalt Paving Technologists, Vol. 71, pp. 816–827.

Roque, R., Birgisson, B., Drakos, C. and Dietrich, B. (2004). Development and field evaluation of energy-based criteria for top-down cracking performance of hot mix asphalt, Journal of the Association of Asphalt Paving Technologists, Vol. 73, pp. 229–260.

Roque, R., Zou, J., Kim, Y.R., Beak, C., Thirunavukkarasu, S., Underwood, B.S. and Guddati, M.N. (2010). Top-down cracking of HMA layers: models for initiation and propagation, NCHRP Web-only Document 162, National Cooperative Highway Research Program, Transportation Research Board of the National Academies.

Roque, R., Zou, J., Kim, Y. R. and Beak, C. (2013). Top-down cracking of Hot-mix asphalt layers: models for initiation and propagation, NCHARP Web-Only Document 162, TRB, National Research Council, Washington, D.C.

Roque, R., Isola, M., Bekoe, M., Zou J. and Lopp, G. (2015). Validation and refinement of mixture volumetric material properties identified in Superpave monitoring project: Phase II, Florida Department of Transportation Research Report for FDOT BDV31-977-18 Contract. Gainesville, FL: University of Florida.

Roque, R., Hernando, D. and Zou J. (2015). Advances in asphalt materials-road and pavement constructions: Chapter 5 Cracking mechanisms in asphalt mixtures, Woodhead Publishing Series in Civil and Structural Engineering: Number 56, pp. 133–167, Elsevier, UK.

Sabouri, M. and Kim, Y.R. (2014). Development of failure criterion for asphalt mixtures under different modes of fatigue loading. Transportation Research Record: Journal of Transportation Research Board, No. 2447, pp. 117–125.

Schapery, R.A. (1984). Correspondence principles and a generalized J integral for large deformation and fracture analysis of viscoelastic media, International Journal of Fracture, Vol. 25, No.3, pp. 195–223.

Shen, S., Airey, G.D., Carpenter, S.H. and Huang, H. (2006). A dissipated energy approach to fatigue evaluation, Road Materials and Pavement Design, Vol.7, Issue 1. pp. 47–69.

Underwood, B.S., Kim, Y.R. and Guddati, M.N. (2006). Characterization and performance prediction of ALF mixtures using a viscoelastoplastic continuum damage model, Journal of Association of Asphalt Paving Technologists, Vol. 75, pp. 577–636.

Underwood, B.S., Y. R. Kim, and M. N. Guddati (2009a). Improved calculation method of damage parameter in viscoelastic continuum damage model, International Journal of Pavement Engineering, Vol. 11, pp. 459–476.

Underwood, B. S., Y. R. Kim, S. Savadatti, S. Thirunavukkarasu, and M. N. Guddati (2009b). Response and fatigue performance modeling of ALF pavements using 3-D finite element analysis and a simplified viscoelastic continuum damage model, Journal of the Association of Asphalt Paving Technologists, AAPT, Vol. 78, pp. 829–868.

Underwood, B. H., E. T. Hou, and Y. R. Kim (2009c). Application of simplified VECD modeling to the fatigue prediction of asphalt concrete mixtures, 7th International RILEM Symposium on Advanced Testing and Characterization of Bituminous Materials, Rhodes, Greece.

Wen, H. and Bahia, H. (2009). Characterizing fatigue of asphalt binders with viscoelastic continuum damage mechanics, Transportation Research Record: Journal of the Transportation Research Board, No.2126, TRB, National Research Council, Washington, D.C., pp. 55–62.

Wang, C., Castorena, C., Zhang, J. and Kim, Y.R. (2015). Unified failure criterion for asphalt binder under cyclic fatigue loading, Road Materials and Pavement Design, Vol. 16, Issue.S2, pp. 125–148.

Wang, C., Zhang, H., Castorena, C., Zhang, J.X. and Kim, Y.R. (2016). Identifying fatigue failure in asphalt binder time sweep tests. Construction and Building Materials, Vol.121, pp. 535–546.

Wang, C., Xie, W., Chen, Y., Diab, A. and You, Z. (2017). Refining the calculation method for fatigue failure criterion of asphalt binder from linear amplitude sweep test, ASCE Journal of Materials in Civil Engineering, Vol. 30, Issue 2.

Yan, Y., Cocconcelli, C., Roque, R., Nash, T., Zou, J., Hernando, D. and Lopp, G. (2015). Performance evaluation of alternative polymer-modified asphalt binders, Road Materials and Pavement Design, Vol. 16, Issue.S1, pp. 389–403.

Yan. Y., Chun. S., Roque, R. and Kim. S. (2016). Effects of alternative polymer modifications on cracking performance of asphalt binders and resultant mixtures, Construction and Building Materials, Vol. 121, pp. 569–575.

Yan. Y., Hernando. D. and Roque. R. (2017). Fracture tolerance of asphalt binder at intermediate temperatures, ASCE Journal of Materials in Civil Engineering, Vol. 29, Issue.9.

Zhang, Z. (2000). Identification of suitable crack growth law for asphalt mixtures using the Superpave indirect tensile test (IDT), PhD dissertation, University of Florida, Gainesville.

Zhang, Z., Roque, R. and Birgisson, B. (2001a). Evaluation of laboratory measured crack growth rate for asphalt mixtures, Transportation Research Record: Journal of the Transportation Research Board, No.1767, TRB, National Research Council, Washington, D.C., pp. 67–75.

Zhang, Z., Roque, R., Birgisson, B. and Sangpetngam, B. (2001b). Identification of verification of a suitable crack growth law, Journal of the Association of Asphalt Paving Technologists, Vol. 70, pp. 206–241.

Zhang, J., Sabouri, M., Guddati, M.N. and Kim, Y.R. (2013). Development of a failure criterion for asphalt mixtures under fatigue loading, Road Materials and Pavement Design, Vol. 14, Issue S2, pp. 1–15.

Zhou, F., Mogawer, W., Li, H., Andriescu, A. and Copeland, A. (2013). Evaluation of Fatigue Tests for Characterizing Asphalt Binders, ASCE Journal of Materials in Civil Engineering, Vol.25, Issue. 5, pp. 610–617.

APPENDIX I ACCURATE CONTROL OF STRAIN LOAD

Preliminary LAS testing results (presented in Task II) indicated that a standard dynamic shear rheometer (DSR) cannot provide accurate control of stepwise increased strain load for the LAS amplitude sweep test, as shown in Figure I-1. More specifically, the first two and the last data points within a strain interval, which consists of 10 data points at the same strain magnitude, became erroneous at strain levels ranging from approximately 10% to 25%. Similarly, data points with unrealistic low or high shear stress and shear strain were also observed in the shear stress versus shear strain curve, as shown in Figure I-2. These outliers must be addressed because they masked the real maximum shear stress, which is used as the indicator of failure in AASHTO TP 101-14. The same observation has been reported by other researchers and they attributed it to machine incompetence (Hintz et al. 2011).
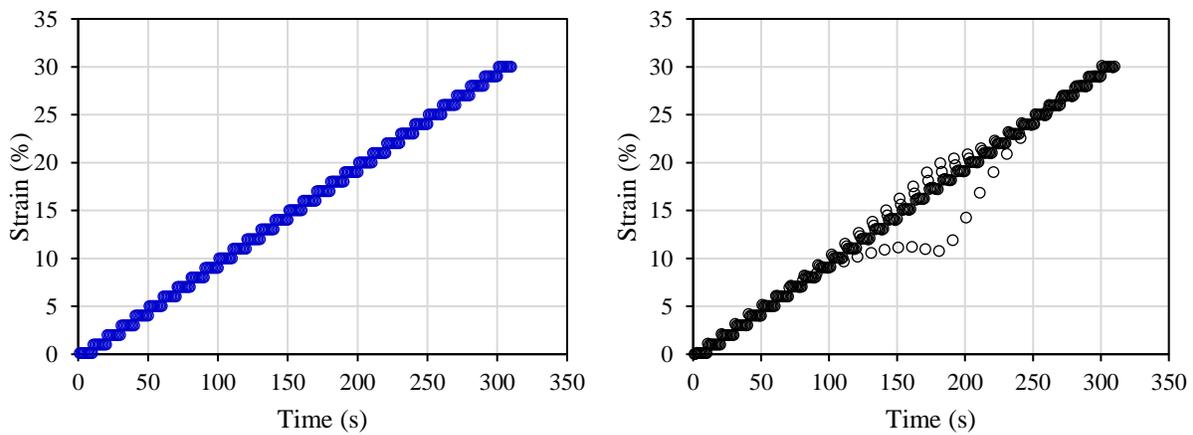

Figure I-1. Stepwise strain loading scheme: (a) target; (b) actual
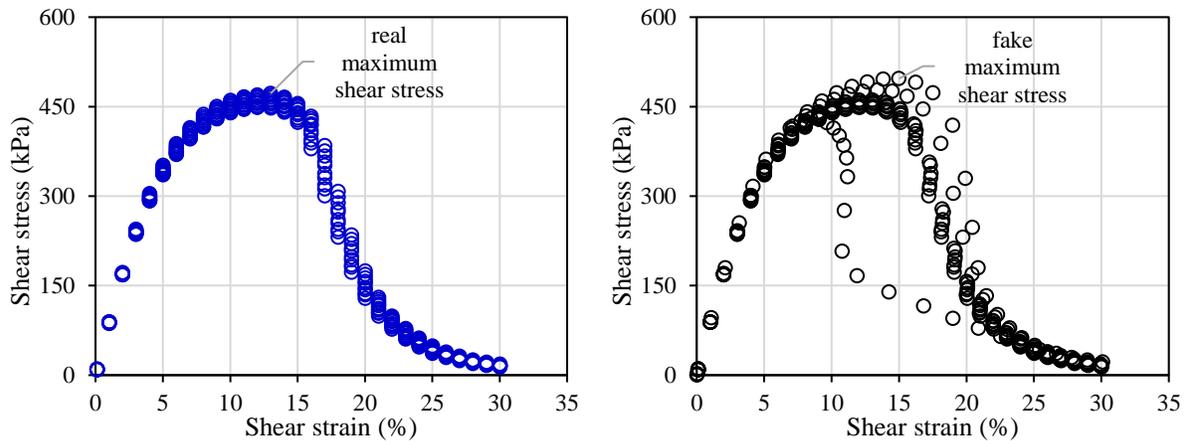
Figure I-2. Shear stress versus shear strain curve: (a) target; (b) actual

Damage accumulation ($D_{(t)}$) was determined following AASHTO TP 101 and the results associated with PG 52-28 are shown in Figure I-3 for illustration purposes. Figure I-3 shows the

material integrity (i.e., $|G^*| \cdot \sin\delta$) versus damage intensity (i.e., damage accumulation) curve. Decreased $|G^*| \cdot \sin\delta$ with increased damage intensity indicates that damage has occurred in the DSR specimen. Some data points were intentionally marked as red circles and they correspond to the strain loads that were previously identified as outliers.
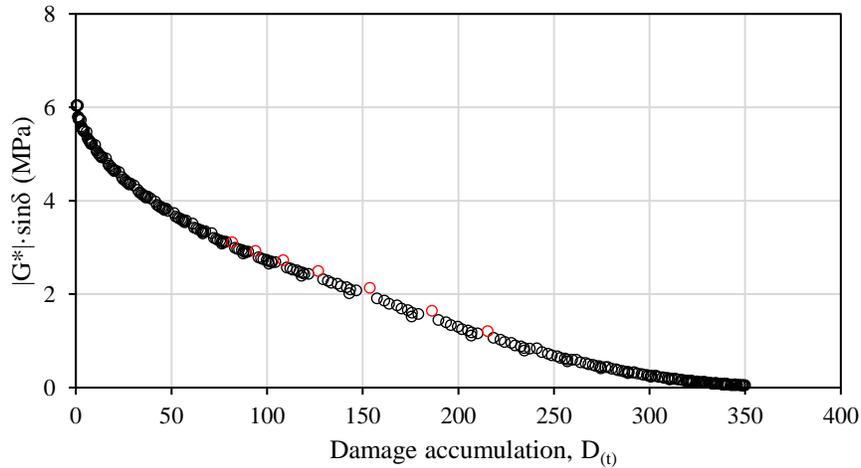

Figure I-3. $|G^*| \cdot \sin\delta$ versus damage plot showing erratic data points

Figure I-4 reveals that the inaccurate strain load did not impact the determination of damage at failure (D_f) when it was correlated to a 35% reduction in undamaged $|G^*| \cdot \sin\delta$. However, the inaccurate strain load can cause a significant impact on D_f when the maximum shear stress was used as the failure indicator. Of note, researchers of this study were recently informed by the developers of the LAS test at UW-Madison that the latter definition of damage at failure (i.e., use of maximum shear stress as the failure indicator) is recommended and AASHTO TP 101-14 shall be followed.
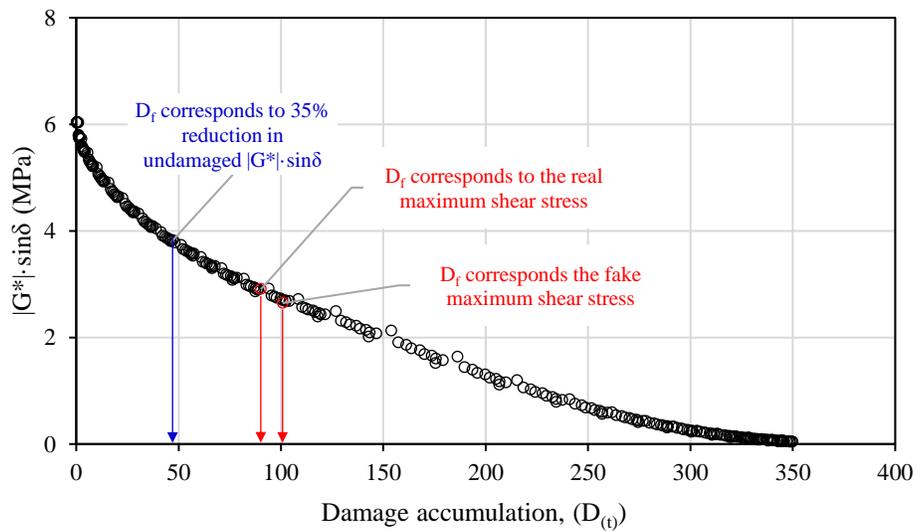
Figure I-4. Determination of damage at failure (D_f) based on different definitions

Figure I-5 reveals that the use of a standard rheometer to perform the stepwise LAS test resulted in approximately 10% overestimated D_f values for five of the six binders tested in this study. The only exception was the PG 67-22 binder, whose fake shear stress peak occurred before the real one (Figure I-6) and, consequently, it yielded an underestimated D_f value.
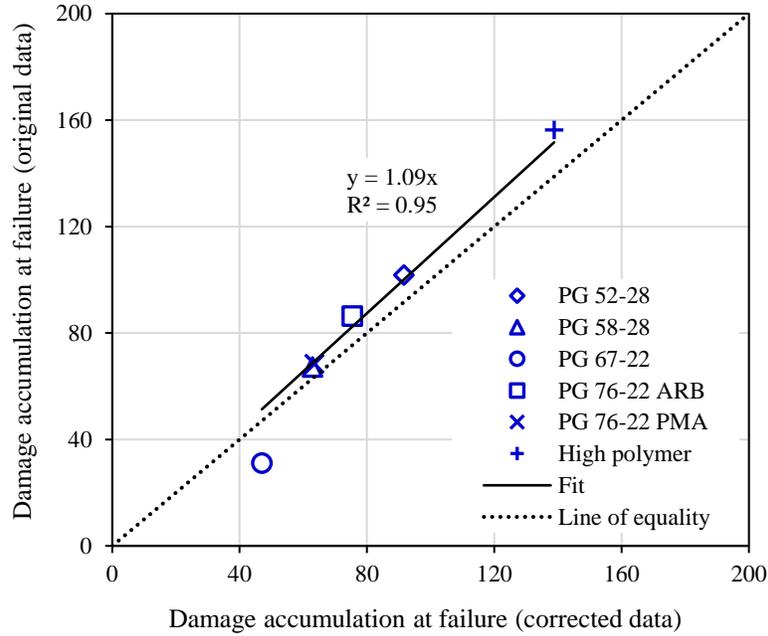
Figure I-5. Comparison in damage accumulation at failure between original and corrected shear stress and shear strain data
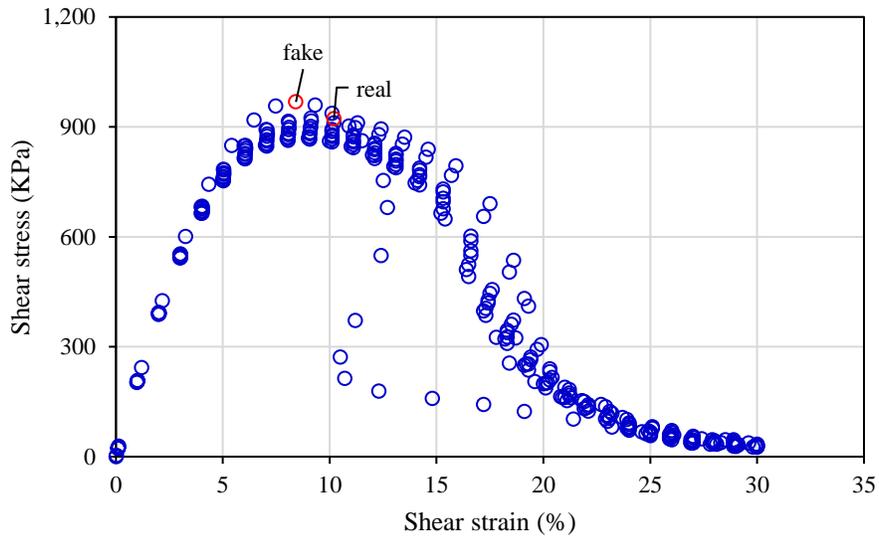
Figure I-6. Shear stress and shear strain curve of the PG 67-22 binder

By using predictive modeling techniques, the LAS test allows for the determination of binder fatigue life for a given pavement structural condition (i.e., employing the maximum expected binder strain for a given pavement structure), as shown in I-7. Two fatigue model parameters A and B can be determined from amplitude sweep and frequency sweep tests, respectively. A larger A value indicates greater fatigue life while a higher magnitude of B decreases fatigue life (at a constant A).

The plot shows the relation:

$$N_f = A \cdot (\gamma_{max})^B$$

with

$$A = \frac{f(D_f)^k}{k(\pi C_1 C_2)^\alpha} \qquad B = 2\alpha$$

where:
f = loading frequency (10 Hz),
C_1 and C_2 = curve-fit coefficients,
$k = 1 + (1 - C_2)\alpha$,
$\alpha = 1/m$, and
m = curve-fit coefficient
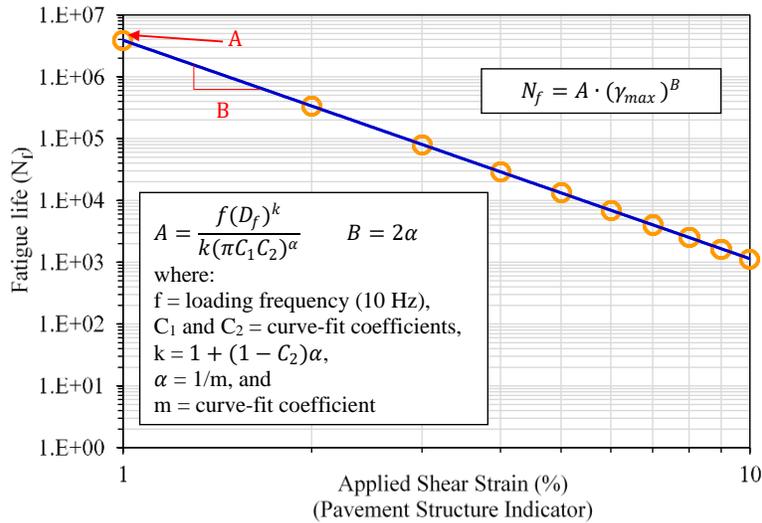
Figure I-7. Plot of fatigue parameter N_f versus applied binder shear strain on a log-log scale

A relationship between a property (e.g., shear stress) and time was established and then, it was used to predict the real shear stress values use time as input. Figure I-8 illustrates the trimming process of the complex shear modulus data.
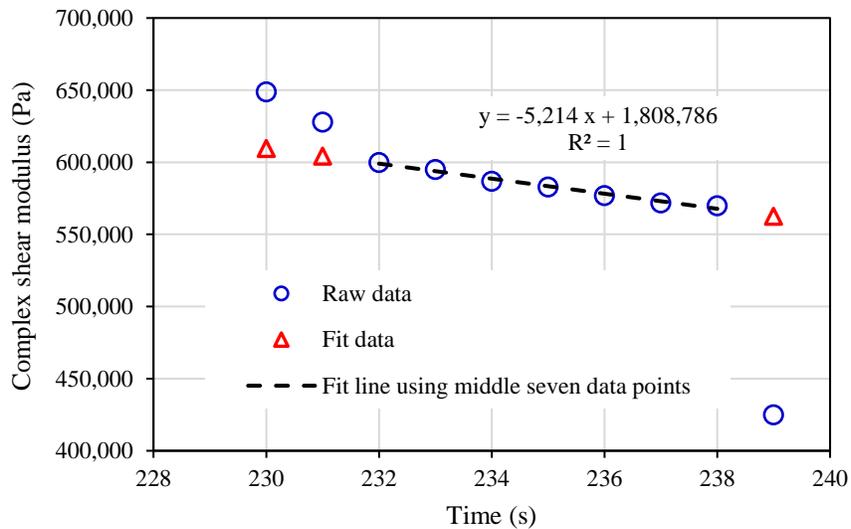

Figure I-8. An example of how to trim the complex shear modulus data for a given strain interval

Figure I-9 compares the results of the LAS fatigue model parameter A of the six binders determined based on original and trimmed raw data. The use of maximum shear stress as the failure indicator was employed for analysis. The A parameter, which is directly related to damage accumulation at failure (D_f), was also found to be overestimated for all binders except for the PG 67-22. The level of overestimation varies; however, they are all greater than what has been previously reported (i.e., 8.47%) by the LAS test developers. Fatigue model parameter B was not affected because it is determined based on data collected from the frequency sweep tests.
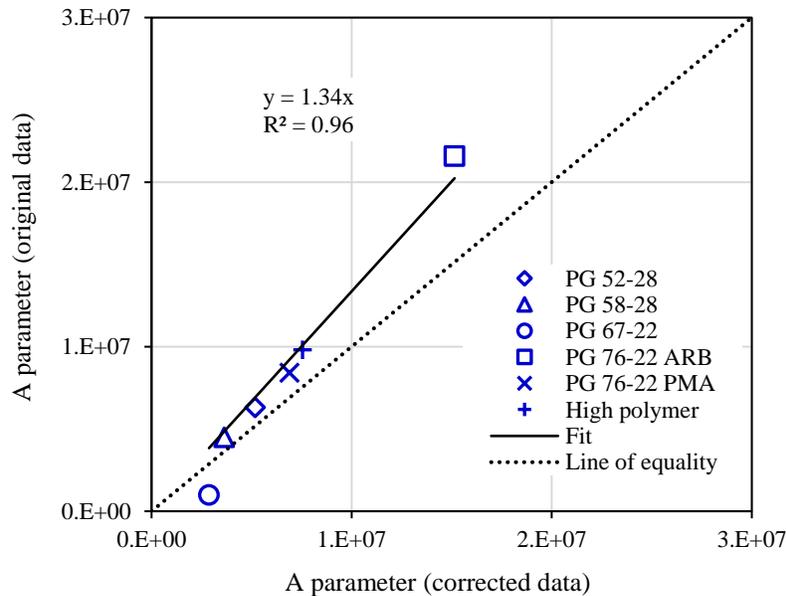

Figure I-9. Comparison of A parameter between original and corrected data

Comparisons were also made in fatigue life (N_f) of the six binders determined based on original and corrected raw data. Two strain levels (2.5% and 5.0%) were applied as structural input for fatigue life predictions. Both Figures I-10 and I-11 indicated the use of original raw data resulted in approximately 30% greater binder fatigue life than that based on corrected raw data. Once again, the only exception is the PG 67-22 binder, which had underestimated fatigue life.

Most of the binders tested in this study exhibited overestimated binder fatigue life; however, it is not clear that in what circumstance, the standard DSR rheometer would yield underestimations. Also, the researchers of the present study were recently informed by the developers of the LAS test that the stepwise strain load in AASHTO TP 101-12 shall be replaced by a linearly increased strain load as described in AASHTO TP 101-14. This change actually made things even worse because the standard DSR used was not able to provide a complete linear strain load (please refer to Task II report Figures 2-15 and 2-16). Therefore, the bituminous laboratory at SMO added a software feature named "TruStrain" to its standard rheometer. This software upgrade allowed for an accurate control of linearly increased strain load, which is necessary for the TP 101-14 and the G^R approach.
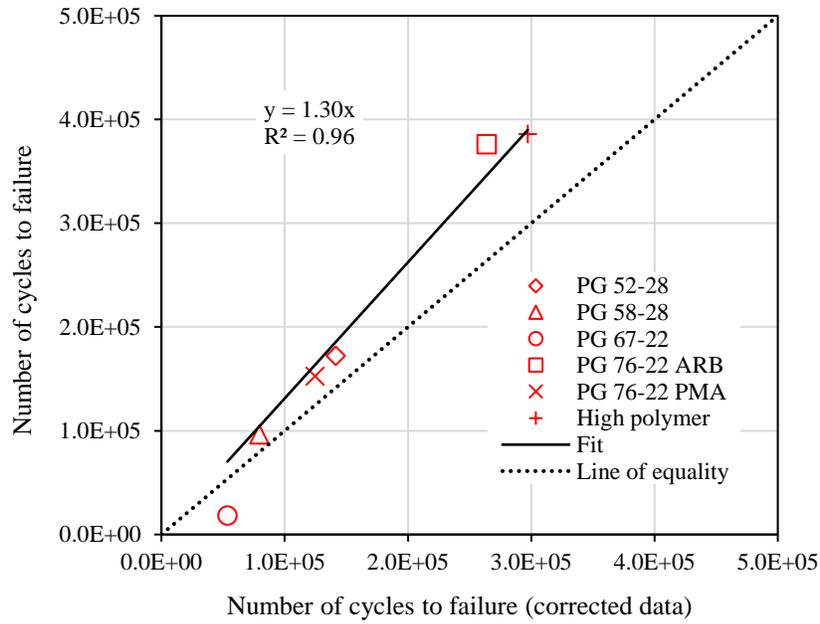
Figure I-10. Comparison of fatigue life (N_f) at 2.5% strain between original and corrected data
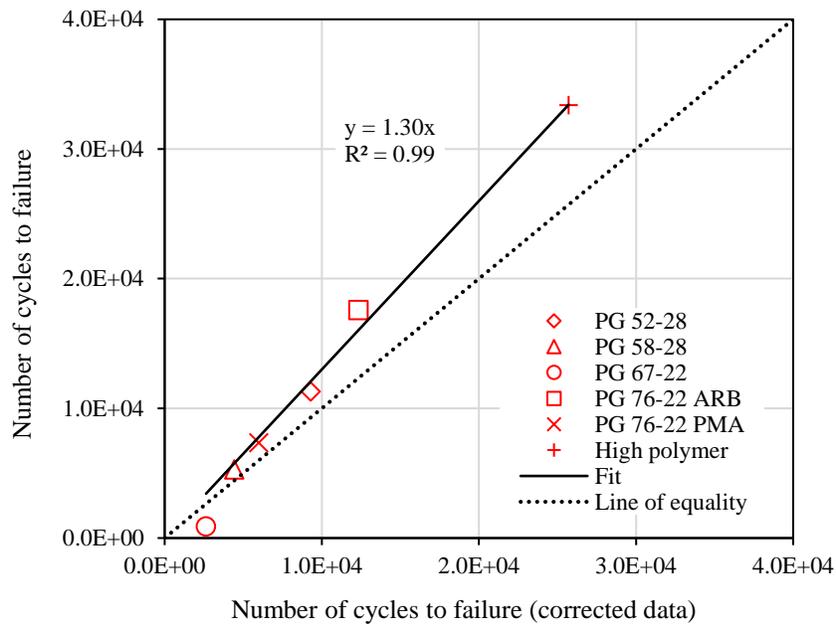
Figure I-11. Comparison in fatigue life (N_f) of 5.0% strain between original and corrected data

APPENDIX II DETERMINATION OF BFE BINDER N_F PARAMETER

According to the hot-mix asphalt-fracture mechanics (HMA-FM) model that has been shown to correlate well with field observations in Florida, it is important to consider both failure limit (e.g., FED) and damage rate as an entire system to predict mixture cracking performance. Thus, it seems logical that a binder parameter that is governed by the binder FED and damage rate is necessary to effectively characterize binder cracking performance.

Binder FED can be determined by performing the BFE test following the AASHTO provisional standard. There are mainly two steps to obtain binder damage rate: 1) performing an alternative interpretation of the true stress-true strain curve of the BFE test to derive the creep strain rate per unit stress (CSR/S) parameter and 2) determining the binder dissipated creep strain energy accumulated per loading cycle (DCSE/cycle). A haversine load consisting of a 0.1-s loading period followed by a 0.9-s rest period has been used to determine mixture DCSE/cycle. The same loading scenario was adopted in this study and Equation 1 can be used to determine binder DCSE/cycle.

$$DCSE/cycle = \frac{1}{20} \cdot \sigma^2 \cdot CSR/S \qquad \text{(Equation 1)}$$

where, σ represents the tensile stress in the pavement structure and 1 MPa (150 psi), which has been used to determine the energy ratio of asphalt mixtures, is employed in this study. Note that the same tensile stress value shall be used for all binders. It can be observed that binder DCSE/cycle is governed by the CSR/S parameter.

CSR/S values of all binders were summarized in Task IV report. In general, stiffer binders had lower CSR/S values, indicating lower rates of damage accumulation. Moreover, the SBS binders exhibited notably lower CSR/S values than unmodified binders. Both observations agree with previous knowledge of mixture damage rate. The BFE binder N_f parameter can simply be obtained by using binder failure limit (i.e., FED) over binder damage rate (i.e., DCSE/cycle).

APPENDIX III MIXTURE SPECIMEN INFORMATION

Table III-1. Superpave IDT specimen of GA granite mixtures

Binder type	Specimen ID	G_{mb}	G_{mm}	Air voids (%)	Thickness (inch)
PG 52-28	I	2.398	2.577	7.0%	1.44
	II	2.397		7.0%	1.49
	III	2.395		7.1%	1.47
PG 58-28	I	2.400	2.575	6.8%	1.43
	II	2.399		6.8%	1.58
	III	2.388		7.3%	1.48
PG 67-22	I	2.393	2.574	7.0%	1.54
	II	2.388		7.2%	1.49
	III	2.392		7.1%	1.47
PG 76-22 ARB	I	2.385	2.572	7.3%	1.48
	II	2.385		7.3%	1.53
	III	2.386		7.2%	1.55
PG 76-22 PMA	I	2.383	2.568	7.2%	1.51
	II	2.388		7.0%	1.52
	III	2.386		7.1%	1.51
High polymer	I	2.392	2.564	6.7%	1.45
	II	2.387		6.9%	1.55
	III	2.386		6.9%	1.46

Table III-2. Superpave IDT specimen of FL limestone mixtures

Binder type	Specimen ID	G_{mb}	G_{mm}	Air voids (%)	Thickness (inch)
PG 52-28	I	2.166	2.329	7.0%	1.56
	II	2.159		7.3%	1.59
	III	2.154		7.5%	1.49
PG 58-28	I	2.162	2.332	7.3%	1.59
	II	2.157		7.5%	1.53
	III	2.172		6.9%	1.45
PG 67-22	I	2.169	2.331	7.0%	1.49
	II	2.165		7.1%	1.57
	III	2.158		7.4%	1.54
PG 76-22 ARB	I	2.164	2.344	7.7%	1.55
	II	2.177		7.1%	1.49
	III	2.182		6.9%	1.56
PG 76-22 PMA	I	2.159	2.325	7.2%	1.58
	II	2.158		7.2%	1.57
	III	2.165		6.9%	1.55
High polymer	I	2.156	2.322	7.1%	1.41
	II	2.157		7.1%	1.55
	III	2.157		7.1%	1.44

APPENDIX IV SUPERPAVE IDT RESULTS

Table IV-1. Superpave IDT results for granite and limestone mixtures

Mixture type	Binder type	Resilient modulus test	Tensile creep test	Tensile fracture test		Damage rate	Failure limit	Cracking performance indicator
		M_R	creep compliance rate	Tensile strength	Failure strain	DCSE/cycle	FED	Number of cycles to failure
		GPa	$GPa^{-1} \cdot sec^{-1}$	MPa	$\mu\varepsilon$	$kJ/m^3/cycle$	kJ/m^3	
FL limestone mixtures	PG 52-28	7.6	2.6E-03	1.46	2523	1.3E-03	2.8	2.1E+03
	PG 58-22	10.9	5.9E-04	1.97	1556	3.0E-04	2.3	7.8E+03
	PG 67-22	12.4	2.2E-04	2.53	1250	1.1E-04	2.3	2.1E+04
	PG 76-22 ARB	12.1	9.2E-5	2.77	1319	4.6E-05	2.5	5.4E+04
	PG 76-22 PMA	11.3	1.3E-04	2.65	1576	6.3E-05	3.1	4.9E+04
	High Polymer	8.1	1.2E-04	1.98	2417	6.2E-05	3.5	5.6E+04
GA granite mixtures	PG 52-28	6.4	1.6E-02	1.33	3638	7.8E-03	3.5	4.5E+02
	PG 58-22	11.3	1.5E-03	2.14	2365	7.6E-04	3.7	4.9E+03
	PG 67-22	12.7	6.3E-04	2.73	1815	3.1E-04	3.5	1.1E+04
	PG 76-22 ARB	13.5	3.3E-04	2.57	1795	1.6E-04	3.2	2.0E+04
	PG 76-22 PMA	14.2	3.3E-04	2.74	1884	1.7E-04	3.7	2.2E+04
	High Polymer	8.9	1.4E-04	2.03	3464	7.2E-05	5.0	7.0E+04

APPENDIX V REVISED TENSILE CREEP TEST

The Superpave IDT tensile creep test is used to capture the permanent strain associated with the time-dependent response of asphalt mixtures. Creep compliance is defined as the ratio of time-dependent strain to stress. Since it well represents the time-dependent response of asphalt concrete, it has been used to evaluate the rate of damage accumulation of asphalt mixture subjected to repeated loads.

Tensile creep tests are performed in a load-controlled mode by applying a static load in the form of a step function to the specimen and then holding it for a period of time. Typically, a 1,000-s tensile creep test has been considered to be enough to isolate the viscous response of asphalt mixtures for intermediate temperatures associated with fatigue cracking (0-25°C). The magnitude of the load is appropriately selected in order to maintain the accumulated horizontal deformation in the linear viscoelastic range. For a 6-in Superpave IDT specimen with a gauge length of 1.5 in, this translates to a total horizontal deformation below 750 micro-inches. During the first 100 seconds of test, a horizontal deformation of no greater than 100 to 130 micro-inches is generally considered to be acceptable to keep the maximum horizontal deformation below 750 micro-inches.

Figure V-1 shows the creep compliance rate of five granite mixtures following the existing test protocol. The HP mixture exhibited a greater damage rate than that of the PG 76-22 PMA and PG 76-22 ARB mixtures. This does not meet the expectation because the HP binder has far more SBS polymer than the other two modified binders. The main benefit of SBS polymer has been proven to be a reduction in mixture damage rate and therefore, a higher SBS polymer content should result in a lower mixture damage rate. The same observation was made on FL limestone mixtures, as shown in Figure V-2.
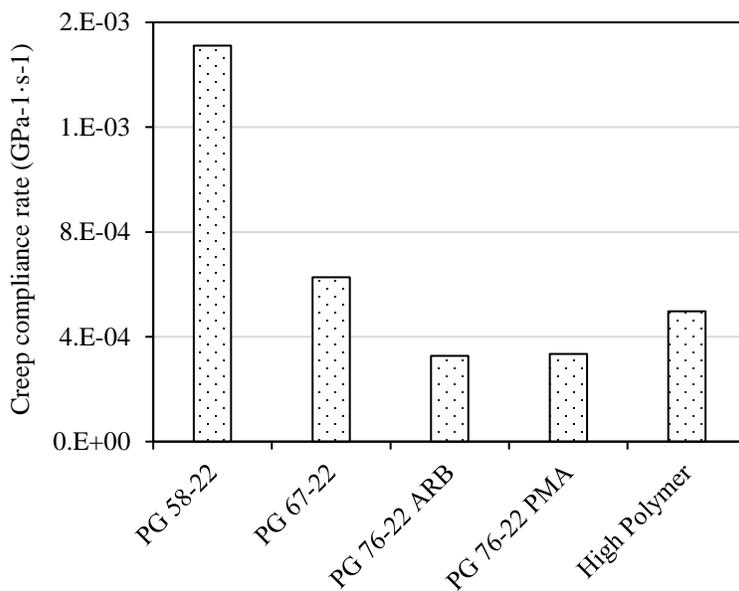

Figure V-1. Creep compliance rate of granite mixtures from 1,000-second creep test
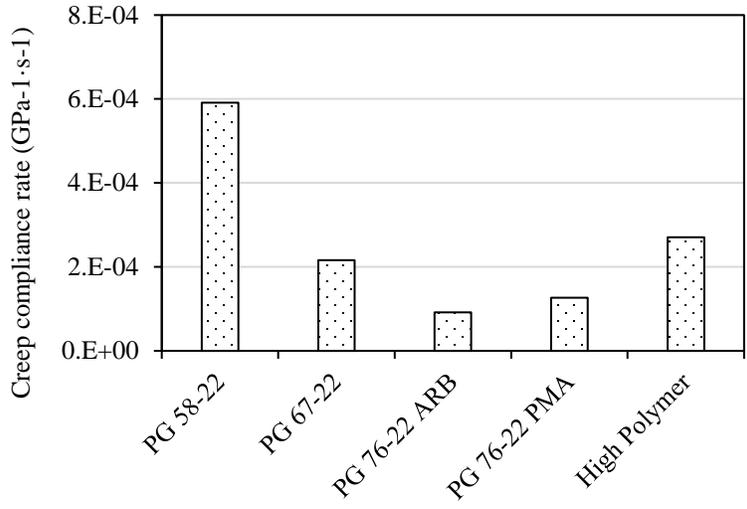
Figure V-2. Creep compliance rate of limestone mixtures from 1,000-second creep test

A preliminary investigation was conducted to explain the potential "high" damage rate of HP mixture. The hypothesis is that 1,000 seconds of testing is not enough time to isolate the viscous response from the delayed elastic response of the HP mixture. Tensile creep tests with a longer loading time period (i.e., 7,500 seconds) were conducted on the HP and the PG 67-22 limestone mixtures to validate the hypothesis.

Figure V-3 plots the creep compliance curve of the two mixtures. Of note, the revised tensile creep tests were also conducted following the previously described rules, i.e., the horizontal displacement at 100 and 1,000 seconds should lower than 100 and 750 micro-inches, respectively. The creep compliance rate (i.e., the slope of the curve) of the PG 67-22 mixture after 1,000 seconds barely changed. This substantiates the effectiveness of the existing protocol in determining the creep compliance of mixtures with commonly used binders in Florida.
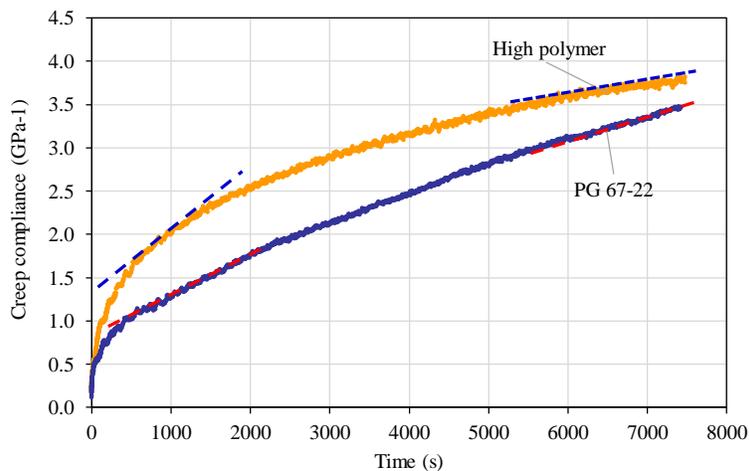

Figure V-3. Creep compliance curve of PG 67-22 and HP limestone mixtures from 7,500-second creep test

Creep compliance rate values (i.e., slope of the creep compliance curve) of the HP mixture were calculated at every 500 seconds from 500 to 7000 seconds. Figure V-4 shows that the creep compliance rate of the HP mixture dropped by a factor of three in the first 2,000 seconds. The decreasing trend continued as time increased until a plateau was reached between 5,500 to 7,000 seconds. Therefore, the creep compliance rate of the HP limestone mixture was reported in this study after 7,000 seconds ($1.24E-4$ $GPa^{-1} \cdot sec^{-1}$).
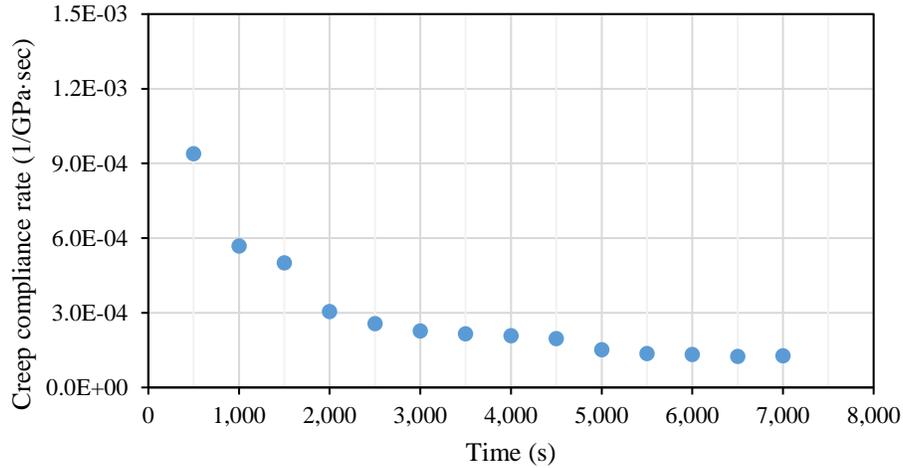

Figure V-4. Creep compliance rate of HP limestone mixture from the 7,500s tensile creep test

The 7,500-s tensile creep test was also conducted on HP granite mixtures and Figure V-5 plots the creep compliance rate of HP granite mixture calculated at every 500 seconds from 500 to 7,000 seconds. The observation made on HP limestone mixture was further validated by the results of HP granite mixture, and the creep complete rate of this mixture used in this study was $1.4E-4$ $GPa^{-1} \cdot sec^{-1}$. More research is recommended to further evaluate the appropriate loading time of the tensile creep tests on mixtures with new modified binders, e.g., the HP binder.
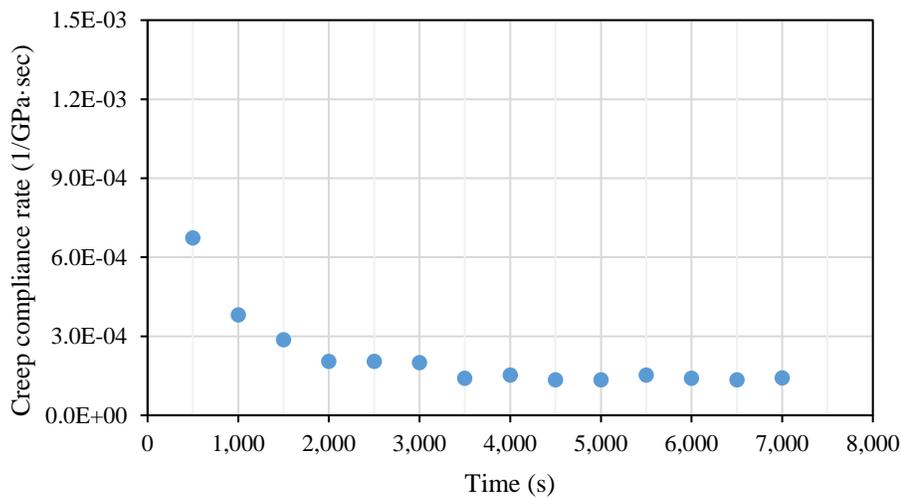

Figure V-5. Creep compliance rate of HP granite mixture from the 7,500s tensile creep test